

Boron in marine biogenic carbonates as a proxy for the carbonate system

by

Karina Kaczmarek

A thesis submitted in partial fulfillment of the requirements
for the degree of Doctor of Philosophy in geoscience

Approved, thesis committee:

Prof. Dr. Jelle Bijma

Prof. Dr. Andrea Koschinsky-Fritsche

Dr. Ingo Horn

Date of Defense: 05.09.2014

School of Engineering and Science

Herewith, I confirmed that this thesis has been written independently and has not been submitted at another University for the conferral of a Degree.

Summary

This thesis has two focus points in the framework of boron in marine biogenic calcium carbonates and its potential as a proxy. Focus point one deals with potential factors, which might influence the boron isotopic composition and boron concentration in marine biogenic calcium carbonates. Since boron in marine biogenic calcium carbonates serves as a proxy for the reconstruction of the carbonate system, the awareness and characterization of potential impacts is of great importance. For that purpose investigations on 1) the effects of temperature and growth rate on the boron concentration and isotopic composition in calcium carbonate were investigated and 2) the potential carbonate system parameters controlling boron incorporation into shells of foraminifers have been determined.

The second focus point introduces a new analytical technique which for the first time allows to determine the boron isotopic composition and boron concentration simultaneously in marine biogenic calcium carbonates. This is a great opportunity for applications in the field of paleoceanography and paleoclimatology since the determination of the boron isotopic composition and boron concentration provides two parameters of the carbonate system which are at least required to reconstruct it.

Contents

Introduction		
1.1	Atmospheric CO ₂	7
1.2	The carbon cycle	9
1.2.1	The global carbon cycle	9
1.2.2	The marine carbon cycle	10
	<i>pH scales</i>	13
	<i>Effects of temperature</i>	14
1.2.3	The carbon pumps	14
1.3	Ocean acidification	15
1.4	Global/ocean warming and ocean deoxygenation	18
1.5	CO ₂ perturbations in the Earth's history and future analogues	19
1.6	Keys to the past	20
1.6.1	Climate archives	20
	<i>History of proxies</i>	20
	<i>Understanding proxies</i>	22
1.6.2	Foraminifers	22
1.6.3	The boron proxy	24
1.7	Outline thesis: Manuscripts with first authorship	26
1.7.1	Topic 1: Effect of Temperature and Growth Rate on the B/Ca and ¹¹ B/ ¹⁰ B Fractionation during Inorganic Calcite Formation	26
1.7.2	Topic 2: Simultaneous determination of δ ¹¹ B and B/Ca in marine biogenic carbonates at nano gram level	27
1.7.3	Topic 3: Boron incorporation in the foraminifer <i>Amphistegina lessonii</i> under decoupled carbonate chemistry	28
1.8	Manuscripts with co - authorship	28
1.8.1	Nano-scale distribution and coordination of boron in foraminifera	28
1.8.2	Decoupled carbonate chemistry controls on the incorporation of boron into <i>Orbulina Universa</i>	29
	References	30

Topic 1

Abstract	36
1 Introduction	37
2 Material and methods	39
2.1 Experimental set up	39
2.2 Precipitation experiments	40
2.3 Analysis of the solutions	41
2.4 Analysis of the B isotopic composition	43
2.5 Conversion of measured $\delta^{11}\text{B}$ into seawater scale	44
3 Results	45
3.1 Chemical composition of the solutions during precipitation	46
3.2 Boron isotopic composition and concentration of precipitated calcite	46
3.2.1 Boron concentration	46
3.2.2 Boron isotopic composition	47
4 Discussion	49
4.1 Boron versus borate	49
4.2 Surface entrapment model (SEMO)	50
4.3 Application of the SEMO	52
4.3.1 Constant growth rate various temperatures	53
4.3.2 Constant temperature various growth rates	53
4.4 Application of the SEMO to $\delta^{11}\text{B}$	55
4.4.1 Constant growth rate various temperatures	55
4.4.2 Constant temperature various growth rates	57
4.5 Decoupling the effect of temperature and growth rate	57
4.6 Implications on paleo proxies	59
5 Conclusion	60
Acknowledgments	61
References	62

Topic 2

Abstract	67
1 Introduction	67
1.1 Sample preparation	69
1.2 Amount of samples needed for analysis	69
1.3 Accuracy and precision	70
1.4 Matrix effects	71
2 Material and methods	71
2.1 Simultaneous determination of B isotopic composition and B concentration	72
2.2 Optical emission analysis	73
2.3 Pre-tests	74
2.4 Isotope analysis	74
2.5 Isotope analysis – acquisition parameters	75
2.6 Isotope analysis – background correction	77
2.7 Comments on errors	80
2.7.1 Isotope analysis	80
2.7.2 Boron concentration	81
2.8 Samples	82

2.8.1	Benthic foraminifers	82
2.8.2	Coral	83
3	Results and discussion	83
3.1	Pre-tests	83
3.2	SRMNIST 610 – accuracy, precision, and reproducibility	85
3.3	Samples	86
3.3.1	Foraminiferal samples	87
3.3.2	Coral sample	90
3.4	Sample consumption	91
3.5	Implications for paleo applications	93
4	Conclusion	94
	Acknowledgments	95
	References	96
	Appendix	99

Topic 3

	Abstract	102
1	Introduction	103
2	Material and Methods	105
2.1	Culturing and experimental set up	105
2.2	Preparation of culture media	106
2.3	Analysis of the culture media	107
2.4	Simultaneous determination of $\delta^{11}\text{B}$ and boron concentration of single tests	108
3	Results and discussion	109
3.1	Carbonate system	109
3.2	The boron isotopic signature of <i>A. lessoniis</i> ' tests	109
3.2.1	The variability in the $\delta^{11}\text{B}$ data	109
3.2.2	$\delta^{11}\text{B}$ of the test versus $\delta^{11}\text{B}$ of borate	112
	<i>The boron standards</i>	113
	<i>Vital effects</i>	114
	<i>The role of $\text{B}(\text{OH})_3$</i>	115
	<i>Boron enrichment of the culture media</i>	115
3.3	The B/Ca of <i>A. lessonii</i>	115
	<i>Further observations</i>	117
4	Conclusion	117
	Acknowledgments	119
	References	120
	Appendix	124

Synthesis & Outlook

	Topic 1	134
	Topic 2	137
	Topic 3	138
	References	141

Introduction

1.1 Atmospheric CO₂

In the last several decades no molecule has caused so much heated debate by researchers, politicians and media as carbon dioxide (CO₂). There are two reasons for this attraction. First, CO₂ is a greenhouse gas and second, its concentration in the atmosphere is increasing.

The greenhouse effect was discovered by Joseph Fourier in 1824 and had been described quantitatively by Svante Arrhenius in 1896: The incoming solar radiation mainly passes through the Earth's atmosphere without being absorbed. The Earth's surface absorbs approximately 50% of the solar radiation and therefore warms itself up. The other part is emitted back to the atmosphere at higher, infrared frequencies. The infrared radiation is absorbed by the gases in the atmosphere which in turn re-radiate much of the energy to the Earth's surface and lower atmosphere. This scenario known as the greenhouse effect causes an average Earth's surface temperature of 14°C. Without the greenhouse effect the average surface temperature would be -18°C. The main atmospheric contributors to the greenhouse effect are: water vapor (36-70%), CO₂ (9-26%), methane (4-9%), and ozone (3-7%). Although CO₂ is not ranking first, its contribution to the increase of the greenhouse effect became more pronounced due to human activities. The anthropogenic CO₂ increase in the atmosphere from approximately 280 to almost 400 ppm is caused by industrial and agricultural activities over the last 200 years. A systematic recording of the atmospheric CO₂ started in 1958 by Charles David Keeling. The history of CO₂ concentration in the atmosphere can be traced even further back in time using data from ice cores (Fig.1). Figure 2 shows the temperature increase for the last 130 years based on satellite data and direct surface measurements. The progressive increase of CO₂ caused by the consumption of fossil fuels, deforestation, agriculture, and cattle industry lead to an increased heat retention in the atmosphere. Consequences of the global warming are sea and glacier ice melts, increased sea level, thawing of permafrost soils, growing of aridity areas, and increasing weather extremes. Approximately 50% of the emitted CO₂ remains in the atmosphere. The other part is redistributed over the terrestrial, biological, and hydrological compartments.

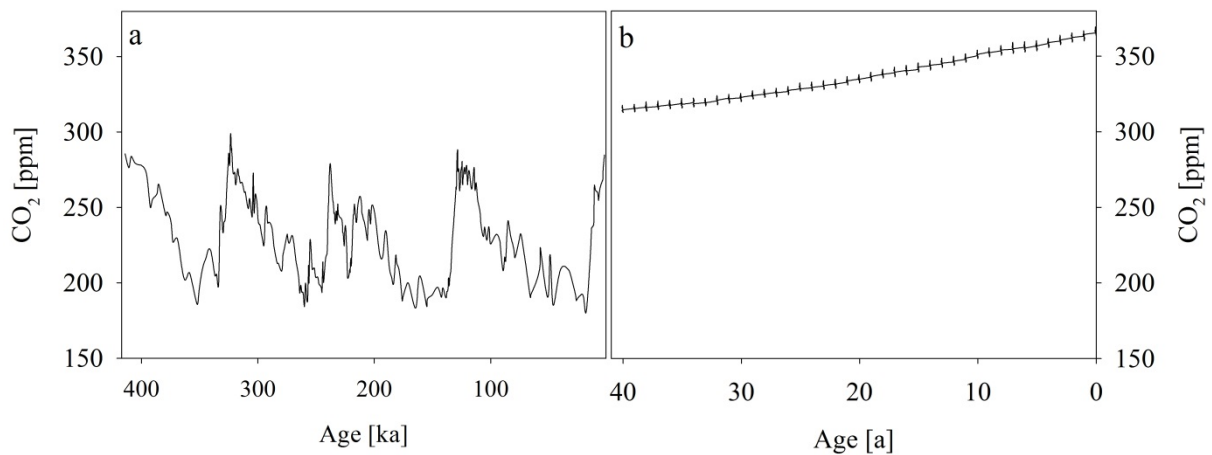


Figure 1: Atmospheric CO₂ concentration over the last 420 000 years. (a) CO₂ data obtained from the Vostok ice core (Petit et al., 1999) (b) data obtained from monthly measurements on Hawaii (Keeling & Whorf, 2000), 0 refers to the year 1998.

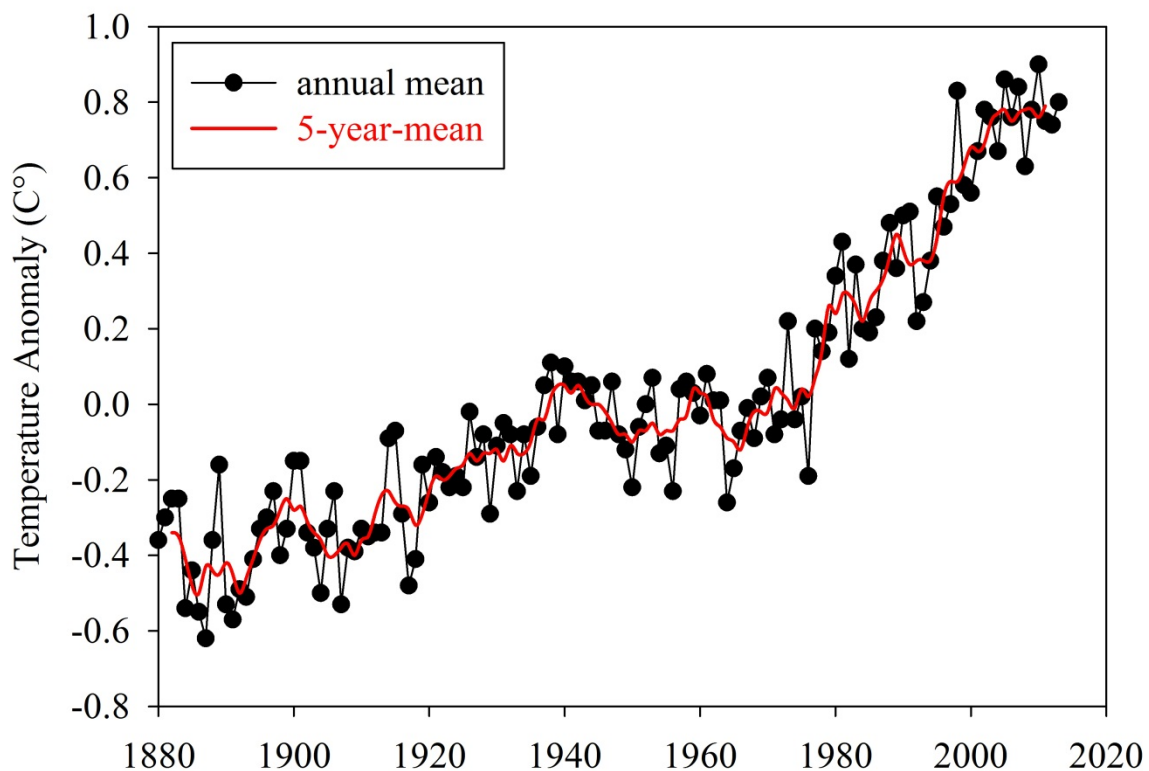


Figure 2: Surface annual temperature anomalies relative to 1951-1980 from surface air measurements at meteorological stations, and ship, and satellite surface sea temperature measurements. Data from (Hanson et al., 2006).

1.2. The Carbon Cycle

1.2.1. The Global Carbon Cycle

Carbon is cycled between four reservoirs: lithosphere, hydrosphere, atmosphere, and biosphere. Most of the carbon is stored in the lithosphere of which 80% is bound in limestone and calcium carbonate. The remaining 20% is stored as kerogen formed by the sedimentation and burial of terrestrial organisms under high heat and pressure. Carbon release to the atmosphere occurs in two ways which have very different time scales. It is removed from the lithosphere by exploitation of fossil fuels which enter the atmosphere by burning and during tectonic activity when CO_2 in carbonate rocks is released by volcanism above subduction zones and hotspots. While the tectonic driven release takes place over millions of years the removal of CO_2 from the atmosphere into the hydrosphere and terrestrial biosphere operates much faster. For example, terrestrial plants require CO_2 to build up bio mass. Plants directly consume CO_2 by photosynthesis and produce O_2 . After decay of plants and more complex organisms carbon is buried in the pedosphere. In the ocean the so called biological pump transforms the dissolved carbon to organic matter along different trophic steps. The significant decomposition, recycling, and repackaging of carbon take place in the mesopelagic zone (100-1000m). Mineralized carbon parts such as lids of coccolithophores and shells of organisms aggregate with organic matter increasing the carbon flux to the ocean floor. Approximately 30% of the carbon from the mixed layer reaches depths below 500 m. This process builds up ocean sediments with an average sedimentation rate of ca. 1cm/1000 years. However, the stability of carbon aggregates decreases with increasing depth leading to dissolution of those aggregates in the deep ocean. The average carbon content of ocean sediments after burial is less than 0.5% of the carbon fixed in the photic zone becoming part of the geological compartment. An overview of the global carbon cycling is given in Figure 3.

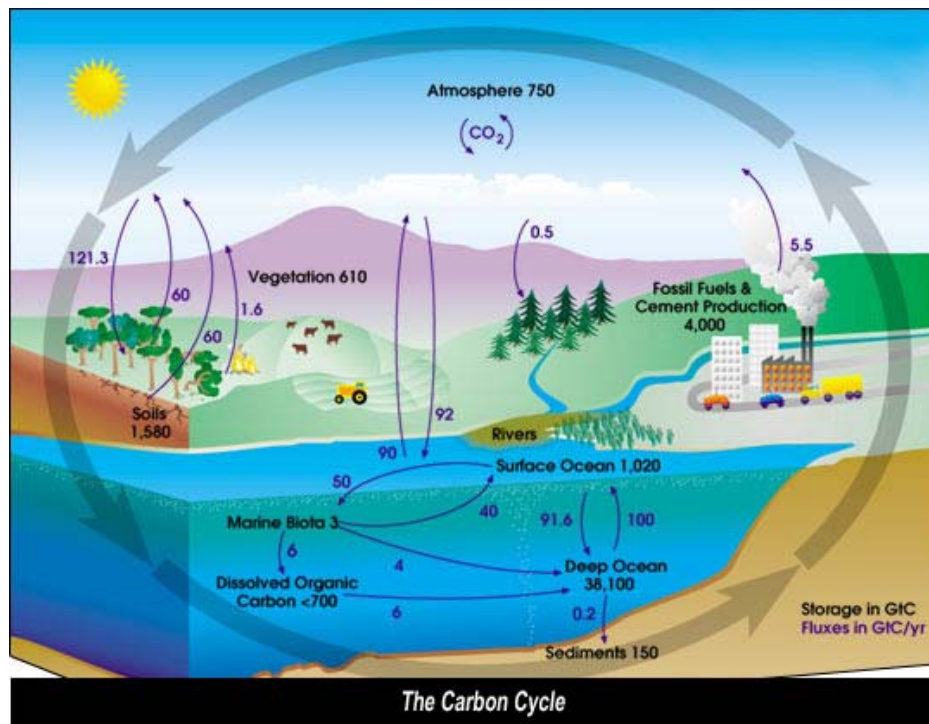
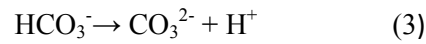
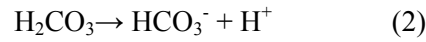


Figure 3: Illustration of the global carbon cycle showing the fluxes between the four carbon reservoirs: atmosphere, hydrosphere, biosphere, and lithosphere. Storage (black) in GtC, fluxes (purple) in GtC. Source: <http://www.global-greenhouse-warming.com/global-carbon-cycle.html>.

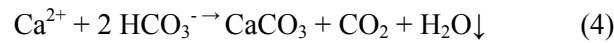
1.2.2. The Marine Carbon Cycle

About 27% of the anthropogenically emitted CO₂ dissolves in the oceans (Le Quéré et al., 2013). Similar to the scenario on land CO₂ is directly consumed by photosynthesis of phytoplankton being partly converted to organic matter. About half of the CO₂ is autotrophically respired. Some of the organic carbon sinks into the mesopelagic ocean as detritus which in turn is partly dissolved. When CO₂ dissolves in seawater it forms carbonic acid which in turn dissociates into bicarbonate and carbonate. These two compounds are essential components for marine calcifiers which secrete shells out of calcium carbonate. The chemical reactions describing the dissolution and dissociation of CO₂ in seawater are:





The formation of calcium carbonate (CaCO_3) by marine calcifiers like corals, molluscs, foraminifers, and coccolithophorides is described by the following equations:



and/ or



As can be seen from reactions 2 and 3 the dissolution of CO_2 in the oceans leads to the formation of hydrogen ions (H^+) whose negative logarithmic value of the concentration is known as pH:

$$\text{pH} = -\log[\text{H}^+] \quad (6)$$

Carbonic acid does not dissociate equally into bicarbonate (HCO_3^-) and carbonate (CO_3^{2-}). At pH 8.1 which equals the average value of the modern oceans the carbon species $[\text{HCO}_3^-]$, $[\text{CO}_3^{2-}]$, $[\text{CO}_2]$ ratio is 100:10:1. The sum of these three species is called dissolved inorganic carbon (DIC):

$$\text{DIC} = [\text{CO}_2] + [\text{HCO}_3^-] + [\text{CO}_3^{2-}] \quad (7)$$

Figure 4 shows the relationship between the carbon species and pH. This Figure is also known as the Bjerrum plot. The ratio between the carbon species determines the pH of the seawater. On the other hand changing the pH of the seawater for example by the addition of H^+ will shift the ratio of the carbon species. Another important parameter of the carbonate system is total alkalinity (TA). It is defined as: “the number of moles of hydrogen ion equivalent to the excess of proton acceptors in one kilogram of sample” (Dickson, 1981).

$$\begin{aligned} \text{TA} = & [\text{HCO}_3^-] + 2[\text{CO}_3^{2-}] + [\text{B}(\text{OH})_4^-] + [\text{OH}^-] + [\text{HPO}_4^{2-}] + 2[\text{PO}_4^{3-}] + [\text{H}_3\text{SiO}_4^-] + [\text{NH}_3] + \\ & [\text{HS}^-] - [\text{H}^+] - [\text{HSO}_4^-] - [\text{HF}] - [\text{H}_3\text{PO}_4] \quad (8) \end{aligned}$$

The sum of charges of the major cations is not fully balanced by the sum of the major anions (as presented in equation 8). Therefore TA can also be considered as a charge balance where the anions of the carbon species play a prominent role in compensating the imbalance:

$$\begin{aligned}
 TA &= \sum \text{conservative cations} - \sum \text{conservative anions} \\
 &= [\text{HCO}_3^-] + 2[\text{CO}_3^{2-}] + [\text{B}(\text{OH})_4^-] + [\text{OH}^-] + [\text{H}^+] \quad (9)
 \end{aligned}$$

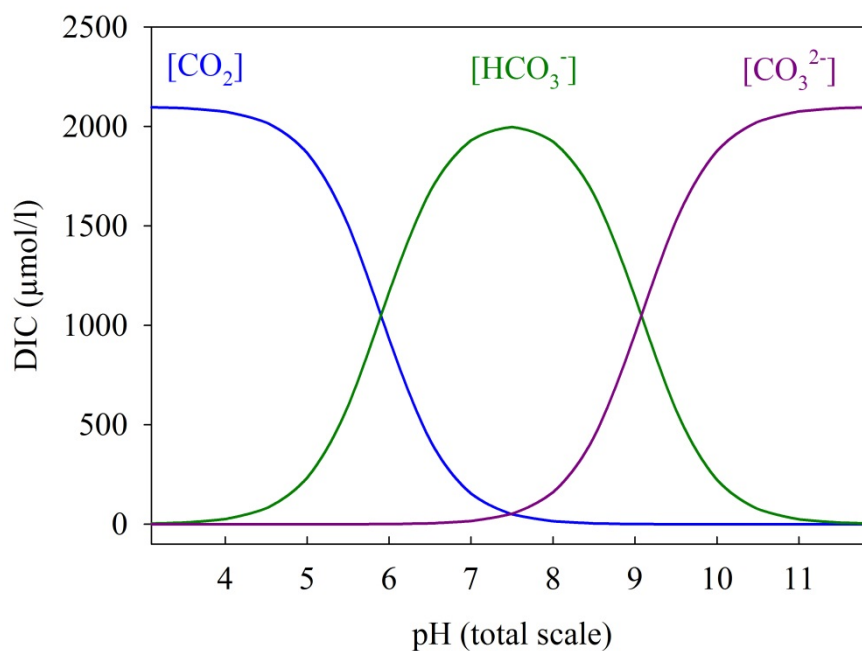


Figure 4: The Bjerrum plot showing the pH dependent distribution of CO_2 , HCO_3^- , and CO_3^{2-} in seawater at 20°C , $S = 32$; $P = 1\mu\text{atm}$, and $\text{DIC} = 2100 \mu\text{mol/l}$.

TA is a conservative parameter of the carbonate system which means that changes in temperature and pressure do not affect it. The addition (e.g. sea-ice melting) or the removal (evaporation, sea-ice formation) of fresh water to surface ocean waters changes TA. As a consequence TA changes with salinity. TA but also DIC are also influenced by biogeochemical processes. For instance, precipitation of CaCO_3 removes CO_3^{2-} from the seawater decreasing DIC by 1mol and TA by 2 mol for every mol CaCO_3 produced (Wolf-Gladrow et al., 2007). The production of organic matter by photosynthesis of algae consumes CO_2 and lowers DIC. At the same time the uptake of NO_3^- by algae accompanied by

the uptake of H^+ maintains electroneutrality which in turn increases TA.

The sum of the relationships between the above introduced parameters (pH, DIC, TA, CO_2 , HCO_3^- , CO_3^{2-}) is known as the marine carbonate system. While four of these parameters can be measured (pH, DIC, TA, CO_2) the rest can be calculated. At least two of its parameters should be known in order to determine the whole carbonate system.

pH scales

Four different pH scales exist. As already pointed out, pH is the negative logarithm of the hydrogen ion concentration. In theory, activity instead of concentration should be used. Unfortunately, measurements of the hydrogen ion activity are impossible. The NBS pH scale was introduced as an alternative definition by the International Union of Pure and Applied Chemistry (IUPAC). The pH NBS scale is based on a series of standard buffer solutions with assigned pH values whose negative hydrogen ion concentration is similar to their activities. This implies that the ionic strength of the buffer solutions is much lower (0.1) than for seawater (0.7). The difference in ionic strength causes significant changes in pH when seawater is measured by NBS calibrated pH electrodes. Hence, buffers with an ionic strength close to that of seawater are required. pH scales based on an artificial seawater matrix are the free scale (pH_F), the total scale (pH_T), and the seawater scale (pH_{SWS}) (Zeebe & Wolf-Gladrow, 2001):

$$pH_{F=} = -\log[H^+]_F \quad (10)$$

$$pH_T = -\log([H^+]_F + [HSO_4^{2-}]) \quad (11)$$

$$pH_{SWS} = -\log([H^+]_F + [HSO_4^{2-}] + [HF]) \quad (12)$$

The difference between those scales is the chemical composition of the buffer solution on which the scale is based. Values can be converted into another scale using the relationship:

$$pH_F = pH_T + \log(1 + S_T/K_S^*) \quad (13)$$

$$pH_F = pH_{SWS} + \log\left(1 + \frac{S_T}{K_S^*} + \frac{F_T}{K_F^*}\right) \quad (14)$$

Where K_s^* is $([H^+][SO_4^{2-}])/[HSO_4^-]$ and K_F^* is $([H^+][F^-])/[HF]$.

The conversion from NBS scale to total scale can be performed by measuring a Tris/Tris-HCl seawater buffer prepared in accordance with the recipe described in (Dickson et al., 2007).

Effects of temperature

Changes in temperature affect the dissociation between the carbon species. At thermodynamic equilibrium the rates of the forward and backward reactions are equal. A change in temperature changes the rate of the forward and backward reaction differently. The direction in which a reaction will proceed during a temperature change depends on the ratio between the activation energies of the forward and backward reactions. The activation energy of an endothermic reaction is higher for the forward reaction than for the backward reaction which means that the rate for the forward reaction is more sensitive to a temperature change. Therefore, the rate of the forward reaction increases faster with increasing temperature than for the backward reaction. Considering the transformations of CO_2 into HCO_3^- , and HCO_3^- into CO_3^{2-} (which are endothermic reactions) an increase in temperature of the seawater results in a faster transformation of CO_2 into HCO_3^- , and HCO_3^- into CO_3^{2-} . Consequently, warmer seawater contains more CO_3^{2-} ions. A cooling favours the backward reactions to proceed. Endothermic reactions proceed faster in warm environments whereas exothermic reactions in cold environments. Since the dissolution of CO_2 in seawater is an exothermic reaction its solubility increases with decreasing water temperature.

1.2.3. The Carbon Pumps

Dissolved CO_2 is transported from the ocean's surface to its interior. Two processes are responsible for this carbon flux:

The physical carbon pump is based on the difference in CO_2 solubility between warm and cold waters and the fact that the formation of cold and dense water in high latitudes transports it to the deep ocean. On the other hand, upwelling of CO_2 rich, cold, deep water leads to warming and the release of CO_2 .

The biological carbon pump is driven by biological CO_2 fixation into organic matter in the euphotic zone, its subsequent sinking, remineralisation, and dissolution in the deep sea. The biological pump

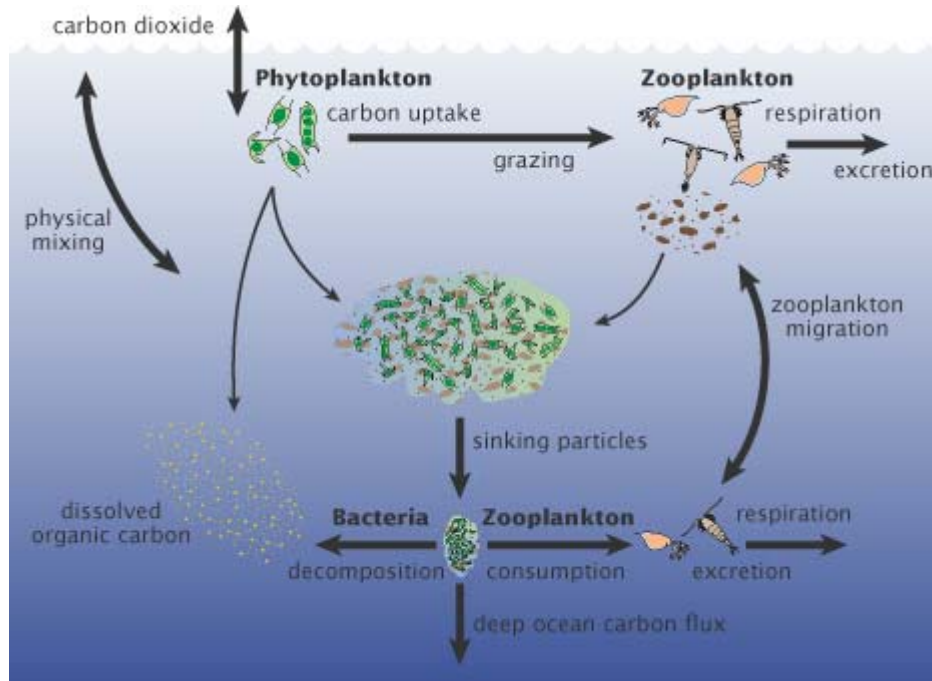


Figure 5: The biological carbon pump.

Source: <http://earthobservatory.nasa.gov/Features/Phytoplankton/page2.php>

(Fig. 5) can be divided into two parts: the soft tissue pump which describes the CO_2 fixation by photosynthesis performed by phytoplankton and the carbonate pump which represents the removal of carbon by formation of CaCO_3 secreted by calcifiers. The ratio describing the export of carbon by these two pumps is called the rain ratio (r) and determines the net flux of CO_2 between the surface ocean and the atmosphere.

$$r = \frac{\text{rate of } \text{CaCO}_3 \text{ export}}{\text{rate of tissue export}} \quad (15)$$

The modern ocean exhibits a rain ratio range between 0.05 and 0.25 (Sarmiento et al., 2002).

1.3. Ocean Acidification

The dissolution of atmospheric CO_2 leads to the formation of $[\text{H}^+]$ and leads to a decrease in pH, a process known as ocean acidification (OA). A decrease in pH drives reactions 2 and 3 backwards. As a consequence, the concentrations of CO_3^{2-} decrease, and the concentration of HCO_3^- increases. A

progressive dissolution of CO₂ will make CaCO₃ formation more difficult if the calcifiers depend on CO₃²⁻ as building blocks. The stability of calcium carbonate is expressed by the saturation state (Ω):

$$\Omega = \frac{[Ca^{2+}] \times [CO_3^{2-}]}{K_{sp}} \quad (16)$$

Where K_{sp} is the solubility product defined as:

$$K_{sp} = [Ca^{2+}]_{sat} \times [CO_3^{2-}]_{sat} \quad (17)$$

Where the subscript “sat” refers to equilibrium concentrations of Ca²⁺ and CO₃²⁻ in water. At Ω equal 1 the reaction is in chemical equilibrium which means that the speed of the forward and backward reaction with respect to equations 4 and 5 is equal. If Ω is > 1, the concentrations of Ca²⁺ and CO₃²⁻ are higher than at equilibrium and therefore, the system compensates this imbalance by CaCO₃ precipitation. If Ω is < 1, the concentrations of Ca²⁺ and CO₃²⁻ are lower than at equilibrium condition. Establishing chemical equilibrium is achieved by dissolution of CaCO₃. Since the Ca concentration in the ocean is nearly constant Ω is mainly controlled by the CO₃²⁻ concentration. The solubility of CaCO₃ increases with decreasing temperature and increasing pressure. As a consequence deep sea water is under saturated with respect to CaCO₃ and sediments of the deep sea are CaCO₃ free. Calcium carbonate has two polymorphs found in the skeletons/shells of marine calcifiers: calcite and aragonite. The depth at which $\Omega = 1$ is called lysocline and is polymorph specific. For calcite the lysocline is found in greater depth than for aragonite. Differences in the seawater’s composition shift the position of the lysocline for both polymorphs. The deep water of the Pacific is more corrosive to CaCO₃ because 1) its CO₃²⁻ concentration is lower than that of the Atlantic and 2) the CO₂ concentration of the deep water formed in the North Atlantic flowing towards the Pacific increases steadily due the dissolution of sinking aggregates containing carbon. Therefore, the lysocline in the Pacific is found at smaller depths. The depth at which no CaCO₃ exists is called calcium carbonate compensation depth (CCD). Surface sea water is 4 to 6 times supersaturated (Millero, 2007) with respect to CaCO₃, but spontaneous inorganic precipitation does not take place due to inhibiting effects of magnesium and phosphate (Morse et al., 2007).

During the last 650 000 years the atmospheric CO₂ concentration varied between 180 and 300 μatm (Petit et al., 1999; Siegenthaler et al., 2005). Since the beginning of the industrial revolution the atmospheric CO₂ concentration has steadily increased by approximately 100 ppm reaching a current value of approximately 390 μatm. This change is associated by a pH decrease of 0.1 units (Gruber, 2011). Although this decrease appears to be small, it should be noted that the pH scale is logarithmic. A pH drop of 0.1 unit corresponds to an [H⁺] increase of 30% which equates a CO₃²⁻ concentration decrease of 17%. Currently, the buffer capacity of HCO₃⁻ and CO₃²⁻ slow down the AO process, but progressive anthropogenic CO₂ emissions gradually lead to faster consumption of this buffer and hence to a faster pH decrease. The ocean's buffer capacity depends on the relatively slow weathering of rocks, a process which supplies the ocean with ions contributing to the ocean's alkalinity. An enhanced dissolution of atmospheric CO₂ (as currently occurring) overwhelms the ability of the ocean and sediments to regulate Ω leading to a coupled decline of pH and Ω (Ridgwell & Schmidt, 2010).

Predictions on future CO₂ concentration in the atmosphere based on different scenarios and models reveal an increase between 300 and 800 μatm by the end of this century (Meehl et al., 2007). In the latter scenario pH will be decreased by 0.3 units corresponding to a decrease in CO₃²⁻ concentration by 44% when comparing to the modern surface ocean. These changes will have consequences not only for marine calcifiers but possibly for the marine ecosystem as a whole (Bijma et al., 2013). Due to the decrease in CO₃²⁻ concentration the saturation state of CaCO₃ will be reduced in the surface water and formation of CaCO₃ by marine calcifiers will decrease. The magnitude of the effects caused by OA may vary among taxa. A recent study synthesizes the results of 228 studies investigating biological responses to OA: While effects on fish growth are not reported, growth increases by 22% among fleshy algae, and by 18% among diatoms. All calcified taxa show a similar magnitude in mean growth reduction (9-17%) (Kroeker et al., 2013).

1.4. Global/ocean warming and deoxygenation

Approximately 80% of the heat produced by the anthropogenic enhancement of the greenhouse effect is taken up by the oceans (Levitus et al., 2005) leading to a temperature increase of the surface ocean of approximately 0.7 °C over the last 100 years (Trenberth & Fasullo, 2009). Due to the large volume of the ocean its warming is 0.04°C for the same time span. As a consequence of global warming the arctic and antarctic regions are more affected than the lower latitudes. Melting of sea-ice decreases the sea ice-albedo feedback causing a stronger warming of the surface water in the northern hemisphere. Reduced formation of cold and dense deep water is slowing down the thermohaline circulation and the transport of dissolved CO₂ into the deep ocean.

Ocean warming leads also to an oxygen depletion since the solubility of oxygen decreases with increasing temperature. An excess of atmospheric O₂ has been recently reported (Manning & Keeling, 2006) and attributed to the O₂ outgassing from the surface ocean due to increasing temperatures. While the surface ocean absorbs more heat, warming of its interior proceeds much slower. Sinking of heavier water masses is subject to density gradients. Due to ocean warming deep water formation in the northern hemisphere is hampered leading to a stronger oxygen stratification in the ocean preventing ventilation of deep water.

Marine life is affected by changes in temperature and deoxygenation. Stronger stratification will decrease mixing of nutrient rich deep water with the upper ocean affecting the ocean's productivity negatively. A reduction in the oxygen concentration will mostly affect active organisms that have a high oxygen demand. Many crustacea and fishes cannot tolerate oxygen concentrations below 60 μmol/kg, and concentrations below 20 μmol/kg are lethal to all higher organisms (Jin & Gruber, 2003).

The three ocean stressors (AO, ocean warming, deoxygenation) operate simultaneously and in part synergistically. Their combination affects seriously the marine ecosystem, the carbonate systems, and the interactions between those. Releasing high amounts of carbon not only leads to a fast consumption of the ocean's alkalinity, but it exposes organisms to a fast changing environment, which demands fast adaptation for survival. The rate of carbon perturbation is the most critical factor not only today but

also during previous periods in earth history (Bijma et al., 2013).

1.5. CO₂ perturbations in the Earth's history and future analogues

Major as well as minor mass extinctions can be identified in Earth history. Most, if not all, are linked to dramatic changes in global carbon cycle affecting the atmospheric CO₂ inventory leading to global and ocean warming, anoxia, and OA (Hönisch et al., 2012; Bijma et al., 2013). Since all three ocean stressors are currently observed, the question arises whether a future mass extinction is imminent or is already ongoing (Barnosky et al., 2011). Investigations of past mass extinctions such as the one during the Paleocene-Eocene Thermal Maximum (PETM) allow to provide a look into our future. The PETM refers to a geologically short (~ 170 000) climate event of extreme warmth, which began abruptly 56 Ma ago. The PETM is a focal point in the field of paleoceanography and paleoclimatology as it probably provides the best past analogue of our future helping to understand the consequences of global warming and ocean acidification including changes in the marine ecosystem. For the PETM an increase in the global surface ocean temperature of 8°C in equatorial and of 5°C in mid and high latitude was reported (Weijers et al., 2007). This temperature increase is attributed to a large release of ¹³C depleted carbon into the reservoirs at the Earth's surface which is reflected in a large decrease of the ¹³C/¹²C ratio in terrestrial and marine carbonates (Kennett & Stott, 1991; Koch et al., 1992). Massive dissociation of oceanic methane hydrate has been suggested as a possible source of the carbon (Dickens et al., 1997). Changes in the ocean carbonate chemistry were a decrease in pH and in the calcium carbonate saturation state the latter leading to a shoaling of the CCD by ca. 2 km (Zachos et al., 2005). The biological diversity of deep-sea benthic foraminifers decreased worldwide by 30-50% in a few thousand years most probably due to the rise of the lysocline whereas their planktonic relatives and dinoflagellates diversified (Thomas & Shackleton, 1996).

1.6. Keys to the past

1.6.1. Climate Archives

Information about the Earth's climate history is stored in climate archives that allow climate researchers to reconstruct past climate conditions. A variety of climate archives exist, these include for example tree rings, stalagmites, and lake sediments for terrestrial records. The CO₂ and O₂ content of gas bubbles in ice cores are excellent recorders of the atmospheric CO₂ and the air temperature. Ocean sediment cores contain small shells of marine organisms whose elemental and isotope composition hold information about past chemistry conditions of the ocean serving as archive for the oceanic record. The elemental and isotope signatures of these shells can be used to reconstruct chemical condition during the shell formation and are called proxies, also nicely described by:

“Those parameters that have a close relationship to environmental parameters are called “proxy variables” (“proxies” for short). Proxies are measurable descriptors for desired (but unobservable) variables.” (Wefer et al., 1999).

Using climate archives and proxies allows to obtain knowledge of the interactions between past climate changes and the marine ecosystem during that time. Understanding the responses of past ocean chemistry and marine ecosystem due to environmental changes like OA, warming and deoxygenation caused by global warming is a primary task in paleoceanography since it allows to project the consequences of progressive CO₂ release on ocean chemistry including its ecosystem. The awareness of dramatic environmental changes in the past due to carbon perturbations should make the human society realize that the decrease of anthropogenic CO₂ emissions is urgent.

History of proxies

The first proxy was introduced by Urey (1947) who calculated on a theoretical basis that oxygen (and carbon) isotope fractionation in inorganic (but by extension also biogenic) carbonates are temperature dependent (Urey, 1947). He wrote:

“A change from 0°C to 25°C should change the ¹⁸O content of carbonate by 1.004 relative to liquid water and the ¹³C content by 1.003. Accurate determinations of the ¹⁸O content of carbonate rocks could be used to determine the temperature at which they were formed.”

Only a few years later the temperature dependence was experimentally confirmed by McCrea (1950) and described as a quadratic function:

$$T(^{\circ}\text{C}) = 16.0 - 5.17 \times (\delta_c - \delta_w) + 0.092 \times (\delta_c - \delta_w)^2 \quad (18)$$

Where $\delta_c = \delta^{18}\text{O}$ of CO_2 released from the calcite after reaction with H_3PO_4 , and $\delta_w = \delta^{18}\text{O}$ of CO_2 equilibrated with the water at 25°C. This was the first, so called, paleotemperature equation.

The first application on biogenic carbonates was performed by Epstein et al. (1953). He demonstrated that marine molluscs almost exactly followed McCrea’s paleo temperature equation. In his seminal paper on “Pleistocene temperatures” Emiliani (1955) was the first to apply the (mollusc!) paleotemperature equation to planktonic foraminifers from sediment cores. From this he concluded that the Pleistocene was characterized by periodic temperature oscillations of about 6°C due to glacial/interglacial cycles. The first paleotemperature equation on planktonic foraminifera developed under controlled laboratory condition was produced by Erez & Luz (1983).

Shackleton (1974) attributed part of the change in the foraminiferal $\delta^{18}\text{O}$ to a change in the isotopic value of seawater due to the waxing and waning of the continental ice sheets. Fairbanks (1989) used U/Th dating of “drowned” surface water inhabiting corals to produce the first deglacial sea level curve. By tying $\delta^{18}\text{O}$ of benthic foraminifers to the sea level curve and assuming that the deep ocean temperature remained more or less constant over glacial/interglacial cycles, Labeyrie (1987) could reconstruct seawater $\delta^{18}\text{O}$ evolution during the deglaciation. These changes in the seawater isotopic composition (and salinity) were confirmed by pore water analyses and modelling (Schrag et al., 1996). Spero et al. (1997) found that the oxygen isotope composition in foraminifers also depends on the carbonate ion concentration in seawater. Using laboratory cultures (Bijma et al., 1998) and modelling approaches (Wolf-Gladrow et al., 1999; Zeebe et al., 1999) our understanding of the factors controlling the oxygen isotopic composition of biogenic calcites and aragonites have grown over the

year and may be considered as one of the most robust proxies (Bemis et al., 1998). Since the pioneering days of Urey (1947), the paleoceanographers proxy toolbox has exponentially increased and include next to geochemical proxies also organic compounds (“biomarkers”) and statistical methods based on assemblage distributions (Wefer et al., 1999).

Understanding proxies

Before applying proxies to fossil records, a good understanding of proxy incorporation is required. Ideally, a proxy records only one variable but this is hardly ever the case. Culture experiments with foraminifers allow to vary a parameter under investigation while keeping other parameters constant. This approach allows e.g. to decouple the carbonate chemistry and has become an established tool to assess the impact of environmental chemistry changes on marine calcifiers. Culture work under controlled laboratory conditions allows to calibrate proxies giving the opportunity for correct interpretations of fossil records and predictions of organism’s behavior to an acidifying ocean. Proxy calibrations have been made for planktonic e.g. (Lea et al., 1995; Spero et al., 1997; Bijma et al., 1998; Russell et al., 2004) and benthic foraminifers (e.g. Toyofuku et al., 2000; Dueñas-Bohórquez et al., 2011; Hintz et al., 2006). An important task of calibration work is to assess the impact of biologically driven and species specific effects, the so called vital effects, on element incorporation and isotope fractionation in biogenic calcium carbonate. This can be realized by comparison to inorganic calcium carbonate precipitation experiments. This approach creates an inorganic baseline allowing the classification of species specific deviations from the inorganic system on which proxy work is often based.

1.6.2. Foraminifers

Ocean sediments are the most resourceful archive for paleoceanographers since they contain remains of fossil organisms. The most widely used are tests (shells) of fossil foraminifers. Foraminifers are a phylum of amoeboid protists that have been present in the world’s oceans since the Cambrian (Culver, 1991). Within the Protozoa they belong to the major group of Rhizaria. Most are marine and live on or within the seafloor sediment (benthic foraminifers) whereas a small number of species live as floaters

in the water column at various depths (planktonic foraminifers) (Fig. 6). The foraminiferal cell consists of a granular endoplasm and a transparent ectoplasm that can branch out forming a pseudopodial network used for locomotion, anchoring, and capturing food. A number of species bears algae as symbionts. The symbiosis is characterised by the foraminiferal host supplying CO_2 (from respiration and calcification), which is used for symbiont photosynthesis. The symbionts provide O_2 and raise pH which increase $[\text{CO}_3^{2-}]$ the building blocks for calcifiers. Calcification refers to the process in which a test/shell is secreted by the foraminifer mainly made out of CaCO_3 . These tests are made up of one or several chambers usually less than 1 mm in diameter, but some are larger. Minor foraminifers are naked. The tests of foraminifers are preserved in sediments and make ideal proxy records in paleoceanography. The incorporation of minor/trace elements and isotopic fractionation in the test are used to reconstruct changes in the chemical micro environment of a foraminifer.



Figure 6: Planktonic foraminifer *Globigerinoides ruber* (left) with symbionts located on the pseudopodial network, source: <http://blogs.denison.edu/geosciences/2011/10/02/geosbiol-308-the-paleocene-eocene-thermal-maximum-paleoclimate-change-documented-in-foraminifera-fossils/foraminefera/>.

Benthic foraminifer *Heterostegina depressa* (right), source:
<http://pedagogie.ac-toulouse.fr/svt/serveur/geoltheque/pages/ornac/interp1.htm>

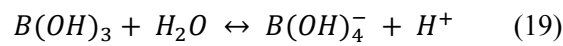
Concentrations of magnesium (Nürnberg et al., 1996), lithium (Misra & Froelich., 2012), and uranium (Russell et al., 2004) correlate to changes in the water temperature, continental weathering, and the carbonate system respectively, while isotope signatures of oxygen, carbon, and boron provide insight

into changes in temperature, biological activity, and pH, respectively.

1.6.3. The boron proxy

Boron (B) has attracted much interest of paleoceanographers because its incorporation into the foraminifers' tests hold information about the carbonate system. The fundamental concept behind the B proxy is that only a particular B species is incorporated into the shells whose concentration and isotopic composition is pH dependant.

Dissolved B has two major species: boric acid $B(OH)_3$ and borate $B(OH)_4^-$ whose dissociation is given by the reaction:



As can be seen from reaction 19, the concentration of these species is a function of pH. At low pH (~6) B is mostly present as $B(OH)_3$ whereas at high pH (~10) $B(OH)_4^-$ is the dominant species in seawater. The boric acid – borate equilibrium is established within 95 μ s in seawater at temperature $T = 25^\circ\text{C}$ and salinity $S = 35$ (Zeebe et al., 2001). The average B concentration in seawater is 416 $\mu\text{mol/kg}$ (Lemarchand et al., 2000). Boron has two stable isotopes: ^{10}B and ^{11}B whose abundances are 19.82% and 80.18% (IUPAC, 1998). Since $B(OH)_3$ is enriched in ^{11}B compared to $B(OH)_4^-$, the boron isotopic composition of both species changes with pH. Isotopic equilibration takes 125 μ s (Zeebe et al., 2001). At any pH the B isotopic composition of modern seawater is ~39.5‰. At low pH (when all B is present as $B(OH)_3$) the B isotopic composition of $B(OH)_3$ equals the value of seawater. The same is true at a high pH when all B is present as $B(OH)_4^-$. Changing the pH from low to high transforms the heavy $B(OH)_3$ into a heavier $B(OH)_4^-$ with a constant offset of ~27‰ (Klochko et al., 2006). Figure 7 summarizes the behaviour of B in seawater with changing pH. The reconstruction of pH using B isotopes can be calculated using Zeebe & Wolf-Gladrow (2001):

$$pH = pK_B - \log \left(- \frac{\delta^{11}B_T - \delta^{11}B_{CaCO_3}}{\delta^{11}B_T - \alpha_B \times \delta^{11}B_{CaCO_3} - \epsilon_B} \right) \quad (20)$$

Where pK_B is the dissociation constant between boric acid and borate, $\delta^{11}B_T$ is the B isotopic composition of modern seawater, α_B is the B isotope fractionation factor between boric acid and

borate, and ϵ_B is $(\alpha-1) \times 1000$.

Although the exact mechanisms of B incorporation into the calcite lattice are still unknown, first measurements of the B isotopic composition of biogenic carbonates show the signature of borate suggesting that the charged borate is the only species being incorporated into carbonates (Hemming & Hanson, 1992). Based on this assumption the boron isotopic composition of foraminifers has been applied to reconstruct paleo pH (Palmer et al., 1998; Pearson & Palmer 2000; Sanyal & Bijma, 1999; Hönisch et al., 2005; Yu et al., 2010).

Based on Figure 7a we expect the boron concentration in biogenic carbonates to increase with increasing pH. Indeed, Allen et al. (2011) report a positive correlation between the foraminiferal B/Ca

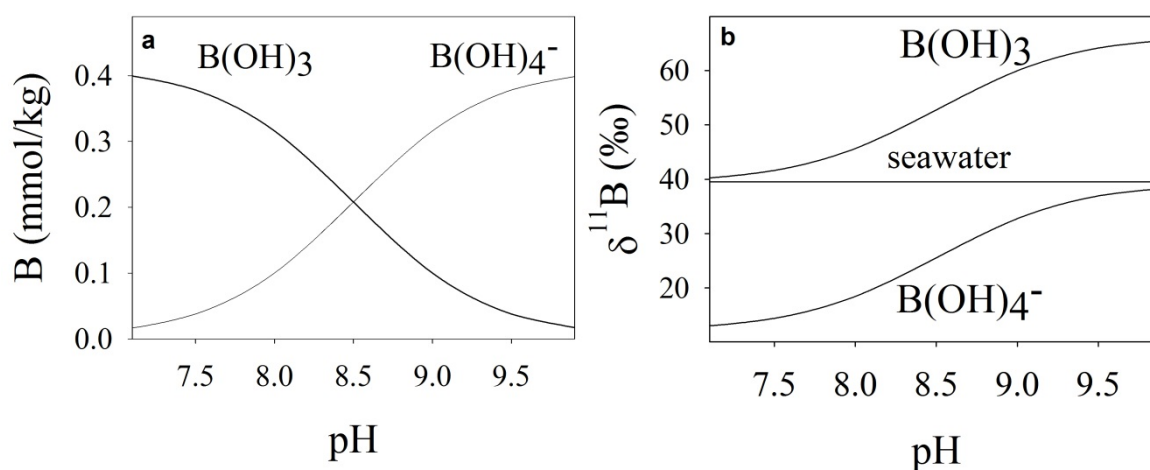
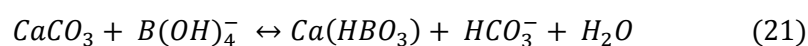


Figure 7: Boron species distribution (a) and isotope fractionation (b) in seawater as a function of pH at 20°C, $S = 32$, and $P = 1 \mu\text{atm}$ and pH.

and pH. Hemming & Hanson (1992) suggested the following mechanism for B substitution at the CO_3^{2-} site:



The distribution coefficient, K_D , for B substitution is expressed as:

$$K_D = \frac{[HBO_3^{2-} / CO_3^{2-}]_{solid}}{[B(OH)_4^- / HCO_3^-]_{fluid}} \quad (22)$$

Since the concentrations of HBO_3^{2-} and CO_3^{2-} cannot be measured, Yu & Elderfield (2007) simplified the relationship by replacing these species by B and Ca since their molar ratios are unity in $CaCO_3$:

$$K_D = \frac{[B/Ca]_{solid}}{[B(OH)_4^- / HCO_3^-]_{fluid}} \quad (23)$$

The observed linear correlation between B/Ca and $\Delta[CO_3^{2-}]$ (saturation state of CO_3^{2-}) by Yu & Elderfield (2007) seem to suggest that the boron concentration is driven by the $[CO_3^{2-}]$. However, $[CO_3^{2-}]$ and pH co-vary in natural seawater and one could argue that, in fact, the observed relationship is driven by pH. Finally, this co-variation does not allow to determine the controlling parameter of foraminiferal B/Ca. On the contrary, the concentration of $B(OH)_4^-$ increases with increasing pH whereas the HCO_3^- concentration decreases. As K_D is constant, and the denominator in equation 23 increases with increasing pH so must the numerator, which is the B/Ca ratio in the test. Hence, the boron concentration in foraminiferal tests could also be explained as a function of the ratio of borate to bicarbonate in seawater. By decoupling the carbonate chemistry in controlled laboratory experiments Allen et al., (2012) suggest that B/Ca is most probably dependant on $B(OH)_4^- / HCO_3^-$.

1.7 Outline thesis

Manuscripts with first authorship

1.7.1 Topic 1

Karina Kaczmarek, Gernot Nehrke, Sambuddha Misra, Jelle Bijma (under review)

Effects of Temperature and Growth Rate on the B/Ca and $^{11}B/^{10}B$ Fractionation during Inorganic Calcite Formation. Chemical Geology.

The incorporation of boron into biogenic calcium carbonates for example foraminifers shows a temperature dependence being also species specific. A temperature effect on the B isotopic

composition of foraminiferal test has yet not been studied but in theory such an effect is very likely. The investigation of potential temperature impacts on B incorporation in foraminifers is hindered by processes influencing the B incorporation which are 1) directly correlated with a change in temperature (for example growth rate) and 2) **not** directly correlated with a change in temperature (for example nutrient supply). In order to investigate temperature and growth rate effects adequately manipulation of the medium must guarantee growth of calcium carbonate at one temperature and different growth rates, one growth rate and different temperatures and without biology driven effects. The aim of this investigation is to create an inorganic baseline for possible effects of temperature and growth rate on the B/Ca and $^{11}\text{B}/^{10}\text{B}$ fractionation in inorganically precipitated calcite.

1.7.2 Topic 2

Karina Kaczmarek, Ingo Horn, Gernot Nehrke, Jelle Bijma (under review)

Simultaneous determination of $\delta^{11}\text{B}$ and B/Ca in marine biogenic carbonates at nano gram level.

Chemical Geology

So far the opportunity of simultaneous determination of $\delta^{11}\text{B}$ and B/Ca was not taken. Studies focused on the reconstruction of the carbonate system using the boron proxies rely on sufficient sample material in order to analyze the B concentration and B isotopes separately. The aim of this investigation is to introduce a new *in situ* technique which allows the determination of the B isotopic composition and B/Ca simultaneously at the nanogram level on single tests of foraminifers. Compared to bulk analytical methods the new technique offers a several fold reduction in the number of tests required for the analysis and in the time for sample preparation. The simultaneous determination of the B isotopic composition and B/Ca ratios provides two parameters of the carbonate system which are at least necessary to reconstruct it at one time.

1.7.3 Topic 3

Karina Kaczmarek, Gerald Langer, Gernot Nehrke, Ingo Horn, Sambuddha Misra, Max Janse, Jelle Bijma (submitted)

Boron incorporation in the foraminifer *Amphistegina lessonii* under decoupled carbonate chemistry. Earth and Planetary Science Letters

Because of the co-variation of pH and $[\text{CO}_3^{2-}]$ and the inverse correlation between these two parameters and $[\text{HCO}_3^-]$ in seawater it is not clear which carbonate system parameter influences the B incorporation in biogenic calcium carbonates. The aim of this investigation is to identify this parameter based on a decoupled pH- $[\text{CO}_3^{2-}]$ chemistry. For that purpose foraminifers were cultured. The B analysis was performed using the new developed technique mentioned in 1.7.2.

1.8 Manuscripts with a co-authorship

1.8.1 Oscar Branson, Karina Kaczmarek, Simon Redfern, Sambuddha Misra, Gerald Langer, Tolek Tyliczszak, Jelle Bijma, Henry Elderfield (submitted)

Nano-scale distribution and coordination of boron in foraminifera. Nature Geoscience

Assuming not the solely incorporation of the tetrahedral pyramidal $\text{B}(\text{OH})_4^-$ into the tests of foraminifers but also the isotopically heavier, trigonal planar $\text{B}(\text{OH})_3$ the boron isotopic composition would result in a heavier composition than that of $\text{B}(\text{OH})_4^-$. Indeed, a heavier $\delta^{11}\text{B}$ has been observed in biogenic carbonates. In order to shed light whether a $\text{B}(\text{OH})_3$ incorporation occurs, several studies used magic angle spinning (MAS) nuclear magnetic resonance (NMR) to determine the B coordination in biogenic carbonates. So far studies report different results in B coordination showing 1) a trigonal coordination of B in synthetic and biogenic calcite (Mg-rich alga) (Sen et al., 1994), 2) a trigonal and tetrahedral coordination in almost equal abundances in calcite (foraminifers) (Klochko et al., 2009), 3) a trigonal and tetrahedral coordination but in different proportions in aragonite (coral) depending on the coral microstructure (Rollion-Bard et al., 2011). In this study it was demonstrated

that B is solely hosted in a trigonal coordination in the calcite shell of the benthic foraminifera *Amphistegina lessonii*. It has been suggested that in calcite B undergoes a coordination changes from tetrahedral to trigonal during incorporation (Hemming et al., 1995) suggesting that the atomic structure of the calcium carbonate polymorphs dictates the coordination of B in the mineral. Furthermore, a banding of B concentration to the direction of growth was observed.

1.8.2 Ella Howes, Markus Raitzsch, Antje Mewes, Karina Kaczmarek, Nienke Bijma, Ingo Horn, Sambuddha Misra, Jean-Pierre Cattuso, Jelle Bijma (in preparation)

Decoupled carbonate chemistry controls on the incorporation of boron into *Orbulina universa*

In this study we address the question which carbonate parameter impacts the boron incorporation in the planktonic foraminifers *O. universa*. The boron analysis of the cultured foraminifers was performed by the new *in situ* technique introduced in chapter 1.7.2. Preliminary results show that the B/Ca ratio in the foraminifers is clearly dependant on the $\text{B(OH)}_4^-/\text{HCO}_3^-$ ratio in the culture media and that $\delta^{11}\text{B}$ is a function of pH.

REFERENCES

- Allen, K.A., Hönisch, B., Eggins, S.M., Rosenthal, Y., 2012. Environmental controls on B/Ca in calcite tests of the tropical planktic foraminifer species *Globigerinoides ruber* and *Globigerinoides sacculifer*. *Earth and Planetary Science Letters* 351–352, 270-280.
- Allen, K.A., Hönisch, B., Eggins, S.M., Yu, J., Spero, H.J., Elderfield, H., 2011. Controls on boron incorporation in cultured tests of the planktic foraminifer *Orbulina universa*. *Earth and Planetary Science Letters* 309, 291-301.
- Barnosky, A.D., Matzke, N., Tomiya, S., Wogan, G.O.U., Swartz, B., Quental, T.B., Marshall, C., McGuire, J.L., Lindsey, E.L., Maguire, K.C., Mersey, B., Ferrer, E.A., 2011. Has the Earth's sixth mass extinction already arrived? *Nature* 471, 51-57.
- Bemis, B.E., Spero, H.J., Bijma, J., Lea, D.W., 1998. Reevaluation of the oxygen isotopic composition of planktonic foraminifera: Experimental results and revised paleotemperature equations. *Paleoceanography* 13, 150-160.
- Bijma, J., Hemleben, C., Huber, B.T., Erlenkeuser, H., Kroon, D., 1998. Experimental determination of the ontogenetic stable isotope variability in two morphotypes of *Globigerinella siphonifera* (d'Orbigny). *Marine Micropaleontology* 35, 141-160.
- Bijma, J., Pörtlner, H.-O., Yesson, C., Rogers, A.D., 2013. Climate change and the oceans – What does the future hold? *Marine Pollution Bulletin* 74, 495-505.
- Culver, S.J., 1991. Early Cambrian Foraminifera from West Africa. *Science* 254, 689-691.
- Dickens, G.R., Castillo, M.M., Walker, J.C.G., 1997. A blast of the gas in the latest Paleocene: Simulating first order effects of massive dissociation of oceanic methane hydrate. *Geology* 25, 259-262.
- Dickson, A.G., 1981. An exact definition of total alkalinity and a procedure for the estimation of alkalinity and total inorganic carbon from titration data. *Deep Sea Research Part A. Oceanographic Research Papers* 28, 609-623.
- Dickson, A.G., Sabine, C.L., Christian, J.R., (Eds.), 2007. *Guide to Best Practices for Ocean CO₂ Measurements*. PICES Special Publication 3, 191.
- Dueñas-Bohórquez, A., Raitzsch, M., de Nooijer, L.J., Reichart, G.-J., 2011. Independent impacts of calcium and carbonate ion concentration on Mg and Sr incorporation in cultured benthic foraminifera. *Marine Micropaleontology* 81, 122-130.
- Emiliani, C., 1955. Pleistocene Temperatures. *The Journal of Geology* 63, 538-578.
- EPSTEIN, S., BUCHSBAUM, R., LOWENSTAM, H.A., UREY, H.C., 1953. REVISED CARBONATE-WATER ISOTOPIC TEMPERATURE SCALE. *Geological Society of America Bulletin* 64, 1315-1326.
- Erez, J., Luz, B., 1983. Experimental paleotemperature equation for planktonic foraminifera. *Geochimica et Cosmochimica Acta* 47, 1025-1031.
- Fairbanks, R.G., 1989. A 17,000-year glacio-eustatic sea level record: influence of glacial melting rates on the Younger Dryas event and deep-ocean circulation. *Nature* 342, 637-642.
- Gruber, N., 2011. Warming up, turning sour, losing breath: ocean biogeochemistry under global change. *Philosophical Transactions of the Royal Society A: Mathematical, Physical and Engineering Sciences* 369, 1980-1996.

- Hanson, J., Sato, M., Reudy, R., Lo, K., Lea, D.W., Medina-Elizade, M., 2006. Global temperature change. *PNAS* 103, 14288-14293.
- Hemming, N.G., Hanson, G.N., 1992. Boron isotopic composition and concentration in modern marine carbonates. *Geochimica et Cosmochimica Acta* 56, 537-543.
- Hintz, C.J., Shaw, T.J., Bernhard, J.M., Chandler, G.T., McCorkle, D.C., Blanks, J.K., 2006. Trace/minor element:calcium ratios in cultured benthic foraminifera. Part II: Ontogenetic variation. *Geochimica et Cosmochimica Acta* 70, 1964-1976.
- Hönisch, B., Hemming, N.G., 2005. Surface ocean pH response to variations in pCO₂ through two full glacial cycles. *Earth and Planetary Science Letters* 236, 305-314.
- Hönisch, B., Ridgwell, A., Schmidt, D.N., Thomas, E., Gibbs, S.J., Sluijs, A., Zeebe, R., Kump, L., Martindale, R.C., Greene, S.E., Kiessling, W., Ries, J., Zachos, J.C., Royer, D.L., Barker, S., Marchitto, T.M., Moyer, R., Pelejero, C., Ziveri, P., Foster, G.L., Williams, B., 2012. The Geological Record of Ocean Acidification. *Science* 335, 1058-1063.
- Jin, X., Gruber, N., 2003. Offsetting the radiative benefit of ocean iron fertilization by enhancing N₂O emissions. *Geophysical Research Letters* 30, 2249.
- Keeling, C.D., Whorf, T.P., 2000. Monthly carbon dioxide measurements on Mauna Loa, Hawaii from 1958 to 1998.
- Kennett, J.P., Stott, L.D., 1991. Abrupt deep-sea warming, paleoceanographic changes and benthic extinctions at the end of the Paleocene. *Nature* 353, 225-229.
- Klochko, K., Kaufman, A.J., Yao, W., Byrne, R.H., Tossell, J.A., 2006. Experimental measurement of boron isotope fractionation in seawater. *Earth and Planetary Science Letters* 248, 276-285.
- Klochko, K., Cody, G.D., Tossell, J.A., Dera, P., Kaufman, A.J., 2009. Re-evaluating boron speciation in biogenic calcite and aragonite using ¹¹B MAS NMR. *Geochimica et Cosmochimica Acta* 73, 1890-1900.
- Koch, P.L., Zachos, J.C., Gingerich, P.D., 1992. Correlation between isotope records in marine and continental carbon reservoirs near the Paleocene/Eocene boundary. *Nature* 358, 319-322.
- Kroeker, K.J., Kordas, R.L., Crim, R., Hendriks, I.E., Ramajo, L., Singh, G.S., Duarte, C.M., Gattuso, J.-P., 2013. Impacts of ocean acidification on marine organisms: quantifying sensitivities and interaction with warming. *Global Change Biology* 19, 1884-1896.
- Labeyrie, L.D., Duplessy, J.C., Blanc, P.L., 1987. Variations in mode of formation and temperature of oceanic deep waters over the last 125,000 years. *Nature* 327, 477-482.
- Le Quéré, C., et al., 2013. The global carbon budget 1959-2011. *Earth System Science Data* 5, 165-185.
- Lea, D.W., Martin, P.A., Chan, D.A., Spero, H.J., 1995. Calcium uptake and calcification rate in the planktonic foraminifer *Orbulina universa*. *The Journal of Foraminiferal Research* 25, 14-23.
- Lemarchand, D., Gaillardet, J., Lewin, E., Allegre, C.J., 2000. The influence of rivers on marine boron isotopes and implications for reconstructing past ocean pH. *Nature* 408, 951-954.
- Levitus, S., Antonov, J., Boyer, T., 2005. Warming of the world ocean, 1955–2003. *Geophysical Research Letters* 32, L02604.

- Manning, A.C., Keeling, R.F., 2006. Global oceanic and land biotic carbon sinks from the Scripps atmospheric oxygen flask sampling network. *Tellus B* 58, 95-116.
- McCrea, J.M., 1950. On the Isotopic Chemistry of Carbonates and a Paleotemperature Scale. *The Journal of Chemical Physics* 18, 849-857.
- Meehl, G.A., Stocker, T.F., Collins, W.D., Friedlingstein, P., Gaye, A.T., Gregory, J.M., Kitoh, A., Knutti, R., Murphy, J.M., Noda, A., Raper, S.C.B., Warrington, I.G., Weaver, A.J., Zhao, Z.-C., 2007. Global Climate Projections. In: *Climate Change 2007: The Physical Science Basis. Contribution of Working Group I to the Fourth Assessment Report of the Intergovernmental Panel on Climate Change* [Solomon, S., Qin, D., Manning, M., Chen, Z., Marquis, M., Averyt, K.B., Tignor, M., Miller, H.L. (eds.)]. Cambridge University Press, Cambridge, United Kingdom and New York, NY, USA.
- Millero, F.J., 2007. The Marine Inorganic Carbon Cycle. *Chemical Reviews* 107, 308-341.
- Misra, S., Froelich, P.N., 2012. Lithium Isotope History of Cenozoic Seawater: Changes in Silicate Weathering and Reverse Weathering. *Science* 335, 818-823.
- Morse, J.W., Arvidson, R.S., Lüttge, A., 2007. Calcium Carbonate Formation and Dissolution. *Chemical Reviews* 107, 342-381.
- Nürnberg, D., Bijma, J., Hemleben, C., 1996. Assessing the reliability of magnesium in foraminiferal calcite as a proxy for water mass temperatures. *Geochimica et Cosmochimica Acta* 60, 803-814.
- Palmer, M.R., Pearson, P.N., Cobb, S.J., 1998. Reconstructing Past Ocean pH-Depth Profiles. *Science* 282, 1468-1471.
- Pearson, P.N., Palmer, M.R., 2000. Atmospheric carbon dioxide concentrations over the past 60 million years. *Nature* 406, 695-699.
- Petit, J.R., Jouzel, J., Raynaud, D., Barkov, N.I., Barnola, J.M., Basile, I., Bender, M., Chappellaz, J., Davis, M., Delmotte, G., Delmotte, M., Kotlyakov, V.M., Legrand, M., Lipenkov, V.Y., Lorius, C., Pepin, L., Ritz, C., Saltzman, E., Stievenard, M., 1999. Climate and atmospheric history of the past 420,000 years from the Vostok ice core, Antarctica. *Nature* 399, 429-436.
- Ridgwell, A., Schmidt, D., 2010. Past constraints on the vulnerability of marine calcifiers to massive carbon dioxide release. *Nature Geoscience* 3, 196-200.
- Rollion-Bard, C., Blamart, D., Trebosch, J., Tricot, G., Mussi, A., Cuif, J., 2011. Boron isotopes as pH proxy: A new look at boron speciation in deep-sea corals using ^{11}B MAS NMR and EELS. *Geochimica et Cosmochimica Acta* 75, 1003-1012.
- Russell, A.D., Hönisch, B., Spero, H.J., Lea, D.W., 2004. Effects of seawater carbonate ion concentration and temperature on shell U, Mg, and Sr in cultured planktonic foraminifera. *Geochimica et Cosmochimica Acta* 68, 4347-4361.
- Sanyal, A., Bijma, J., 1999. A comparative study of the northwest Africa and eastern equatorial Pacific upwelling zones as sources of CO₂ during glacial periods based on boron isotope paleo-pH estimation. *Paleoceanography* 14, 753-759.
- Sarmiento, J.L., Dunne, J., Gnanadesikan, A., Key, R.M., Matsumoto, K., Slater, R., 2002. A new estimate of the CaCO₃ to organic carbon export ratio. *Global Biogeochemical Cycles* 16, 1107.
- Schrag, D.P., Hampt, G., Murray, D.W., 1996. Pore Fluid Constraints on the Temperature and Oxygen Isotopic Composition of the Glacial Ocean. *Science* 272, 1930-1932.

- Sen, S., Stebbins, J.F., Hemming, N.G., Gosh, B., 1994. Coordination environments of B impurities in calcite and aragonite polymorphs: A ^{11}B MAS NMR study. *American Mineralogist* 79, 819-825.
- Shackleton, N.J., 1974. Attainment of isotope equilibrium between ocean water and benthonic foraminifera genus *Uvigerina*: isotopic changes in the ocean during the last glacial. *Colloque international du CNRS* 219, 203-210.
- Siegenthaler, U., Stocker, T.F., Monnin, E., Lüthi, D., Schwander, J., Stauffer, B., Raynaud, D., Barnola, J.-M., Fischer, H., Masson-Delmotte, V., Jouzel, J., 2005. Stable Carbon Cycle–Climate Relationship During the Late Pleistocene. *Science* 310, 1313-1317.
- Spero, H.J., Bijma, J., Lea, D.W., Bemis, B.E., 1997. Effect of seawater carbonate concentration on foraminiferal carbon and oxygen isotopes. *Nature* 390, 497-500.
- Thomas, E., Shackleton, N.J., 1996. The Paleocene-Eocene benthic foraminiferal extinction and stable isotope anomalies. *Geological Society, London, Special Publications* 101, 401-441.
- Toyofuku, T., Kitazato, H., Kawahata, H., Tsuchiya, M., Nohara, M., 2000. Evaluation of Mg/Ca thermometry in foraminifera: Comparison of experimental results and measurements in nature. *Paleoceanography* 15, 456-464.
- Trenberth, K.E., Fasullo, J.T., 2009. Global warming due to increasing absorbed solar radiation. *Geophysical Research Letters* 36, L07706.
- Urey, H.C., 1947. The thermodynamic properties of isotopic substances. *Journal of the Chemical Society (Resumed)*, 562-581.
- Weijers, J.W.H., Schouten, S., Sluijs, A., Brinkhuis, H., Sinninghe Damsté, J.S., 2007. Warm arctic continents during the Palaeocene–Eocene thermal maximum. *Earth and Planetary Science Letters* 261, 230-238.
- Wefer, G., Berger, W.H., Bijma, J., Fischer, G., 1999. Use of Proxies in Paleooceanography: Examples from the South Atlantic. *Springer-Verlag Berlin Heidelberg*, 1-68.
- Wolf-Gladrow, D.A., Bijma, J., Zeebe, R.E., 1999. Model simulation of the carbonate chemistry in the microenvironment of symbiont bearing foraminifera. *Marine Chemistry* 64, 181-198.
- Wolf-Gladrow, D.A., Zeebe, R.E., Klaas, C., Körtzinger, A., Dickson, A.G., 2007. Total alkalinity: The explicit conservative expression and its application to biogeochemical processes. *Marine Chemistry* 106, 287-300.
- Yu, J., Elderfield, H., 2007. Benthic foraminiferal B/Ca ratios reflect deep water carbonate saturation state. *Earth and Planetary Science Letters* 258, 73-86.
- Yu, J., Foster, G.L., Elderfield, H., Broecker, W.S., Clark, E., 2010. An evaluation of benthic foraminiferal B/Ca and $\delta^{11}\text{B}$ for deep ocean carbonate ion and pH reconstructions. *Earth and Planetary Science Letters* 293, 114-120.
- Zachos, J.C., Röhl, U., Schellenberg, S.A., Sluijs, A., Hodell, D.A., Kelly, D.C., Thomas, E., Nicolo, M., Raffi, I., Lourens, L.J., McCarren, H., Kroon, D., 2005. Rapid acidification of the ocean during the paleocene-eocene thermal maximum. *Science* 308, 1611-1615.
- Zeebe, R.E., Bijma, J., Wolf-Gladrow, D.A., 1999. A diffusion-reaction model of carbon isotope fractionation in foraminifera. *Marine Chemistry* 64, 199-227.

Zeebe, R.E., Sanyal, A., Ortiz, J.D., Wolf-Gladrow, D.A., 2001. A theoretical study of the kinetics of the boric acid–borate equilibrium in seawater. *Marine Chemistry* 73, 113-124.

Zeebe, R.E., Wolf-Gladrow, D.A., 2001. *CO₂ in seawater: equilibrium, kinetics, isotopes*. Elsevier Science B.V., Amsterdam.

Topic 1

Effects of Temperature and Growth Rate on the B/Ca and $^{11}\text{B}/^{10}\text{B}$ Fractionation during Inorganic Calcite Formation

Karina Kaczmarek^{a*}

* corresponding author: Email: karina.kaczmarek@awi.de

Gernot Nehrke^a

Sambuddha Misra^b

Jelle Bijma^a

^a Alfred-Wegener-Institut Helmholtz-Zentrum für Polar- und Meeresforschung, Am Handelshafen 12, 27570 Bremerhaven, Germany

^b Department of Earth Science, University of Cambridge, Downing Site, CB2 3EQ Cambridge, UK

ABSTRACT

To separate the effect of temperature and growth rate on the boron incorporation and isotope fractionation, seeded calcite precipitation experiments were performed at a constant temperature and various growth rates and at a constant growth rate and various temperatures. We show that boron incorporation into the precipitated calcite increases with increasing growth rate but decreases with increasing temperature. With increasing growth rate the boron isotopic composition ($\delta^{11}\text{B}$) gets lighter and with increasing temperature heavier. At the investigated temperature range (12 – 32°C) and growth rates (0.18 – 1.5 mg mg⁻¹ h⁻¹) the effects of temperature and growth rate shift the $\delta^{11}\text{B}$ with nearly equal amplitudes in opposing directions. Therefore, their effects on boron incorporation and $\delta^{11}\text{B}$ of inorganically precipitated calcite are easily masked if temperature and growth rate are not experimentally decoupled. At the lowest temperature and growth rate (representing near equilibrium growth conditions) $\delta^{11}\text{B}$ of the calcite equals the $\delta^{11}\text{B}$ of $\text{B}(\text{OH})_4^-$ of the solution. The latter is in excellent agreement with the assumption that $\text{B}(\text{OH})_4^-$ is the only boron species incorporated during calcite precipitation. Furthermore, we successfully applied the surface entrapment model (SEMO) of

Watson and Liang (1995) to our data and demonstrate that the observed effects of temperature and growth rate can be explained by processes in the near surface layer of the calcite crystal.

Our findings could have important consequences for paleo applications using boron in marine calcifiers. We discuss possible effects of temperature and growth rate on the foraminiferal boron signature which is often used as a proxy for the reconstruction of the carbonate system.

1. INTRODUCTION

The elemental signature of marine biogenic carbonates can serve as a powerful tool to reconstruct the physio-chemical conditions of their formation ((Urey, 1947); (Boyle, 1988)Wefer et al., 1999). The incorporation of boron (B) into coral and foraminiferal calcium carbonate (CaCO_3) is of particular interest since its concentration and isotopic composition records information about the marine carbonate system of its growth habitat. In seawater B mainly exists as boric acid (B(OH)_3) and borate (B(OH)_4^-) whose species distribution and isotopic composition are strongly pH dependent (DOE, 1994); (Hemming and Hanson, 1992). Even though controversially discussed (Klochko et al., 2009) there is strong evidence that B(OH)_4^- is the only species incorporated during calcite formation substituting for CO_3 (Hemming and Hanson, 1992). Consequently, the isotopic signature of B incorporated in calcite reflects the isotopic composition of B(OH)_4^- in solution. While the isotopic signature of B is used to reconstruct past seawater pH (Sanyal et al., 1996; Hönish & Hemming, 2005), the B/Ca of several species of foraminifers was used to infer past seawater CO_3 concentrations (Yu and Elderfield, 2007); (Yu et al., 2007). However, there are indications that temperature might impact the B/Ca ratio and the $^{11}\text{B}/^{10}\text{B}$ signature in foraminifers (Wara et al., 2003).

The first theoretical estimate of temperature dependence of B isotopic composition of the two dissolved species was given by (Kakihana et al., 1977). The authors demonstrate that the fractionation factor α defined as:

$$\alpha_{(B(OH)_3)-B(OH)_4^-} = \frac{{}^{11}B(OH)_3 / {}^{10}B(OH)_3}{{}^{11}B(OH)_4^- / {}^{10}B(OH)_4^-} \quad (1.1)$$

has a temperature sensitivity of $4.8 \times 10^{-5}/^{\circ}\text{C}$. The latter is based on reduced partition function ratio calculations using data on molecular vibrations obtained from spectroscopic measurements. (Zeebe, 2005) showed that the calculation of α is sensitive to the choice of the theoretical method used to calculate the forces in the molecule and the molecular vibration frequencies. Based on these observations the temperature sensitivity of α for three different theoretical methods (KK77, B-LYP, UBFF) was found to be 5.25×10^{-5} , 1.2×10^{-4} , and $1.83 \times 10^{-4}/^{\circ}\text{C}$. Furthermore, Zeebe (2005) suggested an almost linear decrease in α over a temperature range from 0 to 40 °C by 2, 5, and 7 ‰ for the theoretical methods mentioned above. The first experimental study was performed by (Klochko et al., 2006) using spectrometric pH measurements in order to determine α from differences in the pK_B of ${}^{11}\text{B}(\text{OH})_3$ and ${}^{10}\text{B}(\text{OH})_3$. They concluded that temperature does not affect α in seawater over a temperature range from 25 to 40°C.

With respect to the temperature dependency of the B concentration in planktonic foraminifers published data are inconsistent. Yu et al. (2007) show a positive correlation with temperature whereas Allen et al. (2011) concluded that within a 10°C temperature range there is no effect on the B concentration in *Orbulina universa*. To our knowledge there are no studies on the effect of temperature on the B incorporation during inorganic calcite formation. Hence, the impact of temperature on the incorporation of B in calcite needs to be further investigated.

Changes in the temperature of a system alter the kinetics of many chemical processes. In a biological system this will affect many physiological processes involved in the biomineralization process. From the inorganic point of view a strong temperature dependence of the growth rate of a crystal will have consequences for the element and isotope fractionation (Lorens, 1981; Rimstidt et al., 1998; Gussone et al., 2005). In terms of growth rate of foraminifers Ni et al. (2007) reports a correlation between B/Ca, ${}^{11}\text{B}/{}^{10}\text{B}$ and the test size of *Globigerinoides sacculifer*. However, a larger test size does not necessarily relate to higher growth rates. Biogenic mineral formation does not represent a continuous process like inorganic precipitation under constant supersaturation conditions but rather has periods in which growth occurs and other periods in which the foraminifer is not growing (intermittent chamber formation). Furthermore, the timing of these growth periods can

change during the ontogeny of an organism. For inorganically formed calcite Ruiz-Agudo et al. (2012) suggested an effect of growth rate on the B incorporation based on AFM investigations.

As the physiological processes involved in biomineralization of foraminifers are poorly understood, it is not possible to systematically investigate the fundamental effects of temperature and growth rate on B/Ca and $^{11}\text{B}/^{10}\text{B}$ by means of culture experiments. A fundamental understanding obtained from inorganic systems will allow comparing them to systems with higher complexity such as controlled culture experiments. In this study we assess the role of temperature and growth rate on the B concentration and its isotopic composition in calcite using highly controlled precipitation experiments 1) within a temperature range of 20°C (12 to 32°C) having the same growth rate and 2) at one temperature (22°C) and different growth rates.

2. MATERIAL AND METHODS

2.1 Experimental setup

Calcite precipitation was performed in a 250 ml quartz-glass beaker containing 150 ml of a solution supersaturated with respect to calcite (for details on solution compositions see 2.2.). In order to trigger precipitation, five mg of calcite powder (Aldrich; 50 – 100 μm big aggregates containing 5 – 10 μm big grains, as characterized by SEM) were added to the supersaturated solution. In order to quickly transfer the powder into the quartz-glass beaker, 1 ml of solution was withdrawn with a pipette and given into a 2 ml Eppendorf vial containing the pre-weighted calcite powder. The solution-powder mix was then transferred back into the quartz-glass beaker using a pipette. This step was repeated twice to transfer all powder into the quartz-glass beaker. During the precipitation of calcite the Ca and B concentration, pH, and Ω were kept constant using a chemostat system. This chemostat system consists of a titrator (Titrand 902, Metrohm), three burettes (Dosino 800, Metrohm), a Ca-ion selective electrode (6.1241.050, Metrohm), and a pH electrode (6.0262.100 Ecotrode Plus, Metrohm). The chemostat system was controlled by a computer system using the tiamo 2.3 (Metrohm) software. Burette 1 contained a 0.02 M CaCl_2 , 0.04 M $\text{B}(\text{OH})_3$, and 0.7 M NaCl solution. Burette 2 contained a 0.02 M Na_2CO_3 and a 0.7 M NaCl (all chemicals were obtained from Merck in the quality suprapure®). A decrease in the Ca concentration detected by the Ca sensitive electrode triggered burette 1 and 2 to

add simultaneously the same volume into the solution until the initial Ca concentration was re-adjusted. During precipitation the signals from the Ca and the pH electrode were logged every 60 seconds and temperature every two minutes. The CO₂ produced during the precipitation of calcite would reduce pH and subsequently lower the saturation state with respect to calcite. To maintain pH and the dissolved inorganic carbon (DIC) concentration constant during calcite precipitation, the pH electrode was used to trigger the third burette containing 0.01 M HCO₃/CO₃ (in a ratio equal to that in the solution containing the growing calcite aggregates) and 0.7 M NaCl. To keep the calcite powder in suspension throughout the experiment, the solution was stirred (200 rpm) by an agitator (model BDC250, Caframo) equipped with a teflon coated axial impeller (Bohlender C378-12). The precipitation experiment was terminated when 55 ml of burette 1 and 2 had been added respectively because 1) a sufficient overgrowth of calcite was achieved (~15 times the mass of the initial seeds) 2) the B concentration in the overgrowth was sufficient for B analysis. Subsequently, the solution within the quartz-glass beaker was vacuum filtrated using a 0.2 µm PC filter (Whatman 110606). In order to remove all crystals from the beaker and to remove adsorbed B from the surface of the calcite crystals, the beaker was rinsed three times with 30 ml of a calcite saturated solution (prepared from suprapure calcite powder and di-ionized water). In a second step 90 ml of di-ionized water (resistance = 18.2 Ohm) were used to remove Ca left from the first washing step. Pilot experiments performed with a known mass of powder showed that these washing steps did not lead to a measurable loss of material. Afterwards the calcite crystals were dried in an oven at 50°C for 12 hours and weighed using an analytical balance (Mettler Toledo, XP Excellence Plus) with a resolution of 0.1µg. For B analysis (see section 2.4.) the calcite powder was dissolved in 0.5 M HNO₃ (Merck, suprapure® quality). All experiments were performed in a temperature controlled laboratory.

2.2 Precipitation experiments

Precipitation experiments were performed at three temperatures: 12, 22, and 32°C. However, since changes in temperature strongly affect the precipitation rate, it was necessary to modify the solution compositions for the different experiments to perform the experiments at comparable growth rates independent of temperature. Since it is difficult to quantitatively predict the precipitation rate on theoretical grounds, pilot experiments were performed to narrow down the required chemical

composition at each temperature. One aim of these pre-experiments was to find a precipitation rate which (1) was not too fast (not diffusion limited), (2) still experimentally feasible (allowing the control by the chemostat system without the need to re-calibrate electrodes during the experiment), and (3) resulting in a significant amount of precipitate needed for B analysis. The first step was to calculate the chemistry of the solutions using the chemical speciation code V. MINTEQA3 (Gustafsson, 2008). Based on pilot experiments, a supersaturation ($\Omega = \text{IAP} K_{\text{sp}}^{-1}$) of ~ 4 turned out to be well suited for our experiments. Since it had been shown that the Ca/CO₃ stoichiometry in solution strongly influences the growth rate of calcite (Nehrke et al., 2007; Wolthers et al., 2012), this ratio was used, by changing the calcium concentration, to realize different growth rates (R). The growth rate is defined as:

$$R = (mt_1 - mt_0)/mt_0/t \quad (1.2)$$

where mt_0 is the initial mass of calcite seeds at the beginning of the experiment, mt_1 the mass of calcite at the end of the experiment, and t the duration of the experiment. The pilot experiments showed that it was possible to realize precipitation experiments with the same growth rates at 22 and 32°C. In order to avoid the influence of pH on the B isotopic composition, pH was ~ 8.7 for all experiments. A concentration of NaCl of 0.7 M was used in order to obtain an ionic strength similar to that of seawater. The B concentration was 0.0035 M which is almost 10 times higher when compared to the average value for natural seawater. All chemicals used for the experiments were obtained from Merck (suprapure[®] quality) and dissolved in de-ionized water (resistance = 18.2 Ohm). All experiments were repeated four times. Table 1 shows the chemical parameters of the solutions of all experimental runs.

2.3 Analysis of the solutions

Before and after each experiment salinity of the solution was measured and aliquots were sampled for the analysis of [Ca], [B], $\delta^{11}\text{B}$, and [DIC]. Salinity measurements were performed using a conductivity meter (WTW Multi 340i) interfaced with a TetraCon 325 conductivity sensor. Calcium and B concentrations were determined by a Thermo Elemental (TJA) IRIS Intrepid ICP-OES Spectrometer using a Merck 4 multi element standard. The average internal error as estimated by multiple measurements of the reference material was $\pm 3.5\%$. Determination of [DIC] was performed photometrically in triplicates with a TRAACS CS800 QuAAatro autoanalyzer with an average

Table 1: Chemical composition of the solutions. be = before experiment, ae = after experiment. All concentrations are in mmol/l, B isotope composition in ‰. Calculated parameters are based on calculations in V. MINTEQ 3. For calculations the mean values ((be+ae)/2) of measured parameters are used. SD refers to 1 σ . Boron isotope composition of B(OH)₄⁻ was calculated using equation 5.

12°C	measured											calculated					
	Ca be	Ca ae	B be	B ae	DIC be	DIC ae	pH	S be	Sae	$\delta^{11}\text{B}$ be	$\delta^{11}\text{B}$ ae	B(OH) ₄ ⁻	$\delta^{11}\text{B}$ B(OH) ₄ ⁻	CO ₃ ²⁻	HCO ₃ ⁻	Ca/CO ₃ ²⁻	Ω
RUN 1	1.18	1.21	3.44	3.55	6.33	6.08	8.60	43	42	-17.44	-17.47	1.79	-34.15	0.15	4.47	8.01	2.99
RUN 2	1.17	1.03	3.74	3.70	6.38	6.19	8.66	43	42	-16.52	-15.26	2.00	-29.54	0.17	4.44	6.56	3.11
RUN 3	1.20	1.23	3.66	3.85	6.37	6.20	8.69	43	43	-17.75	-17.44	2.08	-31.73	0.18	4.38	6.78	3.66
RUN 4	1.12	1.22	3.48	3.62	6.46	6.46	8.63	43	42	-16.91	-16.07	1.86	-31.48	0.16	4.62	7.18	3.21
mean \pm SD	1.17\pm0.03	1.17\pm0.08	3.58\pm0.12	3.68\pm0.11	6.38\pm0.05	6.23\pm0.14	8.64\pm0.03	43\pm0.11	42\pm0.43	-17.15\pm0.47	-16.56\pm0.94	1.93\pm0.11	-31.72\pm1.64	0.16\pm0.01	4.48\pm0.09	7.13\pm0.55	3.24\pm0.25
22°C																	
RUN 1	0.72	0.72	3.72	3.56	5.17	5.16	8.76	43	41	-14.43	-13.77	2.30	-22.30	0.22	3.55	3.26	2.82
RUN 2	0.73	0.76	3.67	3.33	5.08	5.08	8.75	43	42	-13.75	-13.49	2.20	-21.65	0.21	3.50	3.48	2.83
RUN 3	0.72	0.75	3.68	3.56	5.29	5.06	8.76	43	42	-14.65	-13.96	2.28	-22.66	0.22	3.56	3.33	2.86
RUN 4	0.72	0.82	3.67	3.49	5.23	4.79	8.75	43	41	-14.37	-13.99	2.25	-22.57	0.21	3.46	3.65	2.88
mean \pm SD	0.72\pm0.003	0.76\pm0.04	3.69\pm0.02	3.49\pm0.09	5.19\pm0.08	5.02\pm0.14	8.76\pm0.003	43\pm0.11	42\pm0.5	-14.29\pm0.33	-13.80\pm0.19	2.26\pm0.04	-22.30\pm0.40	0.21\pm0.004	3.51\pm0.04	3.49\pm0.15	2.85\pm0.02
RUN 1	1.07	1.16	3.67	3.42	5.09	5.12	8.74	43	42	-14.55	-13.90	2.20	-22.91	0.21	3.54	5.37	4.11
RUN 2	1.07	1.03	3.65	3.47	5.07	5.31	8.76	43	41	-14.03	-13.65	2.25	-21.95	0.22	3.57	4.76	4.10
RUN 3	1.05	1.23	3.65	3.44	5.08	4.81	8.75	43	42	-14.38	-13.39	2.22	-22.15	0.21	3.41	5.52	4.12
RUN 4	1.06	1.08	3.61	3.31	5.05	4.89	8.75	43	43	-14.79	-13.81	2.16	-22.88	0.21	3.44	5.21	3.93
mean \pm SD	1.06\pm0.006	1.13\pm0.07	3.64\pm0.02	3.41\pm0.06	5.07\pm0.01	5.02\pm0.19	8.75\pm0.008	43\pm0.11	42\pm0.8	-14.44\pm0.28	-13.69\pm0.19	2.21\pm0.03	-22.47\pm0.43	0.21\pm0.006	3.49\pm0.06	5.22\pm0.29	4.1\pm0.08
32°C																	
RUN 1	0.70	0.76	3.81	3.49	5.20	5.57	8.73	43	43	-14.61	-14.50	2.41	-22.09	0.27	3.82	2.69	3.78
RUN 2	0.71	0.74	3.76	3.51	5.22	5.97	8.73	43	44	-13.86	-13.55	2.39	-20.84	0.28	3.98	2.60	3.89
RUN 3	0.71	0.76	3.79	3.65	5.17	6.03	8.73	43	44	-14.45	-14.42	2.46	-21.83	0.28	3.97	2.59	3.99
RUN 4	0.70	0.75	3.74	3.61	5.12	5.77	8.72	43	43	-13.97	-13.23	2.41	-20.78	0.27	3.88	2.69	3.72
mean \pm SD	0.70\pm0.005	0.75\pm0.008	3.77\pm0.03	3.57\pm0.07	5.18\pm0.04	5.83\pm0.18	8.73\pm0.005	43\pm0.11	43\pm0.5	-14.22\pm0.31	-13.93\pm0.55	2.42\pm0.03	-21.38\pm0.58	0.28\pm0.006	3.91\pm0.06	2.64\pm0.05	3.8\pm0.10

reproducibility of $\pm 10 \mu\text{mol/l}$ based on calibrations of an in-house standard (North Sea Seawater) that is calibrated against certified reference material batch No. 54 of Dickson (Scripps Institution of Oceanography). Before each run the pH electrode was calibrated using NBS buffers (7 and 9, Metrohm) giving at least a R^2 of 98 %.

2.4 Analysis of $\delta^{11}\text{B}$

Boron isotopes were analyzed by Thermo[®] Element XR, a single collector, sector field, high-resolution inductively coupled plasma mass spectrometer, fitted with a high sensitivity interface pump (Jet pump) as described in Misra et al. (2014a). Boron isotopic composition is reported as per mil (‰) deviation from NIST SRM 951a ($^{11}\text{B}/^{10}\text{B} = 4.04362 \pm 0.00137$) (Catanzaro et al., 1970) where:

$$\delta^{11}\text{B} (\text{‰}) = \left(\left[\frac{^{11}\text{B}/^{10}\text{B}_{\text{sample}}}{^{11}\text{B}/^{10}\text{B}_{\text{NIST-951a}}} \right] - 1 \right) \times 1000 \quad (1.3)$$

Boron isotope analyses were made following a Sample – Standard Bracketing (SSB) technique. NIST 951a was used as the standard and samples were concentration matched, typically at $\pm 5\%$, with the standard and were analyzed in quintuplicate. All samples and standards were analyzed in 0.3M HF matrix to facilitate rapid boron wash out (Misra et al., 2014a). We used Savillex[®] self-aspirating C-flow nebulizers with sample uptake rate of $50\mu\text{l}/\text{min}$ for sample aspiration. High performance extraction cones (Jet sampler and 'X' skimmer) were used to boost B sensitivity. The instrumental plasma conditions and mass calibration were appropriately adjusted to eliminate any artificial mass bias caused by $^{20}\text{Ne}^{2+}$ and $^{40}\text{Ar}^{4+}$ peak tailing into the $^{10}\text{B}^+$ peak. Before each analytical session the instrument was optimized for maximum B sensitivity (1 M-cps / ppb on ^{11}B), and samples were analyzed at a signal to blank intensity ratio of > 500 . An optimal analyses time of ~ 12 minutes per sample was adopted to obtain ≥ 2500 $^{11}\text{B}/^{10}\text{B}$ ratios to achieve the desired external precision of $\leq 0.5\text{‰}$ per quintuplicate analysis ($2\sigma/\sqrt{n}$). Based on sample aspiration rate and analysis time at total of ~ 3 ng B was consumed per analysis.

Prior to mass spectrometric analysis B was separated from the sample matrix by a single-step micro-distillation method modified after Gaillardet et al. (2001) and Wang et al. (2010) as described in Misra et al. (2014a). Savillex® Teflon® fin legged 5 ml beakers with conical interior were used as the distillation reservoir. Samples were loaded on to the cap of a pre-cleaned beaker – the beaker was tightly closed to avoid B loss – set on a hotplate at 95°C with the conical end pointing up. The distillation process was carried out for 15 to 18 hours to achieve a quantitative distillation of B from the load into the distillate. Sample load volume was kept below 50 µl to avoid the accumulated droplet at the conical end from dropping back onto the cap. Post distillation beakers were taken off the hotplate, allowed to cool for ~ 15 minutes, then 0.5 ml of 0.3 M HF was added, and the beakers were capped with pre-cleaned caps. The sample residue left on the cap was taken up in 0.1 M HNO₃ for trace element analysis of the precipitated calcite and to determination of the distillation yield (Misra et al., 2014b).

The accuracy and precision of the analytical method was assessed by comparing $\delta^{11}\text{B}$ measurements of seawater and secondary B standards (AE 120, 121, 122) with published/accepted results. Our estimate of $\delta^{11}\text{B}_{\text{SW}}$ of $39.8 \pm 0.4\text{‰}$ (2σ , $n = 30$) is independent of sample size and is in agreement with published values of $39.61 \pm 0.2\text{‰}$ (Foster et al., 2010) and $39.7 \pm 0.6\text{‰}$ (Spivack and Edmond, 1987). Moreover, our $\delta^{11}\text{B}$ estimates of SRM AE-120 ($-20.2\text{‰} \pm 0.5\text{‰}$, $2s$, $n = 33$); SRM AE-121 ($19.8\text{‰} \pm 0.4\text{‰}$, $2s$, $n = 16$); SRM AE-122 ($39.6\text{‰} \pm 0.5\text{‰}$, $2s$, $n = 16$) are similar, within analytical uncertainty, to accepted values (Louvat et al., 2010).

2.5 Conversion of measured $\delta^{11}\text{B}$ into seawater scale

Since the solutions from which the calcite was precipitated had a significantly lighter $\delta^{11}\text{B}$ (-14‰) than natural seawater ($\sim 40\text{‰}$), all values were corrected for this difference in order to scale with published data. Conversion to the seawater scale was performed using the relationship:

$$\delta^{11}\text{B SS}_{\text{calcite}} = \delta^{11}\text{B}_{\text{SW}} - \delta^{11}\text{B}_S + \delta^{11}\text{B}_{\text{calcite}} \quad (1.4)$$

Where SS stands for seawater scale, $\delta^{11}\text{B}_{\text{sw}}$ is the B isotopic composition of seawater (39.95‰), $\delta^{11}\text{B}_S$ represents the B isotope composition of the solution, and $\delta^{11}\text{B}_{\text{calcite}}$ represents the measured B isotope composition of the precipitated calcite. Converted values are listed in Table 2. For comparison between $\delta^{11}\text{B}$ of the precipitated calcite and $\text{B}(\text{OH})_4^-$ of the solutions, $\delta^{11}\text{B}$ of $\text{B}(\text{OH})_4^-$ was calculated using (Zeebe and Wolf-Gladrow, 2001):

$$\delta^{11}\text{B}_{\text{B}(\text{OH})_4^-} = \frac{\delta^{11}\text{B}_{\text{sw}} \times [\text{B}_{\text{sw}}] - \varepsilon_B \times [\text{B}(\text{OH})_3]}{[\text{B}(\text{OH})_4^-] + \alpha_B \times [\text{B}(\text{OH})_3]} \quad (1.5)$$

where α_B is the B fractionation factor between $\text{B}(\text{OH})_4^-$ and $\text{B}(\text{OH})_3$ (1.0272 (Klochko et al., 2006)) and ε_B is $(\alpha_B - 1) \times 1000$. Values for the boron isotopic composition of $\text{B}(\text{OH})_4^-$ are listed in Table 1. $\delta^{11}\text{B}$ of $\text{B}(\text{OH})_4^-$ was also converted to the seawater scale by:

$$\delta^{11}\text{B}_{\text{SS}_{\text{B}(\text{OH})_4^-}} = \delta^{11}\text{B}_{\text{sw}} - \delta^{11}\text{B}_S + \delta^{11}\text{B}_{\text{B}(\text{OH})_4^-} \quad (1.6)$$

Converted values for $\text{B}(\text{OH})_4^-$ can be found in Table 2.

3. RESULTS

3.1 Chemical composition of the solutions during precipitation

The [Ca], [B], [DIC], and pH at the start and the end of each experimental run are nearly identical (Table 1). Figure 1 shows an example of the logged addition of CaCl_2 to the solution and the corresponding signal of the Ca sensitive electrode (A) and the addition of Na_2CO_3 and the corresponding signal of the pH electrode (B) during one run. The almost linear development of added chemicals demonstrates a constant calcite growth rate. The B isotope composition of all solutions during each run did not change significantly.

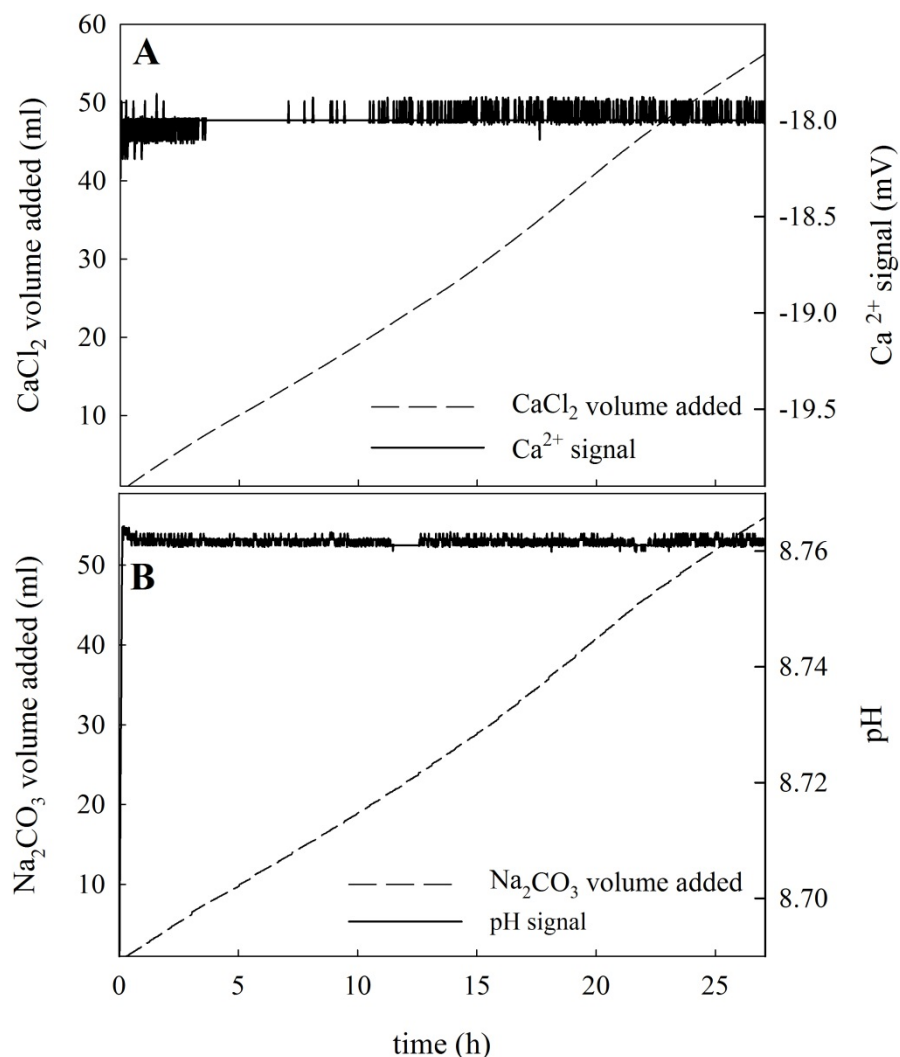


Figure 1: (A) CaCl_2 addition into the solution during crystal growth (left y-axis) and the corresponding Ca^{2+} signal (right y-axis) during an experiment at 22°C and $R = 0.69 \text{ (mg mg}^{-1} \text{ h}^{-1})$. (B) Na_2CO_3 addition (left y-axis) and recorded pH (right y-axis) during the same run. In both cases a linear trend for the volumetric dosing is observed indicating a constant precipitation rate.

3.2 Boron isotope composition and concentration of precipitated calcite

The results of the B analysis of the precipitated calcite are presented in table 2.

3.2.1 Boron concentration

The B concentration data show an influence of both temperature and growth rate on the B incorporation into calcite (Fig. 2A). The highest B concentration was measured at 22°C and $R = 1.44 \text{ mg mg}^{-1} \text{ h}^{-1}$ whereas the lowest boron concentration was observed at 12°C and $R = 0.18 \text{ mg mg}^{-1} \text{ h}^{-1}$.

Table 2: Measured B data of precipitated calcite, calculated growth rates (R), values of B isotope composition of calcite and B(OH)_4^- converted to seawater scale (SS), B/Ca ratios of the calcite (the amount of Ca in the initial seeds was subtracted), and K_D , $\text{SD} = 1\sigma$.

measured (calcite)				calculated			
12°C	B (ppm)	$\delta^{11}\text{B}$ (‰)	R ($\text{mg mg}^{-1} \text{h}^{-1}$)	$\delta^{11}\text{B SS}_{\text{calcite}}$ (‰)	$\delta^{11}\text{B SS}_{\text{B(OH)}_4^-}$ (‰)	B/Ca (mmol/mol)	$K_D \times 1000$
RUN 1	23	-28.86	0.17	28.36	26.87	0.209	0.523
RUN 2	23	-29.62	0.18	26.04	27.55	0.212	0.470
RUN 3	19	-29.51	0.19	26.36	26.51	0.180	0.379
RUN 4	23	-27.84	0.17	28.42	27.19	0.210	0.521
mean±SD	22±1.4	-28.96±0.71	0.18±0.009	27.3±1.1	27.03±0.39	0.203±0.013	0.47±0.06
22°C							
RUN 1	51	-24.63	0.54	29.23	30.00	0.469	0.724
RUN 2	49	-24.08	0.61	29.31	29.92	0.456	0.725
RUN 3	53	-25.26	0.85	28.82	29.98	0.491	0.765
RUN 4	56	-23.83	0.75	30.12	29.90	0.521	0.800
mean±SD	52±2.7	-24.45±0.55	0.69±0.12	29.37±0.47	29.95±0.04	0.484±0.025	0.75±0.03
RUN 1	97	-26.42	1.42	27.57	29.71	0.899	1.447
RUN 2	105	-26.16	1.45	27.45	29.96	0.974	1.546
RUN 3	97	-25.83	1.40	27.83	29.86	0.896	1.372
RUN 4	103	-26.77	1.50	27.30	29.82	0.955	1.517
mean±SD	101±3.6	-26.29±0.34	1.44±0.04	29.84±0.18	29.84±0.09	0.931±0.034	1.47±0.06
32°C							
RUN 1	54	-24.40	1.61	29.93	30.72	0.500	0.794
RUN 2	57	-22.10	1.38	31.37	30.68	0.530	0.882
RUN 3	54	-23.60	1.41	30.60	30.77	0.498	0.802
RUN 4	57	-23.05	1.61	30.32	30.59	0.531	0.856
mean±SD	56±1.5	-23.29±0.84	1.5±0.11	30.55±0.53	30.69±0.06	0.515±0.015	0.83±0.04

Experiments performed at a constant growth rate show that more B is incorporated if temperature decreases. Experiments performed at constant temperature reveal that less B is incorporated as the growth rate decreases.

3.2.2 Boron isotope composition

At a constant growth rate $\delta^{11}\text{B}$ of the precipitated calcite gets heavier with temperature (Fig. 2B). At $R \sim 1.5 \text{ mg mg}^{-1} \text{ h}^{-1}$ the observed temperature sensitivity is 2.3‰ per 10°C. Hence, the incorporation of the heavier isotope is favored with increasing temperature. Calcites precipitated at the same temperature (22°C) but at different growth rates show that $\delta^{11}\text{B}$ gets lighter with increasing growth rate. Hence, faster precipitation (at the same temperature) leads to an enrichment of the lighter isotope. Calcite precipitated

at 12°C and $R = 0.18 \text{ mg mg}^{-1} \text{ h}^{-1}$ shows, within errors, the same B isotopic signature as calcite precipitated at 22°C and $R = 1.44 \text{ mg mg}^{-1} \text{ h}^{-1}$.

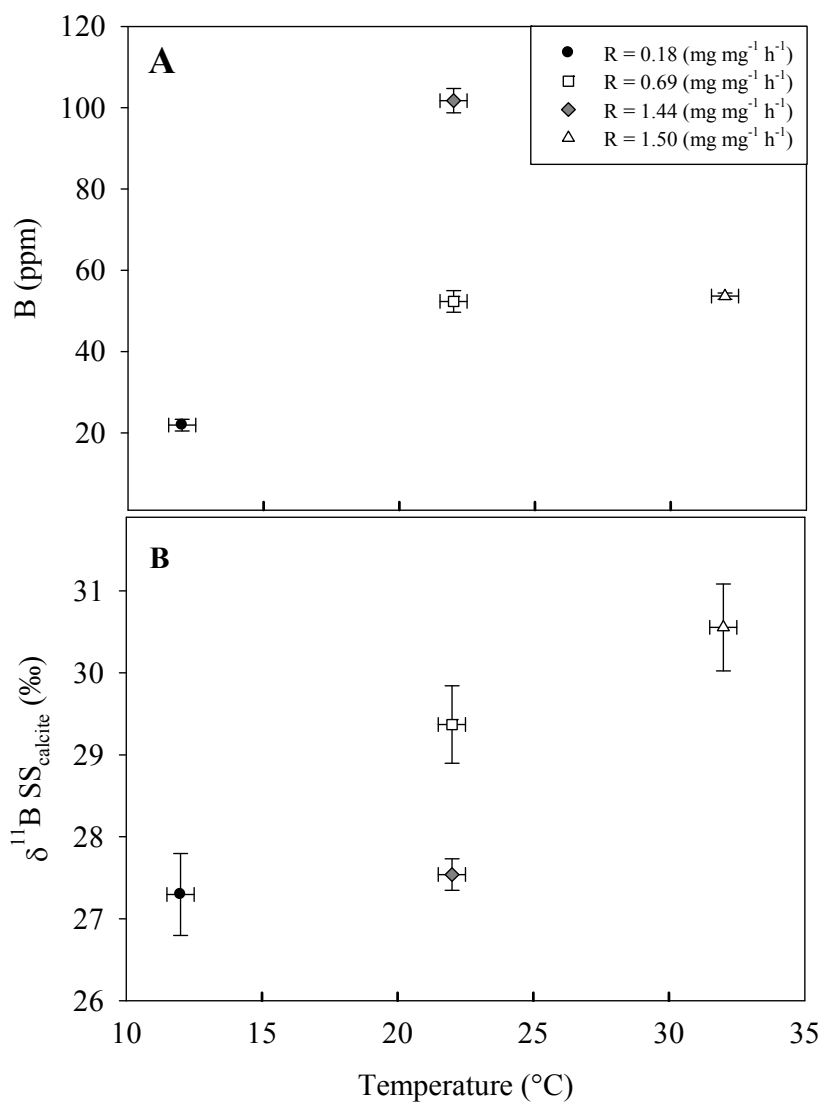


Figure 2: The boron concentration (A) and the B isotope composition (B) of precipitated calcite crystals at 12, 22, and 32°C. Single data points represent mean values of four runs respectively. Error bars represent a SD of 1σ .

4. DISCUSSION

4.1 Total boron versus $B(OH)_4^-$

The data measured and presented in Figure 2 are based on the total B concentration (B_T) in solution. As discussed in the introduction the prevalent opinion is that $B(OH)_4^-$ is the only species being incorporated into inorganic as well as into biogenic calcite. Since the pK_B is temperature dependent, changes in temperature will affect the total concentration of $B(OH)_4^-$ and subsequently its isotope composition. In order to quantitatively evaluate this effect we plotted the K_D for B versus temperature. K_D of B is defined as (Yu & Elderfield, 2007):

$$K_D = \frac{B/Ca_{solid}}{[B(OH)_4^-]/[HCO_3^-]_{liquid}} \quad (1.7)$$

Plotting B_T and K_D against temperature shows a very similar pattern (Fig. 3). The latter is not surprising since the $B(OH)_4^-$ fraction of B_T does not change significantly if the temperature is varied between 12 to 32°C. However, for the B isotope fractionation in calcite this is quite different. Figure 4A shows the differences in $\delta^{11}B$ SS of $B(OH)_4^-$ at 12, 22, and 32°C which is related to the temperature dependence of pK_B together with the $\delta^{11}B$ SS of calcite precipitated in the different treatments. $\delta^{11}B$ SS of $B(OH)_4^-$, the species assumed to be incorporated during calcite formation, changes significantly with temperature. To account for the latter we plotted the $\delta^{11}B$ SS values of the precipitated calcite normalized to the $\delta^{11}B$ SS of $B(OH)_4^-$ (as $\delta^{11}B$ of calcite - $\delta^{11}B$ of $B(OH)_4^-$ of the solution) versus temperature (Fig. 4B). The $\delta^{11}B$ values of the calcite precipitated at 12 and 32°C are very close to the calculated $\delta^{11}B$ of $B(OH)_4^-$ of the solution whereas $\delta^{11}B$ values at 22°C deviate with increasing growth rate from the calculated equilibrium value for borate. However, for calcites precipitated with identical growth rates, the $\delta^{11}B$ of the calcite precipitated at 22°C has the largest deviation from the $\delta^{11}B$ of $B(OH)_4^-$ whereas the $\delta^{11}B$ value at 32°C exactly matches the $\delta^{11}B$ of $B(OH)_4^-$. To summarize; at this point no consistent picture between temperature, growth rate, and B isotope fractionation during calcite precipitation emerges. For a better understanding of the observed pattern we separate the effect of temperature and growth rate by

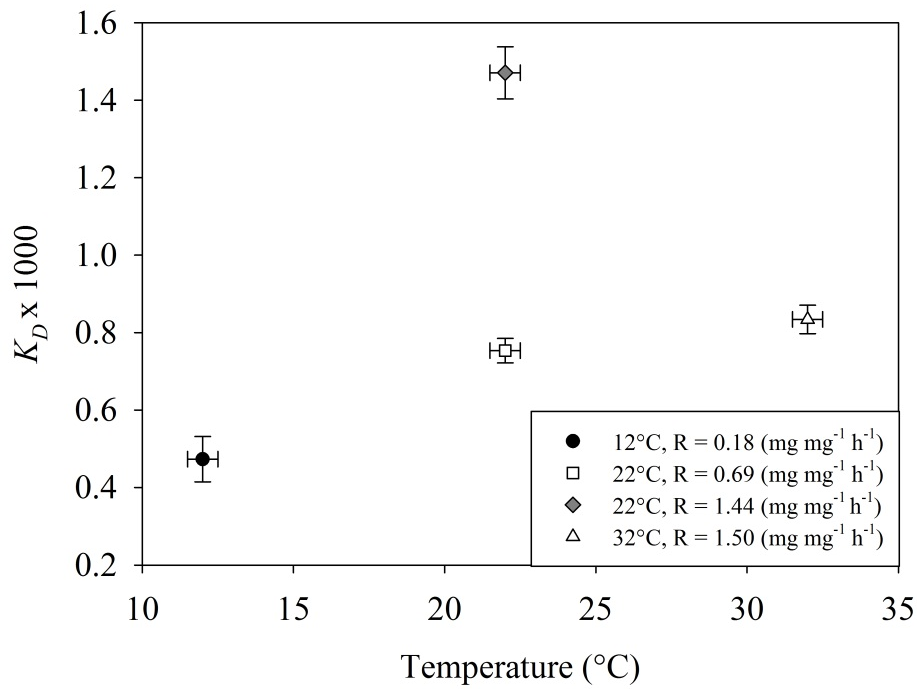


Figure 3: Calculated K_D values vs. temperature. Single data points represent mean values of four runs. Error bars represent a SD of 1σ .

means of the so called Surface Entrapment Model (SEMO) which was conceived in order to explain trace/minor element incorporation and isotope fractionation during crystal growth. The SEMO was introduced and further developed by Watson and Liang, (1995); Watson, (1996); Watson, (2004) and has successfully been applied to experimental data for e.g. Sr incorporation (Tang et al., 2008b) and Ca isotope fractionation (Tang et al., 2008a) in calcite.

4.2 The Surface Entrapment Model (SEMO)

The SEMO is based on the following major assumption: Within a thin surface layer of a crystal in equilibrium with an aqueous solution, the so called “surface boundary layer” (S), trace/minor elements are enriched compared to their concentration in the bulk of the crystal lattice (e.g. (Hall, 1953; Tiller & Ahn, 1980). The enrichment of a trace/minor element in the surface boundary layer relative to the bulk crystal implies that the crystal lattice at the near surface differs from the bulk lattice. Using *in situ* high resolution X-ray reflectivity Fenter et al. (2000) concluded that the outermost two monolayers of a calcite crystal have a different structure from the bulk crystal in terms of orientation and bond length. Given such

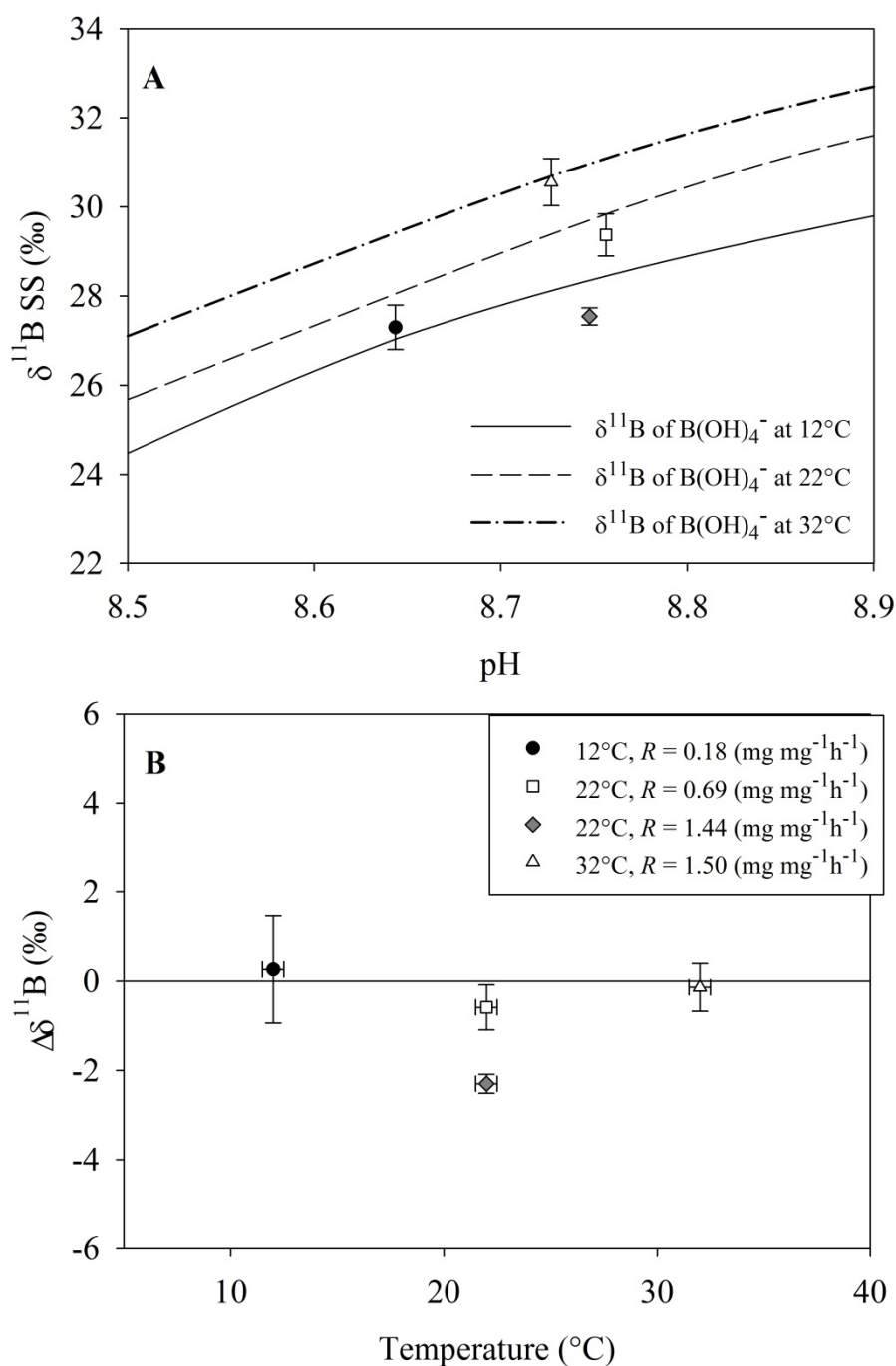


Figure 4: (A) $\delta^{11}\text{B}$ SS of B(OH)_4^- calculated at 12, 22, and 32°C using equations 5 and 6. The temperature dependent distribution of B(OH)_4^- and B(OH)_3 was calculated by $[\text{B(OH)}_4^-] = [\text{B}_T]/(1+[\text{H}^+]/K_B)$ and $[\text{B(OH)}_3] = [\text{B}_T] - [\text{B(OH)}_4^-]$ using temperature corrected K_B values. Also plotted are mean values of $\delta^{11}\text{B}$ SS_{calcite}. Error bars represent a SD of 1σ . (B) Difference between $\delta^{11}\text{B}_{\text{calcite}}$ and $\delta^{11}\text{B}_{\text{B(OH)}_4^-}$ ($\Delta\delta^{11}\text{B}$) for the different treatments.

a structural anomaly allowing ions to migrate more “freely” Watson (2004) proposed that the diffusivity within that area of anomaly reaches higher values than in the bulk crystal. Watson’s (2004) reflections are

also based on the enhanced near surface ion mobility reported in the studies of Stipp et al., (1992), Stipp, (1998), and Hoffmann & Stipp, (2001). During the growth of the crystal the fate of the elements in the surface layer depends on two major processes: (a) diffusivity (D) of elements between S and the newly build crystal layer C_1 and (b) the growth rate (R) of this newly build crystal layer.

Figure 5 illustrates the dynamic processes that take place during the addition of a new layer of atoms to the existing surface of a crystal. For a better conceptual characterization of the processes the surface boundary layer S is divided into an inner layer (S_i , facing towards the bulk of the crystal) and an outer layer (S_o , facing towards the solution). If a new layer (L_1) is formed at the surface of the crystal, it will become the new outer layer of S (nS_o) and at the same time the former inner layer S_i will become part of the bulk crystal lattice (C_1). Concurrently, the former outer layer S_o will become the new inner layer of S (nS_i) and therefore the relative thickness of S will remain constant (Fig. 5 A+B). The growth rate of the crystal i.e. the advancement of S (the attachment rate of L_1) determines the efficiency with which lattice incompatible trace/minor elements present in S get “entrapped” in the newly formed bulk lattice layer C_1 before they can diffuse out. However, the entrapment efficiency also depends on the diffusivity of the trace/minor elements out of C_1 into S. As a consequence incorporation of trace/minor elements is dictated by the competition between the redistribution of the trace/minor element between C_1 and S by diffusion and the addition rate of new layers (Fig. 5 C+D). It should be noted that at very slow growth rates i.e. for a system close to thermodynamic equilibrium, the B incorporation would represent the so called equilibrium fractionation. The elevated B incorporation at higher growth rates i.e. its deviation from equilibrium is the result of an entrapment of lattice incompatible B due to the above described kinetic processes.

In the following two sections we will apply the SEMO to explain the effects of temperature and growth rate on the B concentration and B isotopic data obtained in this study. It should be noted that the literature on incorporation of elements like i.e. Sr or on the Ca isotope fractionation during the precipitation of calcite is huge compared to the data available on B. Therefore, the data required for a quantitative application of the SEMO is lacking in the literature. However, we will show that a qualitative approach is suitable to significantly broaden our understanding of the B incorporation and B isotope fractionation during calcite precipitation.

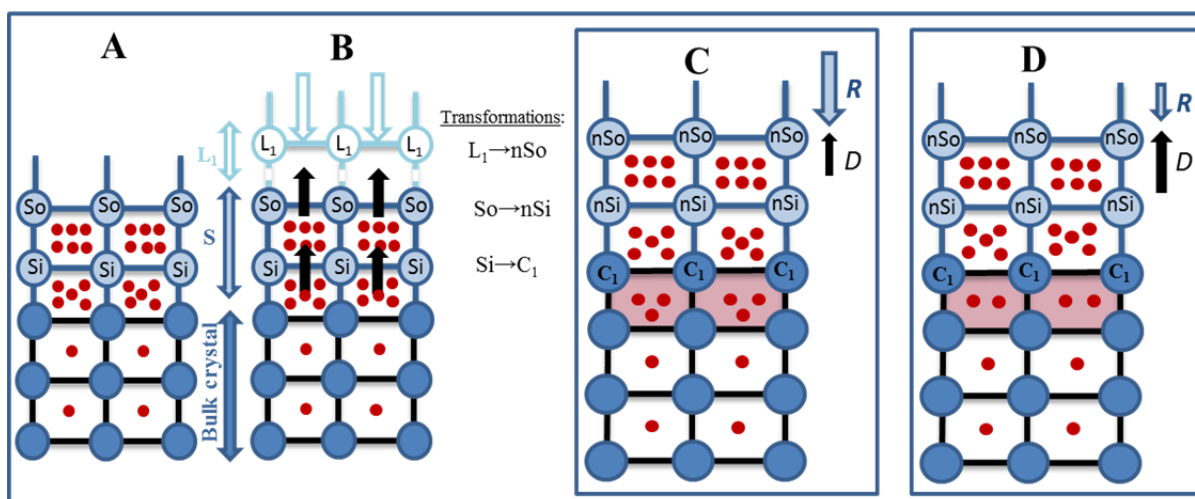


Figure 5: Schematic illustration of the basic principles of the Surface Entrapment Model (SEM). (A) A crystal in contact with a solution. Within the bulk lattice some foreign ions (*i*) are present as illustrated by the red dots. This low concentration is the concentration that would be present in a crystal grown under conditions close to equilibrium. For the sake of convenience the number of red dots is used to exemplify concentration differences within the different layers of the crystal. However, their position within the lattice is highly simplified and does not represent their position in a three dimensional crystal lattice. Due to the greater flexibility of *S*, compared to the bulk lattice, the concentration of foreign ions is highly enriched in the surface layer (*S*) of the crystal. *S* consists of an inner layer *Si* and an outer layer *So*. (B) If a new layer (*L*₁) is added to the crystal surface *Si* becomes part of the bulk crystal (*C*₁) losing its greater flexibility, whereas at the same time *L*₁ will transform into the new *So* (*nSo*) and the old *So* will transform into the new *Si* (*nSi*). At this point the incorporation of *i* depends on 1) the time needed to build *L*₁ as indicated by the white arrows and 2) diffusivity of *i* out of *S* into *L*₁ as indicated by the black arrows. (C) and (D) illustrate the situation after a new layer is added and growth has again stopped. (C) If the formation of *L*₁ (blue arrow) is faster than the diffusivity of *i* (black arrows) ions have less time to escape from *C*₁ into *Si* resulting in a higher enrichment in *C*₁. (D) If the diffusivity (black arrow) is faster than the formation of *L*₁ (blue arrow), less ions are incorporated in *C*₁ then in case (C). The red layer in C and D represents the new overgrowth of the calcite.

4.3 Application of the SEMO to B/Ca

4.3.1 Constant growth rate – various temperatures

If two crystals grow at the same rate, the SEMO predicts that elevated temperatures lead to higher ion diffusivity within *S* resulting in a faster “escape” of *B* from the newly forming layer *C*₁ into the newly forming layer *S*. In case of crystals having the same growth rate the amount of layers added per time is identical i.e. results in the same thickness of *C*₁. Applying this scenario to the *B* incorporation into calcite predicts that with increasing temperatures the diffusivity of *B* out of *S* is enhanced and more *B* can escape from *C*₁ before *C*₁ can be completed i.e. becomes part of the bulk crystal lattice (Fig.6). The latter is exactly what we observe in our experiments (Fig. 2A/3). Experiments performed at a constant growth rate of $\sim 1.5 \text{ mg mg}^{-1} \text{ h}^{-1}$ reveal a decrease in *B* concentration from 101 to 56 ppm when temperature is increased from 22 to 32°C. The equilibrium fractionation for *B* ($[B]_{\text{eq}}$) is temperature dependent. The

latter is the reason why $[B]_{eq}$ in Figure 6 differs for 22 and 32°C.

4.3.2 Constant temperature – various growth rates

According to the SEMO crystals grown at the same temperature show the same diffusivity for B in S. However, with increasing growth rate new layers are added faster to the crystal surface leaving less time for B to diffuse out of S while the inner layer Si becomes part of the bulk lattice of the crystal (C_1). Consequently, the entrapment of B in this new layer C_1 is more effective at higher growth rates (Fig. 6). Exactly this pattern can be seen for our data (Fig. 2A). In experiments performed at the same temperature (22°C) the B concentration within the calcite increases from 52 to 101 ppm if the growth rate increases from 0.69 to 1.44 $mg\ mg^{-1}\ h^{-1}$.

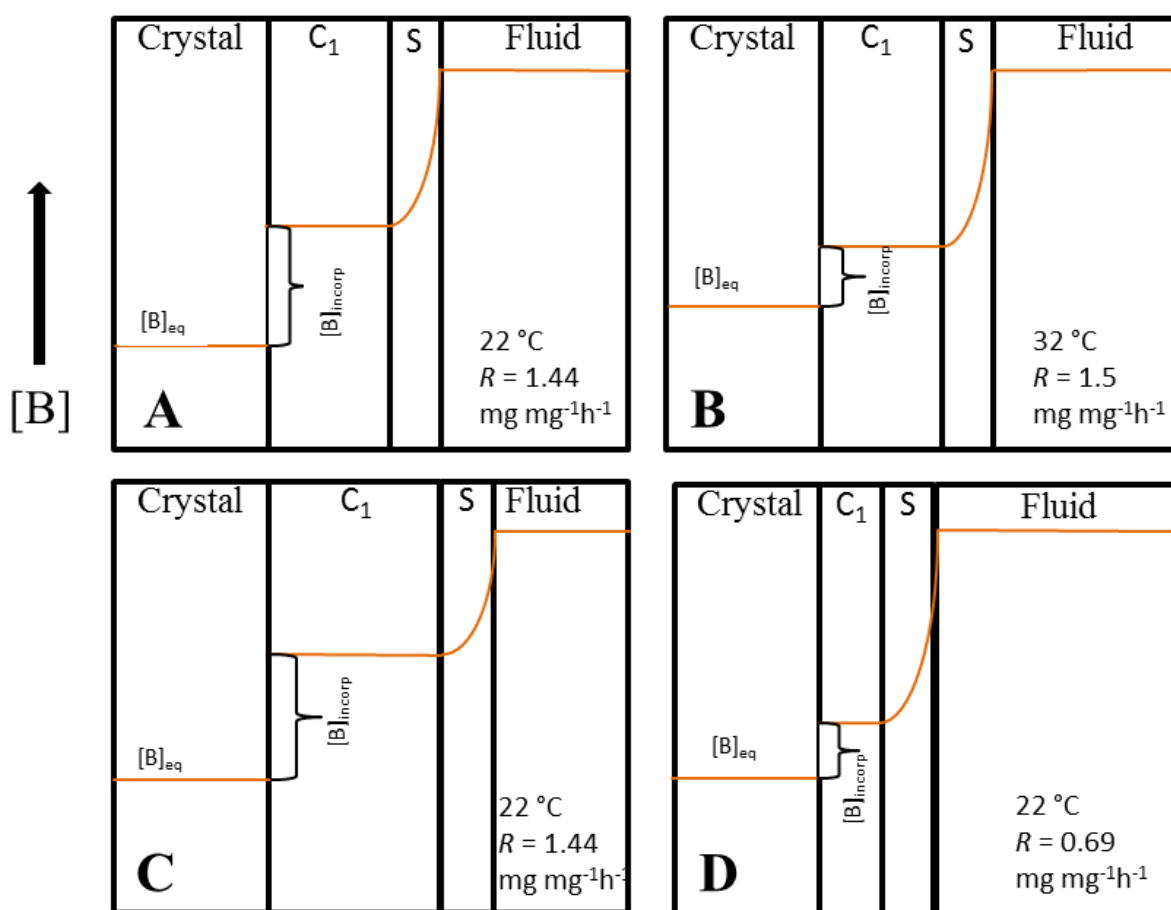


Figure 6: Effects of temperature and growth rate on B incorporation after growth has stopped according to the SEMO. $[B]_{eq}$: boron concentration at equilibrium (temperature dependent), $[B]_{incorp}$: amount of boron being incorporated in the newly formed crystal layer, C_1 .

Constant growth rate at various temperatures (A+B): At a constant growth rate the time for B to diffuse out of S before the latter becomes C_1 is the same. The diffusivity of B on the other hand increases with increasing temperature. This results in a lower B incorporation ($[B]_{incorp}$) with increasing temperature.

Constant temperature various growth rates (C+D): At a constant temperature the B diffusivity is the same. At a higher growth rate C_1 forms faster than at a lower growth rate leaving less time for B to diffuse out of S before the latter becomes C_1 . This results in a higher B incorporation ($[B]_{\text{incorp}}$) with increasing growth rate.

This demonstrates that the effect of growth rate and temperature on the incorporation of B into calcite can be explained by the SEMO assuming the same behavior for B as for Sr (Tang et al., 2008b). It should be noted that this suggests that the incorporation of two so different ions, Sr^{2+} being a divalent cation substituted for Ca^{2+} in the calcite lattice and B most probably incorporated as $\text{B}(\text{OH})_4^-$ at a CO_3^- site, can be explained by the same processes.

4.4 Application of the SEMO to $\delta^{11}\text{B}$ data

The application of the SEMO to isotope data requires some assumptions which will be explained in the following: Tang et al. (2008a) presumed in their study that no significant isotope fractionation occurs close to equilibrium conditions. However, the surface layer is always depleted in the heavier isotope as explained below. Therefore, the surface entrapment factor (F) of ^{11}B (defined as the concentration of ^{11}B in the surface layer divided by the ^{11}B concentration of the bulk crystal corresponding to equilibrium with the fluid) is less than unity (at equilibrium $F = 1$). The authors discuss several reasons for this predicted depletion ranging from the difference in ion radii of the isotopes (Heumann et al., 1977), over differences in binding strength at the surface (Marriott et al., 2004; Gussone et al., 2005), and enhanced diffusion of the lighter isotope at the liquid/solid transitions (Gussone et al., 2003). Furthermore, F shows a temperature dependence: at elevated temperature F is closer to unity. Since the above mentioned arguments are poorly investigated for B, we will use a comparison with Ca isotopes as the best possible starting point. Therefore, we assume that ^{11}B like ^{44}Ca is heavily depleted in S. An illustrative consideration of the SEMO and B isotope fractionation is given in Figure 7.

4.4.1 Constant growth rate – different temperatures

As stated above it is assumed that ^{11}B compared to ^{10}B is depleted in S. If we assume that a crystal grows very slow, i.e. close to equilibrium, no isotope fractionation between solution and crystal is expected i.e. the crystal should carry the isotopic composition of $\text{B}(\text{OH})_4^-$ in solution (as this is the species assumed to be incorporated during calcite precipitation). Comparing two calcite crystals that grow

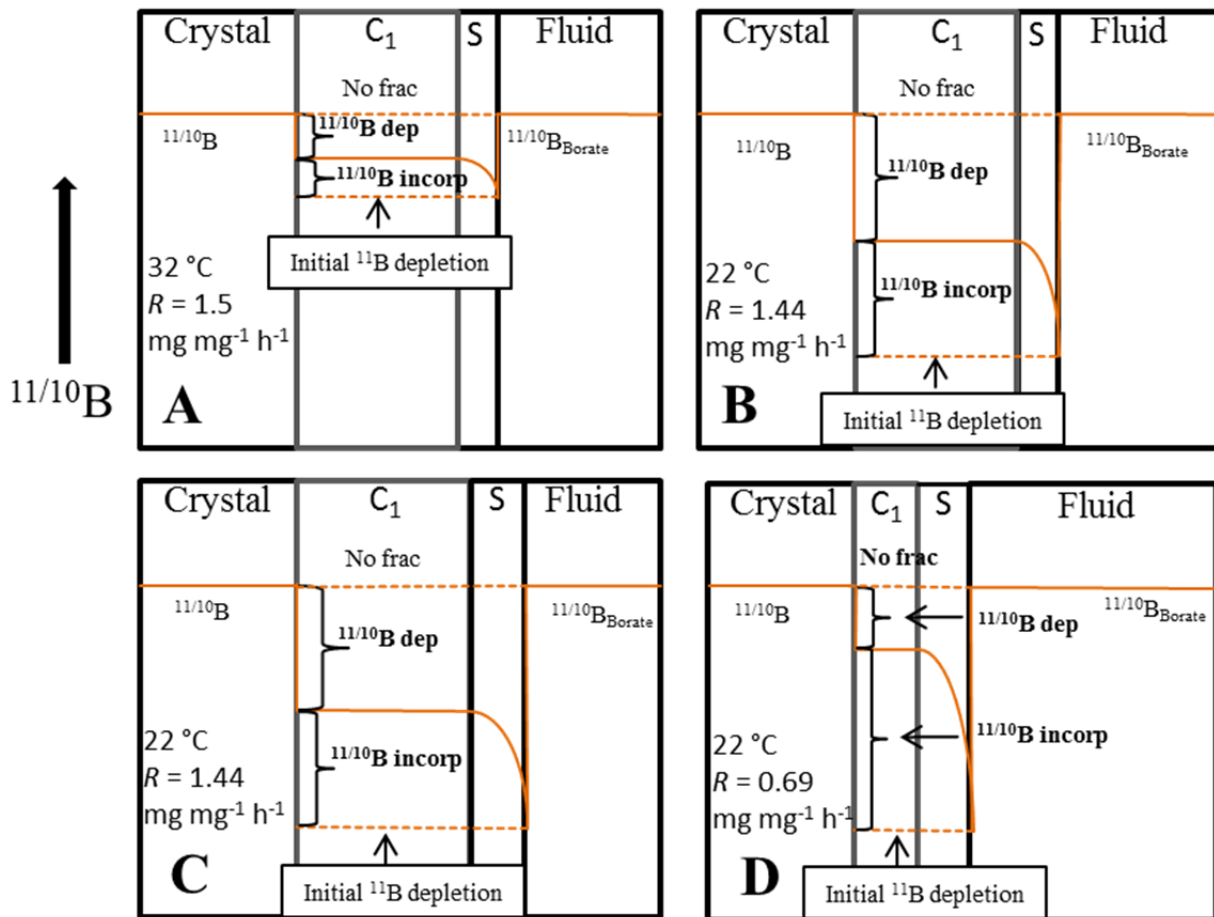


Figure 7: Effects of temperature and growth rate on B isotope fractionation after the growth has stopped according to the SEMO; frac = fractionation; dep = depletion; incorp = incorporation.

Constant growth rate various temperatures (A+B): At the same growth rate the time for B to diffuse out of S before S gets part of the newly formed crystal layer, C_1 , is equal at 22 and 32°C. ^{10}B shows a higher diffusivity than ^{11}B leading to a more efficient escape of ^{10}B compared to ^{11}B . Furthermore, ^{11}B is enriched in S at 32°C compared to 22°C since F is temperature dependent, but ^{11}B is less than ^{10}B at both temperatures (indicated as initial ^{11}B depletion). Both effects lead to a heavier isotopic signature of the crystal as temperature increases.

Constant temperature various growth rates (C+D): With increasing growth rate the time for both B isotopes to diffuse out of S, before S gets part of the newly formed crystal layer C_1 , decreases. Due to the constant temperature the ^{11}B depletion in S is equal in both treatments. Since ^{10}B has the higher diffusivity (compared to ^{11}B) its entrapment relative to ^{11}B increases with increasing growth rate resulting in a lighter isotopic signature of the newly grown C_1 .

with the same rate (significantly away from equilibrium) but at different temperatures, the SEMO predicts that with increasing temperature ^{10}B (as the lighter isotope having the higher diffusivity than ^{11}B) will escape faster than ^{11}B and thus be depleted in C_1 before C_1 becomes part of the bulk crystal lattice.

Additionally, the depletion of ^{11}B in S is less pronounced at 32 than 22°C (due to a higher F). Both factors lead to a relative heavier isotopic signature (Fig.7). This model prediction is in excellent agreement with our experimental results. Experiments performed with the same growth rate of $\sim 1.5 \text{ mg mg}^{-1} \text{ h}^{-1}$ show at

32°C a 2‰ heavier $\delta^{11}\text{B}$ value than at 22°C (Fig. 2B).

4.4.2 Constant temperature – various growth rates

For experiments conducted at the same temperature but at various growth rates, the SEMO predicts that with increasing growth rate new layers are added faster leaving less time for B to diffuse out of S while the inner layer of S becomes part of the bulk lattice of the crystal (C_1). Since ^{10}B has a higher diffusivity than ^{11}B , the time for ^{10}B to diffuse out of C_1 is shorter i.e. depletion in ^{10}B is less effective at higher growth rates. According to the SEMO, the latter leads to a lighter $\delta^{11}\text{B}$ of C_1 at a higher growth rate. This prediction is exactly what we see in our data (Fig. 2B): Experiments conducted at 22°C show a decrease in $\delta^{11}\text{B}$ of 1.3‰ if the calcite growth rate increases from 0.69 to 1.44 $\text{mg mg}^{-1} \text{h}^{-1}$. The same trend can be seen in the data of Sanyal and co-workers (2000). With increasing growth rates the deviation from the isotopic signature of $\text{B}(\text{OH})_4^-$ increases.

Assuming the same behavior for B isotopes as for the Ca isotopes (Tang et al., 2008a) we could show that the SEMO is able to describe the effect of temperature and growth rate on the B isotope fractionation during calcite precipitation. It should be noted that this suggests that the incorporation of very different ions, Ca^{2+} being a divalent cat-ion substituted for Ca^{2+} in the calcite lattice and B, a monovalent an-ion most probably incorporated as $\text{B}(\text{OH})_4^-$ at a CO_3^- site, can be explained by the same processes in which the heavier isotope is depleted in the surface layer of the crystal.

4.5 Decoupling the effect of temperature and growth rate

Since we could separate the effects of temperature and growth rate on the B incorporation using the SEMO, we summarize the processes leading to the observed data in the following conceptual model (Fig. 8). The $\Delta\delta^{11}\text{B}$ value ($\delta^{11}\text{B}$ of calcite normalized to the $\delta^{11}\text{B}$ of $\text{B}(\text{OH})_4^-$) determined at 12°C and R of 0.18 $\text{mg mg}^{-1} \text{h}^{-1}$ shows (within error) no fractionation between calcite and $\text{B}(\text{OH})_4^-$ of solution (first data point). Therefore this is regarded as calcite growth with a B fractionation close to thermodynamic equilibrium. Increasing growth rate (second data point) from 0.18 to 0.69 $\text{mg mg}^{-1} \text{h}^{-1}$ leads to an increasingly negative $\Delta\delta^{11}\text{B}$ value but due to the compensating effect caused by the increased temperature (from 12°C to 22°C) the $\Delta\delta^{11}\text{B}$ value is similar to the value at equilibrium. The third data point, (same

temperature of 22°C but a significantly higher growth rate of 1.44 mg mg⁻¹ h⁻¹) deviates significantly from the equilibrium fractionation. If the temperature is increased to 32°C but the growth rate is unchanged (fourth data point), $\Delta\delta^{11}\text{B}$ of calcite is shifted back again to a value expected for equilibrium fractionation of B isotopes. In summary, the increase in T and R applied in this study changes the B isotopic composition in opposing directions by almost the same magnitude.

The same principle holds for the B incorporation into calcite shown in Figure 3. At the lowest temperature and growth rate, calcite has the lowest K_D . With increasing growth rate K_D increases, but an increase in temperature counteracts/compensates the effect of growth rate. Hence, the values determined at the highest temperature (32°C) and the highest growth rate (1.50 mg mg⁻¹ h⁻¹) are close to the value determined at the lowest temperature (12°C) and the lowest growth rate (0.18 mg mg⁻¹ h⁻¹).

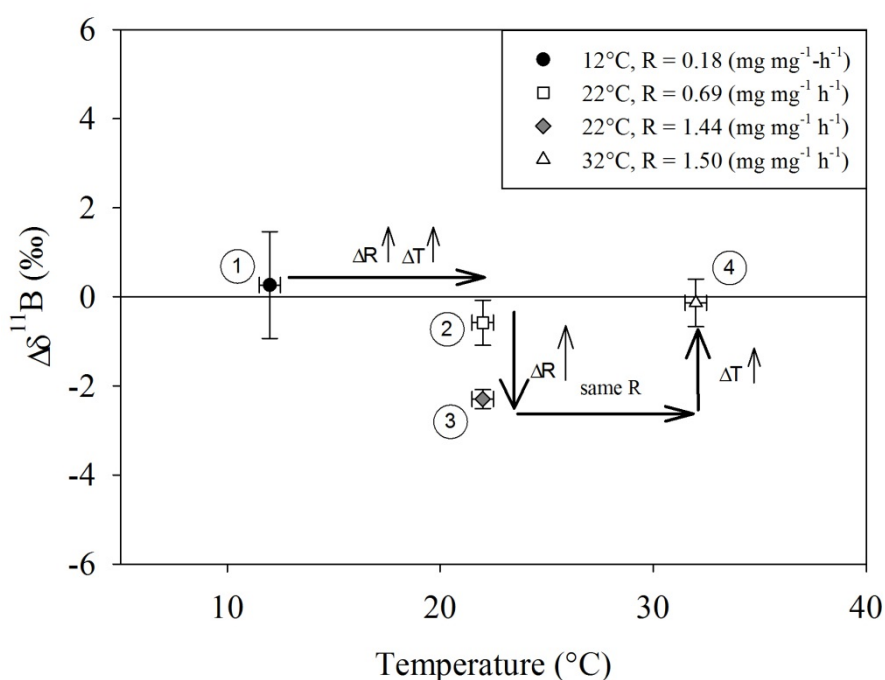


Figure 8: A conceptual illustration summarizing how temperature and growth rate effect the B isotope fractionation in inorganically precipitated calcite. The y-axis shows ($\Delta\delta^{11}\text{B}$), the deviation in $\delta^{11}\text{B}$ of calcite and $\text{B}(\text{OH})_4^-$. The first data point (12°C and $R = 0.18$ (mg mg⁻¹ h⁻¹)) is close to thermodynamic equilibrium and the $\delta^{11}\text{B}$ of the calcite matches the $\delta^{11}\text{B}$ of $\text{B}(\text{OH})_4^-$ very well (no fractionation between solution and calcite). A simultaneous increase in T and R ($T: 12 \rightarrow 22^\circ\text{C}$, $R: 0.18 \rightarrow 0.69$ mg mg⁻¹ h⁻¹) does not change the measured fractionation as seen from the second data point. Even though temperature and growth rate do effect the isotope fractionation, they operate in opposite directions and compensate their effects. Doubling R while keeping T constant ($R = 0.69 \rightarrow 1.44$ mg mg⁻¹ h⁻¹, $T = 22^\circ\text{C}$) leads to a more negative $\Delta\delta^{11}\text{B}$ (as illustrated by the third data point). Keeping R constant but increasing T ($R = 1.5$ mg mg⁻¹ h⁻¹, $22 \rightarrow 32^\circ\text{C}$) as illustrated by the fourth data point compensates again the previously shown effect of R leading to a more positive $\Delta\delta^{11}\text{B}$ of the precipitated calcite.

4.6 Implications on paleo proxies

One of the most ambiguous tasks in finding the component in the biomineralization process is to describe the chemical environment at the site of calcification. Throughout the literature the ideas about the biomineralization processes of foraminifers are diverse ranging from more or less modified seawater being taken up by vacuolization e.g. (Bentov et al., 2009) to selective ion transport to the site of calcification (Nehrke et al., 2013). Even if the exact pathway of ions to the site of calcification is unknown, we can still evaluate whether the B concentration and B isotope fractionation in foraminiferal tests show the same temperature dependence determined for inorganic calcite precipitation.

We could show that for inorganically precipitated calcite the effect of temperature on the B incorporation and B isotope fractionation is compensated by the effect of an increasing growth rate. In a natural system i.e. if temperature and growth rate are not experimentally decoupled a temperature induced change in growth rate would result in a B incorporation and B isotope fractionation that does to all appearances not change with temperature. For foraminifers two different trends for the B incorporation as a function of temperature are described in the literature: no impact (Allen et al., 2011) and an increase (Yu et al., 2007; Wara et al., 2003; Tripathi et al., 2011). This demonstrates that the effect of temperature may be species specific and a general prediction not possible. Unfortunately, no data is available with regard to the effect of temperature on B isotope fractionation in foraminifers.

For a biogenic system it is possible that parameters like light or nutrient availability will lead to changes in calcification rate not associated with changes in temperature. For an increase in growth rate we predict an increase in B incorporation and a lighter $\delta^{11}\text{B}$ of the inorganically precipitated calcite. As mentioned in the introduction it is difficult to determine the growth rate of foraminifers. Often heavier shells are interpreted as related to higher growth rates. Wara et al. (2003) reported for *Globogerinoides sacculifer* that B incorporation decreases and $\delta^{11}\text{B}$ gets heavier with increasing shell mass (the latter with a quite poor R^2 of 0.25). Hönisch & Hemming (2004) report for the same species $\delta^{11}\text{B}$ to be heavier with increasing shell mass. These findings suggest that the trend for the species investigated is the opposite as observed for the inorganic system, or that increased shell mass is an indication for a decreased growth rate rather than an increased one.

5. CONCLUSION

Application of the SEMO to the experimental data obtained in this study showed that temperature and growth rate both effect the B incorporation and isotope fractionation during inorganic calcite precipitation. The effects of temperature and growth rate change the $\delta^{11}\text{B}$ in opposing directions with nearly equal amplitudes under the investigated conditions. Their effects on B incorporation and isotope fractionation are easily masked if temperature and growth rate are not decoupled experimentally. The occurrence of kinetic effects on the B isotope fractionation during calcite precipitation revealed in this study explains why some experimental data (Sanyal et al., 2000) deviate significantly from the isotopic composition of $\text{B}(\text{OH})_4^-$.

A comparison with literature data shows that there is no clear trend between the B concentration and isotope data obtained from inorganic experiments and from foraminifers suggesting that species specific physiological effects dominate over the effects observed for the pure inorganic system.

So far the SEMO has been applied to cat-ions such as Sr and Ca isotopes which are incorporated in a Ca site of the crystal lattice. In this study we could show that the SEMO can also be applied to a system in which a $\text{B}(\text{OH})_4^-$ ion substitutes for CO_3^- .

ACKNOWLEDGMENTS

We thank Sarah Moser and Kerstin Oetjen for assistance during the experiments. For analysis of DIC and elemental measurements we thank Laura Wischnewski, Jana Hölscher and Ilsetraut Stölting. This project was financially supported by the DFG BI 432/7-1.

REFERENCES

- Allen, K.A., Hönlisch, B., Eggins, S.M., Yu, J., Spero, H.J., Elderfield, H., 2011. Controls on boron incorporation in cultured tests of the planktic foraminifer *Orbulina universa*. *Earth and Planetary Science Letters* 309, 291-301.
- Bentov, S., Brownlee, C., Erez, J., 2009. The role of seawater endocytosis in the biomineralization process in calcareous foraminifera. *Proceedings of the National Academy of Sciences* 106, 21500-21504.
- Boyle, E.A., 1988. Cadmium: Chemical tracer of deepwater paleoceanography. *Paleoceanography* 3, 471-489.
- Brown, R.E., Anderson, L.D., Thomas, E., Zachos, J.C., 2011. A core-top calibration of B/Ca in the benthic foraminifera *Nuttallides umbonifera* and *Oridorsalis umbonatus*: A proxy for Cenozoic bottom water carbonate saturation. *Earth and Planetary Science Letters* 310, 360-368.
- Catanzaro, E.J., Champion, C.E., Garner, E.L., Marinenko, G., Sappenfield, K.M., Shields, W.R., 1970. Boric Acid. Isotopic, and Assay Standard Reference Materials Nat. Bur. Stand. (U.S.) Spec. Publ. 260-17, 70.
- DOE, 1994. Handbook of Methods for the Analysis of the Various Parameters of the Carbon Dioxide System in Sea Water; version 2, Dickson, A.G., Goyet, C. eds., ORNL/CDIAC-74.
- Fenter, P., Geissbühler, P., DiMasi, E., Srajer, G., Sorensen, L.B., Sturchio, N.C., 2000. Surface speciation of calcite observed in situ by high-resolution X-ray reflectivity. *Geochimica et Cosmochimica Acta* 64, 1221-1228.
- Foster, G.L., Pogge von Strandmann, P.A.E., Rae, J.W.B., 2010. Boron and magnesium isotopic composition of seawater. *Geochemistry, Geophysics, Geosystems* 11, Q08015.
- Gaillardet, J., Lemarchand, D., Gopel, C., Manhès, G., 2001. Evaporation and sublimation of boric acid: Application for boron purification from organic rich solutions. *Geostandards Newsletter* 25, 67-75.
- Gussone, N., Böhm, F., Eisenhauer, A., Dietzel, M., Heuser, A., Teichert, B.M.A., Reitner, J., Wörheide, G., Dullo, W.-C., 2005. Calcium isotope fractionation in calcite and aragonite. *Geochimica et Cosmochimica Acta* 69, 4485-4494.
- Gussone, N., Eisenhauer, A., Heuser, A., Dietzel, M., Bock, B., Böhm, F., Spero, H.J., Lea, D.W., Bijma, J., Nägler, T.F., 2003. Model for kinetic effects on calcium isotope fractionation ($\delta^{44}\text{Ca}$) in inorganic aragonite and cultured planktonic foraminifera. *Geochimica et Cosmochimica Acta* 67, 1375-1382.
- Gustafsson, J.P., 2008. *Visual MINTEQ Version 3.0*.
- Hall, R.N., 1953. Segregation of Impurities During the Growth of Germanium and Silicon. *The Journal of Physical Chemistry* 57, 836-839.
- Hemming, N.G., Hanson, G.N., 1992. Boron isotopic composition and concentration in modern marine carbonates. *Geochimica et Cosmochimica Acta* 56, 537-543.
- Heumann, K.G., Ginder, F., Klöppel, H., 1977. Dependence of the Calcium Isotope Effect upon the Electrolyte Concentration in Ion-Exchange Chromatography. *Angewandte Chemie International Edition in English* 16, 719-720.
- Hoffmann, U., Stipp, S.L.S., 2001. The behavior of Ni^{2+} on calcite surfaces. *Geochimica et Cosmochimica Acta* 65, 4131-4139.

- Hönisch, B., Hemming, N.G., 2004. Ground-truthing the boron isotope-paleo-pH proxy in planktonic foraminifera shells: Partial dissolution and shell size effects. *Paleoceanography* 19, PA4010.
- Kakahana, H., Kotaka, M., Satoh, S., Nomura, M., Okamoto, M., 1977. Fundamental Studies on the Ion-Exchange Separation of Boron Isotopes. *Bulletin of the Chemical Society of Japan* 50, 158-163.
- Klochko, K., Cody, G.D., Tossell, J.A., Dera, P., Kaufman, A.J., 2009. Re-evaluating boron speciation in biogenic calcite and aragonite using ^{11}B MAS NMR. *Geochimica et Cosmochimica Acta* 73, 1890-1900.
- Klochko, K., Kaufman, A.J., Yao, W., Byrne, R.H., Tossell, J.A., 2006. Experimental measurement of boron isotope fractionation in seawater. *Earth and Planetary Science Letters* 248, 276-285.
- Lorens, R.B., 1981. Sr, Cd, Mn and Co distribution coefficients in calcite as a function of calcite precipitation rate. *Geochimica et Cosmochimica Acta* 45, 553-561.
- Marriott, C.S., Henderson, G.M., Belshaw, N.S., Tudhope, A.W., 2004. Temperature dependence of $\delta^7\text{Li}$, $\delta^{44}\text{Ca}$ and Li/Ca during growth of calcium carbonate. *Earth and Planetary Science Letters* 222, 615-624.
- Misra, S., Owen, R., Kerr, J., Greaves, M., Elderfield, H., 2014 a. Determination of $\delta^{11}\text{B}$ by HR-ICP-MS from Mass Limited Samples: Application to Natural Carbonates and Water Samples. *Geochimica et Cosmochimica Acta* in review.
- Misra, S., Greaves M., Owen, R., Kerr, J., Elmore, A.C., Elderfield, H., 2014 b. Determination of B/Ca of natural carbonates by HR-ICP-MS. *Geochemistry, Geophysics, Geosystems* in press.
- Nehrke, G., Keul, N., Langer, G., de Nooijer, L.J., Bijma, J., Meibom, A., 2013. A new model for biomineralization and trace-element signatures of Foraminifera tests. *Biogeosciences* 10, 6759-6767.
- Nehrke, G., Reichart, G.J., Van Cappellen, P., Meile, C., Bijma, J., 2007. Dependence of calcite growth rate and Sr partitioning on solution stoichiometry: Non-Kossel crystal growth. *Geochimica et Cosmochimica Acta* 71, 2240-2249.
- Ni, Y., Foster, G.L., Bailey, T., Elliott, T., Schmidt, D.N., Pearson, P., Haley, B., Coath, C., 2007. A core top assessment of proxies for the ocean carbonate system in surface-dwelling foraminifers. *Paleoceanography* 22, PA3212.
- Rimstidt, J.D., Balog, A., Webb, J., 1998. Distribution of trace elements between carbonate minerals and aqueous solutions. *Geochimica et Cosmochimica Acta* 62, 1851-1863.
- Ruiz-Agudo, E., Putnis, C.V., Kowacz, M., Ortega-Huertas, M., Putnis, A., 2012. Boron incorporation into calcite during growth: Implications for the use of boron in carbonates as a pH proxy. *Earth and Planetary Science Letters* 345, 9-17.
- Sanyal, A., Hemming, N.G., Broecker, W.S., David, W.L., Spero, H.J., Hanson, G.N., 1996. Oceanic pH control on the boron isotopic composition of foraminifera: Evidence from culture experiments. *Paleoceanography* 11, 513-517.
- Sanyal, A., Nugent, M., Reeder, R.J., Bijma, J., 2000. Seawater pH control on the boron isotopic composition of calcite: evidence from inorganic calcite precipitation experiments. *Geochimica et Cosmochimica Acta* 64, 1551-1555.
- Spivack, A.J., Edmond, J.M., 1987. Boron isotope exchange between seawater and the oceanic crust. *Geochimica et Cosmochimica Acta* 51, 1033-1043.
- Stipp, S.L., Hochella Jr, M.F., Parks, G.A., Leckie, J.O., 1992. Cd^{2+} uptake by calcite, solid-state

diffusion, and the formation of solid-solution: Interface processes observed with near-surface sensitive techniques (XPS, LEED, and AES). *Geochimica et Cosmochimica Acta* 56, 1941-1954.

Stipp, S.L.S., 1998. Surface analytical techniques applied to calcite: evidence of solid-state diffusion and implications for isotope methods. *Palaeogeography, Palaeoclimatology, Palaeoecology* 140, 441-457.

Tang, J., Dietzel, M., Böhm, F., Köhler, S.J., Eisenhauer, A., 2008a. Sr²⁺/Ca²⁺ and ⁴⁴Ca/⁴⁰Ca fractionation during inorganic calcite formation: II. Ca isotopes. *Geochimica et Cosmochimica Acta* 72, 3733-3745.

Tang, J., Köhler, S.J., Dietzel, M., 2008b. Sr²⁺/Ca²⁺ and ⁴⁴Ca/⁴⁰Ca fractionation during inorganic calcite formation: I. Sr incorporation. *Geochimica et Cosmochimica Acta* 72, 3718-3732.

Tiller, W.A., Ahn, K.-S., 1980. Interface field effects on solute redistribution during crystallization. *Journal of Crystal Growth* 49, 483-501.

Tripathi, A.K., Roberts, C.D., Eagle, R.A., Li, G., 2011. A 20 million year record of planktic foraminiferal B/Ca ratios: Systematics and uncertainties in pCO₂ reconstructions. *Geochimica et Cosmochimica Acta* 75, 2582-2610.

Urey, H.C., 1947. The thermodynamic properties of isotopic substances. *Journal of the Chemical Society (Resumed)*, 562-581.

Vogl, J., Rosner, M., 2012. Production and Certification of a Unique Set of Isotope and Delta Reference Materials for Boron Isotope Determination in Geochemical, Environmental and Industrial Materials. *Geostandards and Geoanalytical Research* 36, 161-175.

Wang, B.-S., You, C.-F., Huang, K.-F., Wu, S.-F., Aggarwal, S.K., Chung, C.-H., Lin, P.-Y., 2010. Direct separation of boron from Na- and Ca-rich matrices by sublimation for stable isotope measurement by MC-ICP-MS. *Talanta* 82, 1378-1384.

Wara, M.W., Delaney, M.L., Bullen, T.D., Ravelo, A.C., 2003. Possible roles of pH, temperature, and partial dissolution in determining boron concentration and isotopic composition in planktonic foraminifera. *Paleoceanography* 18, 1100.

Watson, E.B., 1996. Surface enrichment and trace-element uptake during crystal growth. *Geochimica et Cosmochimica Acta* 60, 5013-5020.

Watson, E.B., 2004. A conceptual model for near-surface kinetic controls on the trace-element and stable isotope composition of abiogenic calcite crystals. *Geochimica et Cosmochimica Acta* 68, 1473-1488.

Watson, E.B., Liang, Y., 1995. A simple model for sector zoning in slowly grown crystals: Implications for growth rate and lattice diffusion, with emphasis on accessory minerals in crustal rocks. *American Mineralogist* 80, 1179-1187.

Wefer, G., Berger, W.H., Bijma, J., Fisher, G., 1999. Clues to Ocean History: a Brief Overview of Proxies, in: Fischer, G., Wefer, G. (Eds.), *Use of Proxies in Paleoceanography: Examples from the South Atlantic*. Springer, Berlin, Heidelberg, pp. 1-68.

Wolthers, M., Nehrke, G., Gustafsson, J.P., Van Cappellen, P., 2012. Calcite growth kinetics: Modeling the effect of solution stoichiometry. *Geochimica et Cosmochimica Acta* 77, 121-134.

Yu, J., Elderfield, H., 2007. Benthic foraminiferal B/Ca ratios reflect deep water carbonate saturation state. *Earth and Planetary Science Letters* 258, 73-86.

Yu, J., Elderfield, H., Hönisch, B., 2007. B/Ca in planktonic foraminifera as a proxy for surface seawater pH. *Paleoceanography* 22, PA2202.

Yu, J., Foster, G.L., Elderfield, H., Broecker, W.S., Clark, E., 2010. An evaluation of benthic foraminiferal B/Ca and $\delta^{11}\text{B}$ for deep ocean carbonate ion and pH reconstructions. *Earth and Planetary Science Letters* 293, 114-120.

Zeebe, R.E., 2005. Stable boron isotope fractionation between dissolved $\text{B}(\text{OH})_3$ and $\text{B}(\text{OH})_4^-$. *Geochimica et Cosmochimica Acta* 69, 2753-2766.

Zeebe, R.E., Wolf-Gladrow, D.A., 2001. *CO₂ in seawater: equilibrium, kinetics, isotopes*. Elsevier Science B.V., Amsterdam.

Topic 2

Simultaneous determination of $\delta^{11}\text{B}$ and B/Ca in marine biogenic carbonates at nano gram level

Karina Kaczmarek^{1*}

* corresponding author: Email: karina.kaczmarek@awi.de

Ingo Horn²

Gernot Nehrke¹

Jelle Bijma¹

¹Alfred-Wegener Institut Helmholtz-Zentrum für Polar- und Meeresforschung, am Handelshafen 12, 27570 Bremerhaven, Germany

²Institute of Mineralogy, Leibniz University, Callin street 3, 30167 Hannover, Germany

ABSTRACT

In this study we introduce a new *in situ* technique which allows the determination of the boron isotopic composition and B/Ca ratios simultaneously at the nanogram level on single foraminiferal shells using a combination of optical emission spectroscopy and multiple ion counting MC ICP-MS with laser ablation. This technique offers a new application in the paleo field of oceanography and climatology. The simultaneous determination of the boron isotopic composition and B/Ca ratios provides two independent proxies which allow the reconstruction of the full carbonate system. To test the new technique, we performed measurements on the cultured, benthic foraminifer *Amphistegina lessonii*. Our results yielded an average boron isotopic composition $\delta^{11}\text{B} = 18.0 \pm 0.83\text{‰}$ (SD) with an average internal precision of 0.52‰ (RSE). The boron concentration was $53 \pm 7 \mu\text{g/g}$ (SD). These results agree with the range reported in the literature. The reconstructed mean pH value is in excellent agreement with the measured pH of the seawater in which the foraminifers grew. The analysis of a foraminifer consumed approximately 1200 ng calcium carbonate containing ca. 0.06 ng boron. Compared to bulk analytical methods this new technique requires less material and reduces the time

for sample preparation. However, laser ablation of single foraminiferal tests requires sufficiently large specimens (400 μm) and thick chamber walls (10 μm). Holes caused by laser ablation and a B isotope inhomogeneity lower the internal precision. In addition to the foraminifers a massive piece of a coral (*Porites lutea*) was measured providing sufficient material for laser ablation. The average internal precision improved to 0.29‰ (RSE).

1. INTRODUCTION

Element signatures of biogenic marine calcium carbonates (CaCO_3) are powerful tools to reconstruct the physico-chemical conditions of the environment. The incorporation of boron (B) into biogenic CaCO_3 such as the skeletons of corals or tests (shells) of foraminifers is of particular interest because its concentration and isotopic composition records information about the marine carbonate system which in turn allows the calculation of atmospheric CO_2 concentration.

In seawater B mainly exists as boric acid (BOH_3) and borate (BOH_4^-) whose species distribution and isotopic composition is strongly pH dependent (Dickson, 1990). The B isotopic composition of coral and foraminiferal CaCO_3 provided strong evidence that only borate is incorporated into CaCO_3 (Hemming and Hanson, 1992). Hence, the B isotopic composition of CaCO_3 reflects the B isotopic composition of borate in seawater. Based on this relationship the B isotopic composition of several foraminiferal species was used to reconstruct past seawater pH (Sanyal et al, 1995; Hönisch & Hemming 2005; Yu et al., 2010). The second B based proxy is rooted in the observed linearity between B/Ca ratios determined in foraminifers and CO_3^{2-} concentration in seawater (Yu & Elderfield, 2007; Yu et al., 2010; Brown et al., 2011).

Several analytical techniques are used to measure the B isotopic composition in marine carbonates:

- 1) thermal ionisation mass spectrometry (TIMS) (N-TIMS (e.g. Hemming & Hanson, 1994; Sanyal et al., 1996), P-TIMS (e.g. Gaillardet & Allègre, 1995), TE-TIMS (Foster et al., 2006))
- 2) multi collector-inductively coupled plasma-mass spectrometry (MC-ICP-MS (e.g. Lécuyer et al., 2002; Foster, 2008; Louvat et al., 2010))
- 3) secondary ion mass spectrometry (SIMS (e.g. Kasemann et al., 2009; Rollion-Bard & Erez, 2010))
- 4) laser ablation (LA) MC-ICP-MS (Fietzke et al. 2010).

For TIMS and MC-ICP-MS samples have to be dissolved. For the latter an additional matrix separation of B is needed. SIMS requires a flat sample surface whereas for LA MC-ICP-MS no sample preparation is required.

While TIMS and MC-ICP-MS represent bulk analytical techniques, SIMS and LA MC-ICP-MS are *in situ* techniques which allow determining the isotope ratios and elemental concentrations (but not simultaneously) with high spatial resolution. This needs far less material than bulk analytical techniques which allows performing measurements on e.g. single specimens of foraminifers. Furthermore, it is possible to resolve the spatial variation in the B isotopic composition and B concentration observed in most biogenic carbonates on the μm scale. This can help to develop a process based understanding of B incorporation into foraminiferal CaCO_3 , a process which is still not fully understood but fundamental for the use of B as a paleo proxy. However, due to this inhomogeneity the question arises how many measurements are required to reach a precision comparable to that of bulk analytical techniques.

For a pH reconstruction with a resolution of ~ 0.1 pH unit using boron isotopes a precision better than 1‰ (2SD) is required (Foster et al., 2006). A comparison of the precision of a variety of analytical techniques for B isotope determination is shown in Figure 1. The highest amount of total B is needed for P-TIMS (2000 ng) to achieve a precision (2SD) of 0.5‰. Far less material (30 ng B) is consumed using MC-ICP-MS giving the highest precision of 0.25‰. For the N-TIMS and TE-TIMS

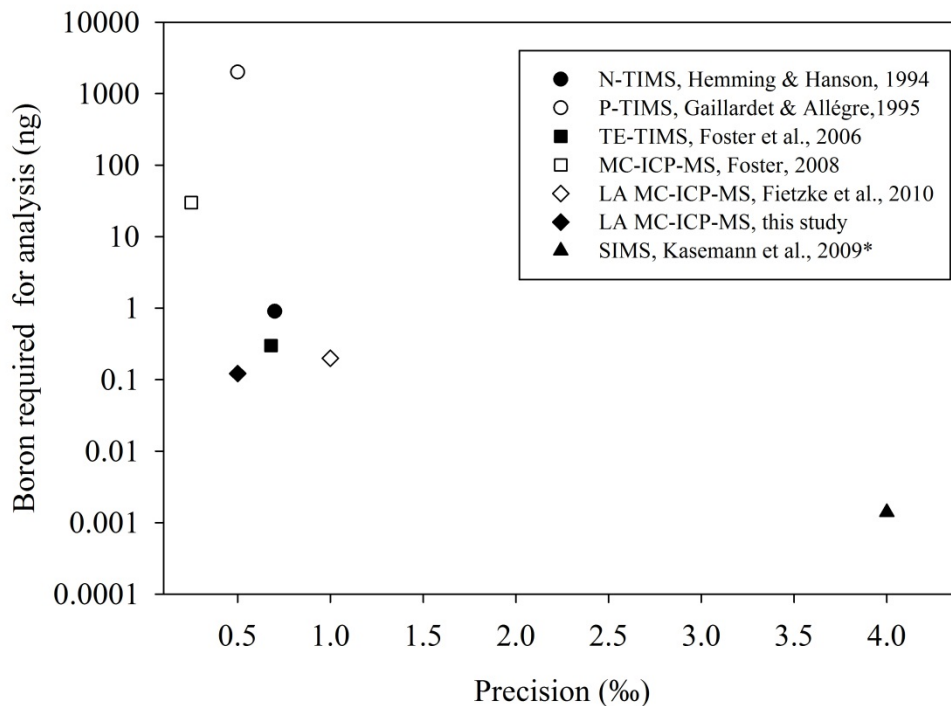


Figure 1: Precision and amount of required boron for various analytical techniques for boron isotope analysis in carbonate matrices (corals) and foraminifers (TE-NTIMS). *Required B amount was calculated assuming a sputter rate of $0.0066\mu\text{m}^3/\text{nAs}$.

approach about three times less B is required resulting in a precision of $\sim 0.7\text{‰}$. Techniques with the lowest demand of B are LA MC-ICP-MS (0.2; 0.03 ng) and SIMS (0.0014 ng). While the latter suffers from the worst precision (4‰), LA MC-ICP-MS achieves a precision ranging between 0.5 and 1‰. Using LA MC-ICP-MS in combination with ion counters instead of faraday cups the required B amount can be reduced by almost a factor of ten.

Although MC-ICP-MS shows a higher instrumental mass bias compared to NTIMS the results obtained by Aggarwal et al. (2004) indicate that mass bias has no significant impact on $\delta^{11}\text{B}$ accuracy and precision. Since boron has only two natural isotopes, it is impossible to perform isotope labelling experiments with known isotopic signatures to assess the amount of fractionation during sample preparation and TIMS measurements. To correct for mass bias during TIMS measurements, the isotope dilution technique (Duchateau & de Bièvre, 1983) is applied and strict protocols are required to achieve a good reproducibility. MC-ICP-MS suffers from the temporal drift and the machine

induced fractionation but these effects can be corrected using the sample standard bracketing procedure.

Several laser ablation studies on B isotopes have been carried out but these studies focused on samples with a silica matrix (le Roux et al., 2004; Tiepolo et al., 2006; Hou et al., 2010; Mikova et al., 2014). The limitation of B measurements on carbonate samples using laser ablation is the absence of a solid matrix matched standard. However, Fietzke et al. (2010) recently carried out B isotopic measurements using LA MC-ICP-MS on silicate glass standards as reference material and showed that no matrix dependent offsets between silicate and carbonate matrices exist suggesting that silicate glass standards may serve as adequate reference material.

Several studies determined $\delta^{11}\text{B}$ and B/Ca on the same set of samples (Wara et al., 2003; Ni et al., 2007; Yu et al., 2010). For these studies the sample requirement was large since the B isotope signature and B concentration were determined separately.

In this study we present a new analytical approach which allows the simultaneous determination of the B isotopic composition and B/Ca ratios in biogenic marine carbonates using LA MC-ICP-MS in combination with ICP-OES and using a silicate glass standard. This new approach offers the possibility to obtain two independent parameters of the carbonate system from the same sample which allows to fully constrain the carbonate chemistry. Since biogenic carbonates are known to be inhomogeneous on the μm scale it is of great importance to be able to directly relate the B isotopic composition obtained at one position with the B concentration at the same position.

This technique can be applied on single foraminiferal tests and no sample preparation is required avoiding the possibility of sample contamination. We determined the $\delta^{11}\text{B}$ and B/Ca ratios of cultured, benthic foraminifers (*Amphistegina lessonii*) and a natural grown coral sample (*Porites lutea*).

2. MATERIAL AND METHODS

2.1. Simultaneous determination of B isotopic composition and B concentration

The measured B intensity of a reference material corresponds to its known B concentration. Based on this relationship the unknown B concentration of a sample can be calculated. However, in our case measurements of the reference material (SRMNIST 610) and samples have not been performed at the same laser repetition rate (as pointed out in section 2.5.) hence, their B ratio is not proportional. The correction for different laser repetition rates e.g. for the amount of material ablated and transported to the ICP can be realized using an optical spectrometer by the collection of Ca on the two high intensity first order emission lines of Ca II at 393.48 and 396.86 nm in cps. This is required as B isotope measurements are performed in static mode of the mass spectrometer. Peak jumping would result in significant loss of time resolution. The detection of Ca cps of SRMNIST 610 and samples (whose Ca concentrations are known: [Ca] of SRMNIST 610 is 8.45%, [Ca] of CaCO₃ is 40%) allows to correct for different laser repetition rates using the equation (Longerich et al., 1996):

$$Ablation\ yield = \left(\frac{Ca\ cps\ NIST610}{8.45 \times 40} \right) / Ca\ cps_{sample} \quad (2.1)$$

Subsequently, the B intensity of the samples is corrected after:

$$Boron\ yield\ corr. = \frac{B\ cps_{sample}}{ablation\ yield \times 100} \quad (2.2)$$

Finally, the B concentration of the sample can be calculated according to:

$$[B](ppm) = \frac{B\ cps_{sample} \times ablation\ yield}{B\ cps_{NIST\ 610} / 351} \quad (2.3)$$

For simultaneous determination of B isotopic composition and B concentration a Fiber Optics Spectrometer (Maya2000 Pro, Ocean Optics) was connected to the torch of a Thermo Finnigan Neptune multiple-collector inductively coupled plasma mass spectrometer (MC-ICP-MS) at the Leibniz University of Hannover. Laser Ablation on reference material and samples was performed by an in-house build UV-femtosecond laser ablation system based on a regenerative one box femtosecond laser (Solstice Newport/Spectra Physics).

2.2. Optical Emission Analysis

Ocean Optics Maya2000 Pro is a high-sensitivity fiber optical spectrometer. It exhibits a measuring range of 250 to 460 nm with a resolution of 0.11 nm covering the first order emission lines of Mg, Ca, Sr, and Ba. It is equipped with a back-thinned 2D FFT-CCD detector, and a grating with a groove density of 1200 lines/mm. More technical information about Maya2000 Pro can be found on <http://www.oceanoptics.com/products/maya.asp>. The optical fiber used is two meters long (attenuation of the photon flux is length dependent) connecting the spectrometer with the coupling lens at the end of the plasma torch. Ca II ion lines were measured at a wavelength of 393.48 nm and 396.86 nm. At these wavelengths the Ca spectra shows no detectable interferences for the matrices used. The acquisition parameters of the foraminiferal measurement session were set to acquire 220 cycles per analysis with an integration time of 1 s for each cycle, the integration time of the coral measurement session was 0.25 s for each cycle acquiring 880 cycles. Because of the stable background (BG) signal detected for the first 40 cycles BG correction was done by subtracting its intensity from the intensity of the reference material and samples. Off peak zeros did not result in improvements of the acquired data.

Average count rates of B and Ca of the samples and the reference material are given in Table 1 together with laser efficiencies.

Table 1: Average intensities for Ca and B isotopes counts yielded at different laser ablation rates. The background counts are subtracted.

	Ca (cps)	¹¹ B (cps)	¹⁰ B (cps)	Laser efficiency (Hz)
Benthic foraminifers	24000	313000	68500	20
NIST 610	840	306000	68000	8
Coral	41600	1960000	400000	20
NIST 610	1750	590000	130000	10

2.3. Pre-tests

In order to examine whether the coupling between the Thermo Finnigan Neptune MC ICP-MS and Maya2000 Pro represents a reliable method of simultaneous determination of B isotopic composition and B concentration two pre-tests were conducted.

As a first step it was verified whether the B concentration in several reference materials with a variable B concentration shows a linearity if measured simultaneously using Maya2000 Pro and a conventional HR-ICP-MS. For that purpose Maya2000 Pro was connected with an optic fibre to the coupling lens at the end of the plasma torch of a ThermoScientific Element XR. Simultaneous collection of B cps (Element XR) and Ca cps (Maya2000 Pro) was performed on a variety of reference materials. The Ca data obtained from Maya2000 Pro was used to calculate the B concentration of these materials according to the method described in section 2.1.

Next, we tested the possibility of simultaneous acquisition of B isotopes and Ca intensities. For that purpose Maya2000 Pro was connected to the torch of a Thermo Finnigan Neptune MC ICP-MS. We chose SRMNIST 610 ([B] 351 $\mu\text{g/g}$, [Ca] 8.45%) and SRMNIST 612 ([B] 37 $\mu\text{g/g}$, [Ca] 8.52%) as analysts. Matching of B intensities between those two standards was achieved by changing the laser repetition rate. The Ca intensity obtained from Maya2000 Pro was used in order to correct for different repetition rates allowing to calculate the B concentration of SRMNIST 612.

2.3. Isotope Analysis - Laser ablation

The in-house built laser ablation system (Solstice Newport/Spectra Physics) is based on a 100 femtosecond Ti-sapphire regenerative amplifier system operating at a fundamental wavelength of 777nm in the infrared spectrum. Subsequent harmonic generations produce the wavelengths 389 nm in the second, 259 nm in the third and 194 nm in the fourth harmonic. The pulse energies measured with a pyroelectric sensor (Molelectron, USA) are 3.2mJ/pulse at 777nm, 0.7 mJ/pulse at 259 nm, and 0.085 mJ/pulse at 194 nm. After the fourth harmonic generation stage, the 194 nm beam is steered by eight dichronic mirrors into a 8x objective (NewWave-Research, USA) and focussed onto the sample. Spot size was set to 50 μm for standard and foraminifers. Within this spot an energy density of 2J/cm² is maintained.

2.5. Isotope Analysis - Acquisition parameters

All measurements are carried out in low mass resolution ($\Delta m/m=350$ where m is the mass of the ion of interest and Δm is the mass difference between its 5 and 95% peak height). Compact discrete dynode multipliers (CDD, Thermo) are attached to faraday cups at the low site on L4 and the high site on H4. The low resolution mode is sufficient enough to resolve potential interferences from doubly charged ions due to the intrinsic high resolution in the low mass region. Possible interferences are the clusters of $^{40}\text{Ar}^{4+}$ or $^{20}\text{Ne}^{2+}$ (le Roux et al., 2004) which are well resolved to the background level. Typically obtained peak shapes are shown in Figure 2 for the background signals for both isotopes. Working with ion counters it necessitates to determine the detector dead time especially for isotope ratios with large isotope abundance differences. The dead time corrections have been performed by measuring the $^{238}\text{U}/^{235}\text{U}$ ratio using SRM 981 in a multidynamic measuring sequence. Subsequently, the dead time has been checked prior to every analytical session by analysing SRMNIST 610 using different repetition rates of laser resulting in a counting range between 300000 – 1000000 cps. An illustration of the procedure is provided in Figure 3 where no change in isotopic ratio is apparent for the bracketing sequence. Prior to each analytical session the instrument was tuned for optimal peak shape. Since the measuring sessions of the foraminifers and coral were performed on two separate days the instrumental parameters for the analysis of the foraminifers and coral vary slightly. They are reported in Table 2. All measurements were performed at plateau voltage of the CDDs which was checked prior to every analytical session. Before the beginning of sample analysis, measurements of SRMNIST 610 were continued until instrumental drift due to warm-up was less than 200 ppm over a bracketing sequence duration of twelve minutes. Boron signal intensities of SRMNIST 610 and samples were matched within 10% in signal intensity by adapting the laser repetition rate. For analysis we adopt the standard sample bracketing procedure using SRMNIST 610 as reference material containing 351 $\mu\text{g/g}$ B and 8.45% Ca. The application of this external calibration technique is required for any stable isotope system and allows the correction of the instrumental mass discrimination and its temporal drift by using a reference material of known isotopic composition prior and after the analysis of the samples. The acquisition parameters in static mode for analysis of SRMNIST 610 and samples were set to acquire 200 cycles of 1 s integrations each.

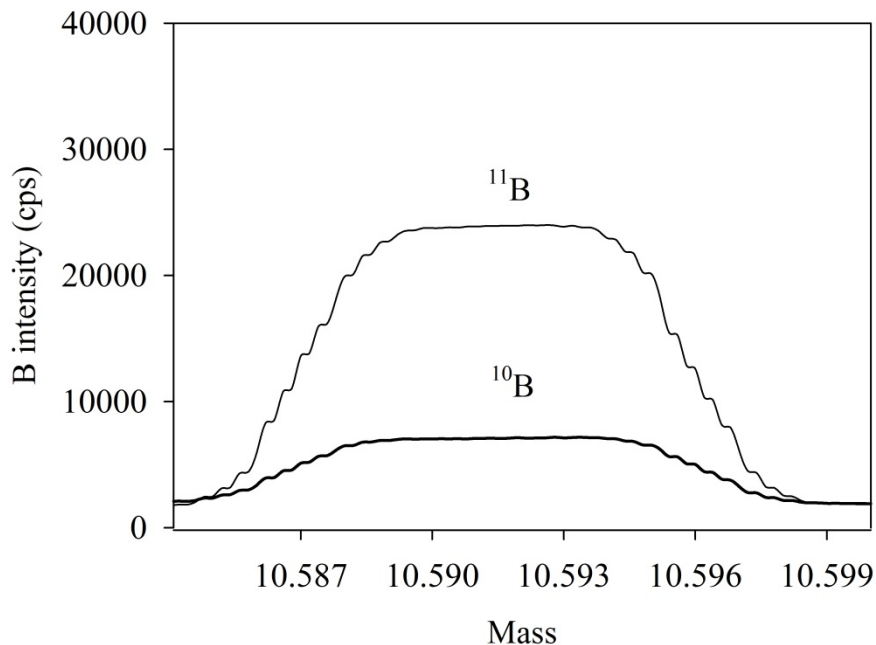


Figure 2: Peak shape of ^{10}B and ^{11}B in low resolution mode. No interferences with Ne^{2+} and Ar^{4+} are observed.

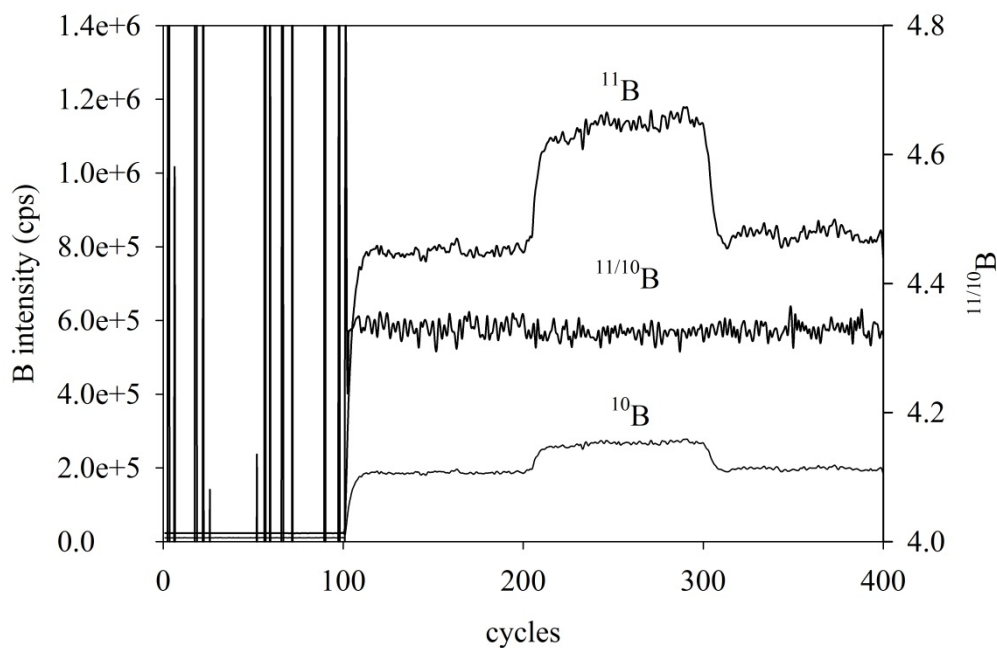


Figure 3: Dead time correction. Spectra of NIST 610 showing the intensity of both isotopes (left y-axis). Ablation was performed by changing the laser repetition rate from 10 (cycles 100-200) to 15 (cycles 200 to 300) to 10 Hz (cycles 300 to 400). The Background was detected from cycle 0 to 100. During the entire measurement the $^{11/10}\text{B}$ remained constant (right y-axis).

Table 2: Instrumental operating conditions for the Neptune MC-ICP-MS and LA.

	benthic foraminifers	coral
Cool Gas[l/min]:	14.6	14.6
Aux Gas[l/min]:	1.2	0.6
Sample Gas[l/min]:	1.3	1.5
Add Gas[l/min]:	0.3	0.4
Operation Power[W]:	1269	1269
Guard electrode:	on	off
Wavelength[nm]:	194	194
Pulse energy[J/cm ²]:	2	2
Pulse width[fs]:	~200	~200
Spot size[μm]:	50	50

During the first 40 cycles the background signal was acquired whereas the remaining cycles represent the sum of the background and reference material, or background and sample signals. A complete measurement consisting of 200 cycles of a single reference material/sample takes four minutes before the next sample can be introduced. Data evaluation was performed using a modified spreadsheet macro ‘LamTool’ initially created for different radiogenic isotope system by Jan Košler. We modified the macro for B isotope analysis. The B isotopic composition is reported using the delta notation:

$$\delta^{11}B_{sample} (\text{‰}) = \left[\frac{(^{11}B/^{10}B)_{sample}}{(^{11}B/^{10}B)_{NIST610}} - 1 \right] \times 1000 \quad (2.4)$$

2.6. Isotope Analysis - Background correction

The BG is a signal noise whose isotopic B ratio (~2.4) differs strongly from that of the reference material and samples (~4). Therefore, a BG correction is essential especially when dealing with constantly decaying background signals. In order to perform a BG correction, the signal of the BG for both isotopes was detected during each measurement in the first 40 cycles by keeping the laser shutter closed and opening for the analysis of the reference material and samples, respectively. Then, the mean value of detected BG intensity was subtracted from the intensity of the reference material/sample for each individual measurement cycle. In general, during the measurement sessions of the foraminifers and the coral we observed a decrease in the BG intensity for both isotopes. By the end of the measurement session of the foraminifers the BG intensity had decreased by 65% for ¹¹B and

47% for ^{10}B (Fig. 4a). By the end of the analysis of the coral the BG intensity decreased by 14% for ^{11}B and 9% for ^{10}B (Fig. 4b). Since we could not assess in how far the continuously changing BG intensity might impact the isotope ratios of the reference material and samples, we performed an additional BG correction by taking the temporal changes in the BG signals into account. This approach represents a time-resolved BG subtraction for each cycle within one measurement. It was performed by the determination of a BG function obtained from plotted BG mean values of all measurements during one analytical session (the daily change in the BG). This BG function determines the BG decrease during the entire measurement session. The best fit through all data points is given when a polynomial of second order is chosen in which “y” represents the BG intensity in cps, “x” represents the time (named as cycles, 1 cycle is 1 s), and the intercept with the y-axis represents the BG of the first measurement of a measurement session (Fig.4a+b). As soon as the BG function was determined for all measurements we used the same function in order to calculate the BG for each cycle within all individual measurements. One measurement consists of 200 cycles. Since we always measured the BG for the first 40 cycles our calculated BG using the BG function should equal the measured BG. The consistence is always larger than 99% when operating at moderate background count rates.

With respect to the foraminifers the comparison between the B isotopic compositions corrected using the conventional BG and the time-resolved BG subtraction shows no significant difference (Table 6). However, an example which shows an influence of the time-resolved BG subtraction is given in the appendix (Table 1A). Here, runs for foraminiferal samples of first test measurements at the beginning of our method development are shown. The difference between the B isotopic compositions corrected using the conventional BG and the time-resolved BG subtraction is up to 2.7‰. With respect to the coral sample a time-resolved BG subtraction could not be performed because the plotted ^{10}B BG intensities show a high scatter and a low R^2 (Fig. 4b). However, in the case of the coral sample we strongly assume that a time-resolved BG subtraction would not change the B isotopic composition much because 1) the decrease in the BG intensity is not as pronounced as observed during the measurement session of the foraminifers 2) the BG intensity detected during the measurement session of the coral was much lower than for the session of foraminifers. In summary, a

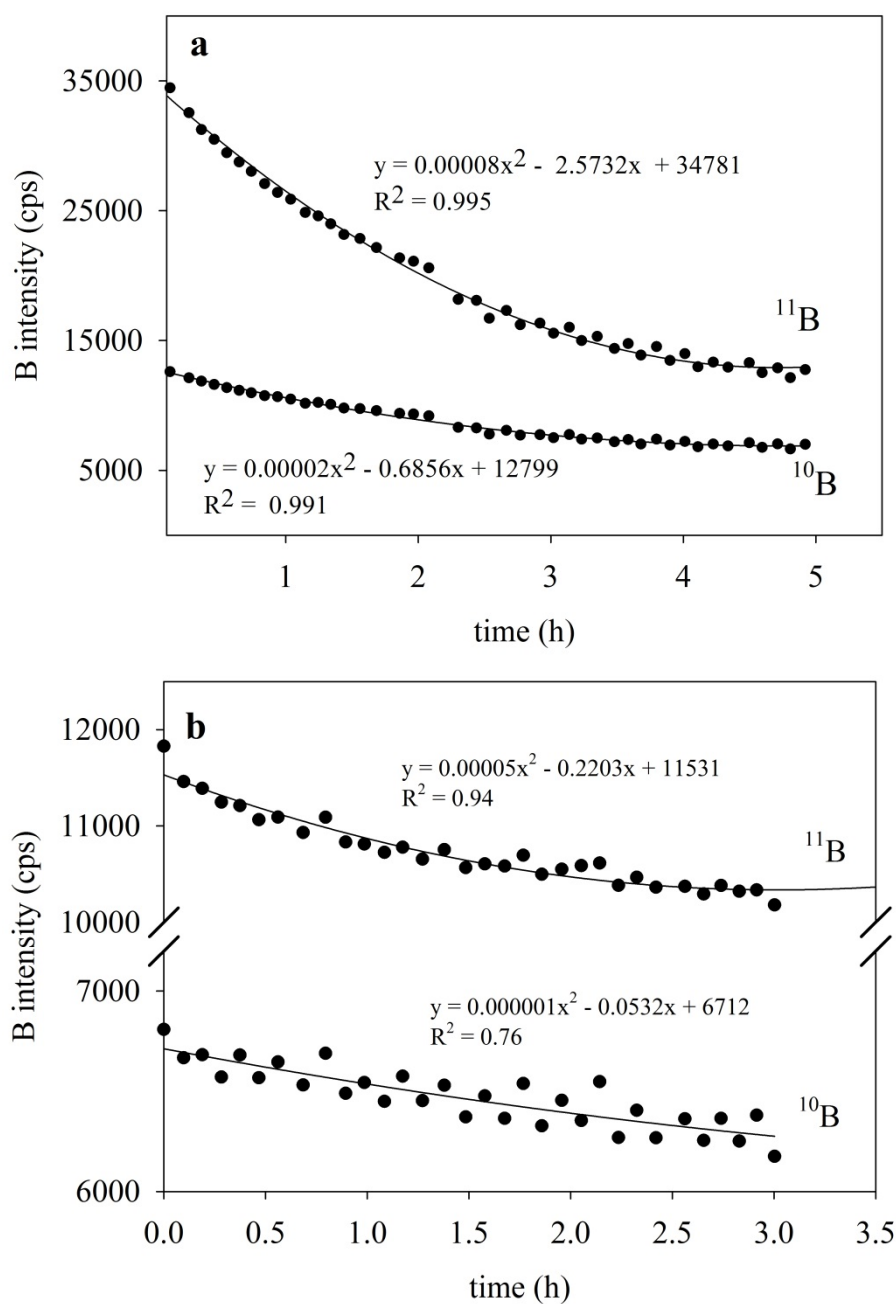


Figure 4: Decrease of the BG signals during the measurement sessions of the foraminifers (a) and the coral (b).

BG correction using the time-resolved BG subtraction is only required when dealing with high and fast decaying BG signal intensities and is important for samples with a low B signal intensity (as shown in Table 1A).

2.7. Comments on errors

In the discussion we will deal with several errors. In order to prevent confusion of the reader we provide a detailed derivation of the errors.

2.7.1. Isotope analysis

One cycle within a measurement corresponds to one $^{11/10}\text{B}$ value. For the analysis of the reference material and the samples we obtain a maximum of 160 $^{11/10}\text{B}$ values ($n=160$) within one measurement. The SD represents the standard deviation of the $^{11/10}\text{B}$ ratios for one measurement. Using SD the standard error (SE) is calculated by SD/\sqrt{n} where n stands for the number of the particular $^{11/10}\text{B}$ ratios obtained for one measurement ($n= 160$). The relative notation of SE (RSE in %) is:

$$RSE(\%) = \frac{SE}{^{11/10}\text{B}} \times 1000 \quad (2.5)$$

Where $^{11/10}\text{B}$ represents the mean value obtained from one measurement. The RSE is an internal error and represents a criterion for the homogeneity of the isotope distribution. If RSE is small the boron isotopes are homogeneously distributed and suggest that one subsample represents a value for the test as a whole. If the B isotope distribution of the sample shows a higher inhomogeneity than the reference material it is recommended to report the RSE of the reference material as an uncertainty of the sample since the analytical uncertainty is assessed more adequately using a homogenous reference material.

The counting statistic error represents a theoretical error estimation which targets the best achievable precision. Practically, calculated errors like RSE (mention above) have to be higher than the best precision determined by counting statistics. In order to assess the error made by counting statistics, we determined the highest and lowest possible counting statistic errors for the measurement sessions of the foraminifers and the coral.

$$|\sigma|_{countstatistic} = \sqrt{\hat{x}_{Bcps} \times n} \quad (2.6)$$

Where n refers to the detection time in s. Absolute errors were calculated taking both isotopes into account. The relative counting statistic error is given by:

$$rel\sigma_{countstatistic}(\%) = \sqrt{\left(\frac{|\sigma|}{\dot{x}_{11Bcps} \times n}\right)^2 + \left(\frac{|\sigma|}{\dot{x}_{10Bcps} \times n}\right)^2} \times 1000 \quad (2.7)$$

The delta notation ($\delta^{11}B$) representing the B isotopic composition of a sample is not a quantity which can be measured directly but depends on two measured quantities ($^{11/10}B$ of SRMNIST 610 and $^{11/10}B$ of sample) and their uncertainties (SE). The error of $\delta^{11}B$ is therefore calculated by error propagation of the ratio $SE/^{11/10}B$ according to the standard bracketing method. It represents an external and absolute error and is expressed as 2RSE:

$$2RSE_{\delta^{11}B}(\%) = \sqrt{\left(\frac{SE}{^{11/10}B}_{NIST-1}\right)^2 + \left(\frac{SE}{^{11/10}B}_{sample}\right)^2 + \left(\frac{SE}{^{11/10}B}_{NIST+1}\right)^2} \times 1000 \times 2 \quad (2.8)$$

Where NIST-1 and NIST +1 represent the reference material measured before and after the sample. The error of $\delta^{11}B$ represents a combination of counting statistics and the homogeneity of B distribution of the analytes.

2.7.2. Boron concentration

For the determination of the relative error of the B concentration and B/Ca we considered the B and Ca concentrations of SRMNIST 610 and their uncertainties known from literature (lit) and the intensities of B and Ca and their uncertainties measured (m) in this study with respect to SRMNIST 610 and the samples where B cps were normalized to Ca cps:

$$RSD_B(\%) = \sqrt{\left(\frac{SD\ B\ conc_{NIST}}{B\ conc_{NIST}}\right)_{lit}^2 + \left(\frac{SD\ Ca\ conc_{NIST}}{Ca\ conc_{NIST}}\right)_{lit}^2 + \left(\frac{SD\ B\ cps_{NIST}}{B\ cps_{NIST}}\right)_m^2 + \left(\frac{SD\ Ca\ cps_{NIST}}{Ca\ cps_{NIST}}\right)_m^2 + \left(\frac{SD\ B\ cps_{sample}}{B\ cps_{sample}}\right)_m^2 + \left(\frac{SD\ Ca\ cps_{sample}}{Ca\ cps_{sample}}\right)_m^2} \times 100 \quad (2.9)$$

2.8. Samples

2.8.1. Benthic foraminifers

Live specimens of the benthic symbiont-bearing foraminifer *Amphistegina lessonii* were obtained from a coral reef aquarium at the Burgers Zoo (Arnhem, The Netherlands). SCUBA divers collected approximately 0.5 kg of sediment containing different species of foraminifers (Ernst et al., 2011). The sediment was transported to the Alfred Wegener Institute – Helmholtz Centre for Polar and Marine Research (Bremerhaven, Germany) immediately. About 30 specimens of *A. lessonii* were transferred to well plates containing North Sea seawater (NSW) and placed in a temperature controlled room at 25°C. After two weeks ~40% of the specimens had reproduced asexually yielding 10-30 juveniles per specimen. Subsequently, juvenile foraminifers were transferred into petri dishes containing NSW (pH 8.08 total scale) and placed in a transparent and gas tight plastic box. Every third day the NSW was replaced by using a freshly opened aliquot from the corresponding batch of NSW. Each time when NSW was replaced, foraminifers were fed with concentrated and sterilized algae *Dunaliella salina*. Before feeding algae were centrifuged to minimize dilution of NSW and exposed to 90°C for 20 minutes after centrifugation in order to reduce bacterial activity. In order to avoid evaporation of NSW in the petri dishes, the air flushing into the plastic box was saturated with water by bubbling it through a fritted wash bottle filled with de-ionized water. A day/night cycle of 12 hours light/dark was applied. Light intensity was 100-150 $\mu\text{mol photons m}^{-2}\text{s}^{-1}$. Foraminifers grew for two months. Afterwards specimens were harvested, bleached in diluted NaOCl (1:3, active chlorine 4.6%) for six hours, rinsed four times using de-ionized water and dried for 12 hours at 50°C. For laser ablation analysis specimens were mounted on a glass slide using double sided sticky tape. We performed raster measurements with a spot size of 50 μm and 20 Hz on the spiral side of the shell. The size of the raster varied depending on the size of the foraminifer. However, the ablated area always covered partly several chambers. Each foraminifer was measured once. Reference material measurements were performed in raster mode (100 μm x 100 μm) with a spot size of 50 μm at 10 Hz.

2.8.2. Coral sample

The coral sample (*Porites lutea*) was collected in the Andaman Sea (Indian Ocean) near the island Miang from a water depth of 15 m in December 2010. The pH of the seawater was 8.01 (total scale). The coral belonged to a previous project performed at the Geomar in Kiel, was embedded in Araldite and cut with a diamond blade using a Buehler IsoMet 1000 precision saw. It should be noted that for the B analysis performed in this study embedding would not have been necessary. We performed raster measurements with a spot size of 50 μm at 20 Hz and different raster sizes (raster size was adapted to measure solid structures showing no pores). One raster was ablated three to four times. Altogether five rasters were measured. Measurements of the reference material (NIST610) were performed in raster mode (100 μm x 100 μm) with a spot size of 50 μm at 10 Hz.

3. RESULTS AND DISCUSSION

3.1 Pre-tests

Table 3 shows the B concentration of the measured reference materials obtained from the Element XR, Maya2000 Pro, and from the Geological and Environmental Reference Material (GeoReM) website. Boron data from GeoReM represents a concentration range based on B concentration values determined from several publications. For more information about these publications the reader is referred to the GeoReM website. The B results of our analysis match the concentration range reported in GeoReM. In addition, the B concentration obtained from Maya

Table 3: B concentrations ($\mu\text{g/g}$) for several reference materials (as listed in GeoReM) and measurements performed using Element XR and Maya2000 Pro.

Reference Material	GeoReM	Element XR (HR ICP-MS)	Maya2000 Pro
T1-G (Diorite Glass)	2.24 - 5.05	6.07	6.04
StHs6/80 (Andesite Glass)	10.6 - 14.6	13.1	12.8
Atho-G (Rhyolite Glass)	5 - 12	5.9	5.6
BHVO-2G (Basalt)	4.6- 6.84	5	4.58

2000Pro and Element XR are linearly related (Fig.5). This confirms our approach of using the optical emission signal for Ca analysis allowing the calculation of B concentration.

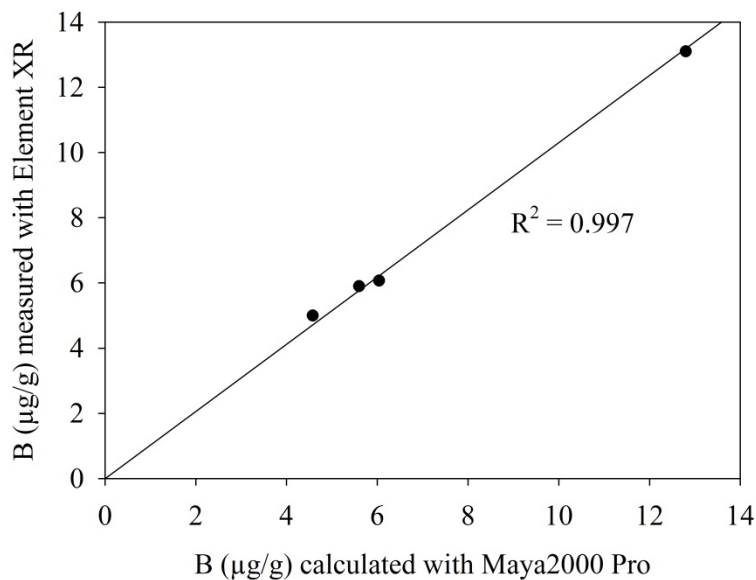


Figure 5: Boron concentration of several reference materials measured by Element XR and calculated based on the emission line of Ca II at 393.48 nm measured by Maya2000 Pro.

Table 4 shows the B data of SRMNIST 612 using SRMNIST 610 as reference material. To our knowledge SRMNIST 610 and SRMNIST 612 have never been measured against each other so far. However, several publications report the B isotopic composition of SRMNIST 610 and SRMNIST 612 measured against SRM951 as reference material, respectively. The B isotopic composition of SRMNIST 610 and SRMNIST 612 using SRM951 as reference material is given in Table 5. Also shown is the B concentration of SRMNIST 612. All data in Table 5 is shown as listed in GeoReM. The comparison between SRMNIST 610 and SRMNIST 612 shows that, within errors, both standards are isotopically equal. Within errors, the B isotopic composition of these two standards measured in this study lies within the range reported in literature. This is also true for the B concentration of SRMNIST 612. Therefore the coupling between the Thermo Finnigan Neptune MC-ICP-MS and Maya2000 Pro represents a reliable opportunity for simultaneous determination of B isotopic composition and B concentration.

Table 4: Boron isotopic signature and concentration of SRMNIST 612. *SD calculated using single values.

$\delta^{11}\text{B}$ (‰)	2RSE (%)	B ($\mu\text{g/g}$)	RSE (%)
-1.80	1.09	38	2.14
-0.86	1.04	38	2.87
-1.69	1.08	39	0.62
-1.69	1.01	39	4.21
-1.26	1.01	39	0.59
mean \pm SD*			
-1.46 \pm 0.35		39 \pm 0.7	

Table 5: Boron isotopic signature of SRMNIST 610 and SRMNIST 612 and B concentration of SRMNIST 612 as listed in GeoReM. * SRMNIST 610 was used as reference material.

NISTSRM 610 measured against NISTSRM 951				
$\delta^{11}\text{B}$ (‰)	Uncertainty	Uncertainty Type	Method	Publication
-0.78	0.7	SD	P-TIMS	Kasemann et al. 2001
-1.31	0.68	SD	N-TIMS	Kasemann et al. 2001
-0.16	0.21	2 SE	MC-ICP-MS	Le Roux et al. 2004
-0.36	0.06	2 SE	MC-ICP-MS	Le Roux et al. 2004
-0.55	0.53	SD	LA MC-ICP-MS	Fietzke et al. 2010
NISTSRM 612 measured against NISTSRM 951				
-1.07	0.85	SD	P-TIMS	Kasemann et al. 2001
-0.29	0.37	2 SE	MC-ICP-MS	Le Roux et al. 2004
-0.8	0.13	2 SE	MC-ICP-MS	Le Roux et al. 2004
-0.56	0.49	SD	LA MC-ICP-MS	Fietzke et al. 2010
NISTSRM 612 B concentration				
B (ppm)	Uncertainty	Uncertainty Type	Method	Publication
36	4.3	2 SD	LA-ICP-MS	Tiepolo et al. 2005
33	5	RSD	LA-ICP-MS	Jacob et. al 2006
34	0.9	SD	LA-ICP-MS	Hu et al. 2009
38	1.48	2 SD	LA-ICP-MS	Liu et al. 2008*
34	9	RSD	LA-ICP-MS	Deschamps et al. 2010
35	1	SD	LA-ICP-MS	Lazarov et al. 2012

3.2. SRMNIST 610 – accuracy, precision, and reproducibility

The analysis of the foraminifers and coral was performed on two different days. The mean internal precision (RSE) of SRMNIST 610 for the foraminifer session was 0.33‰. For the coral session we obtained a better RSE of 0.24‰. The difference in RSE might be caused by the heavily ablated surface of SRMNIST 610 due to previous measurements. After identification of this problem the surface of SRMNIST 610 was polished prior to the analysis of the coral resulting in a lower RSE by almost 0.1‰ during the coral session. A mean RSE of 0.24‰ represents a sufficient homogeneity of B isotopes distribution and makes SRMNIST 610 a suitable standard for LA MC ICP-MS. The $^{11/10}\text{B}$ ratios of SRMNIST 610 reported during both sessions are shown in Figure 6. For the foraminifer session we clearly observe an instrumental drift giving approximately a decrease in $^{11/10}\text{B}$ of 1% by the end of the session. However, the standard sample bracketing procedure accounts for this type of drift. For the coral session the instrumental was stable throughout the analysis.

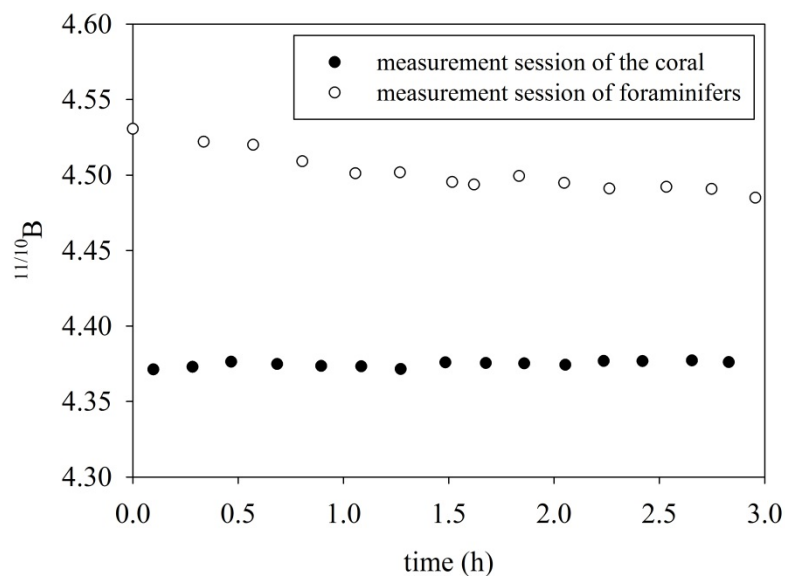


Figure 6: Isotope ratio $^{11/10}\text{B}$ of SRMNIST 610 representing the instrumental drift during the foraminifer and coral sessions illustrating that the standard sample bracketing is adequately correcting for instrumental drift.

3.3. Samples

On average, the B isotopic composition of the samples is $18 \pm 0.8 \text{ ‰}$ (SD) for the foraminifers and $21.1 \pm 0.66 \text{ ‰}$ (SD) for the coral. The B isotopic composition of benthic foraminifers reported in the literature varies between 15 and 20‰ (Vengosh et al., 1991; Foster, 2008; Rae et al., 2011). For corals it ranges between 21 and 27‰ (Hemming and Hanson, 1992; Hemming et al., 1998; Reynaud et al., 2004; Allison and Finch, 2010). Unfortunately, information on pH of the seawater is not reported in every publication. The mean B concentration of the foraminifers investigated here is $53 \pm 7 \text{ } \mu\text{g/g}$ (SD). Values reported in the literature for a variety of benthic foraminifers vary from 10 to 28 $\mu\text{g/g}$ B at an average seawater pH of 8.1 (Foster, 2008). The boron concentration of the same genus as investigated in this study is reported to be 54 $\mu\text{g/g}$ (*Amphistegina* from the Gulf of Aqaba) (Vengosh et al., 1991). The mean B concentration of the coral sample is $61 \pm 3 \text{ } \mu\text{g/g}$ (SD). Values reported in the literature range from 49 to 80 ppm B at an average seawater pH of 8.1 and temperatures between 25 and 29 °C (Vengosh et al., 1991; Hemming and Hanson, 1992; Gaillardet and Allègre, 1995; Trotter et al., 2011). Tables 6 and 7 report i.a. the mean values of the B isotopic signature, B concentration, and B/Ca of both carbonates measured of this study as well as single values. The B isotopic composition and B concentration of the coral had already been determined previously using an Axiom MC-ICP-MS and an AttoM HR ICP-MS both in combination with a NewWave UP193 laser ablation unit at IFM Geomar in Kiel, Germany ($\delta^{11}\text{B} = 22.1 \pm 1.21 \text{ ‰}$ (SD); $[\text{B}] = 26 \text{ to } 67 \text{ } \mu\text{g/g}$). Within the limits of uncertainty (SD) the average B isotopic composition and B concentration obtained in this study is identical to the values measured at IFM Geomar.

The main contributors to the precision of the samples are counting statistics and the homogeneity of the isotope ratio $^{11/10}\text{B}$. In the following we are going to discuss and evaluate these criteria with respect to our samples.

3.3.1. Foraminiferal Sample

For the analysis of foraminifers raster measurements were performed in average 160 μm long, 140 μm wide and 20 μm deep (for detail see section 3.3.3). The homogeneity with respect to the isotope ratio $^{11/10}\text{B}$ corresponds to the internal RSE of $^{11/10}\text{B}$ and is on average 0.52%. In comparison

Table 6: Boron analysis of the foraminifers. * BG subtracted, ** time-resolved BG subtraction as described in section 2.1. °SD calculated using single values. Details on errors see section 2.7.

single measurements of benthic foraminifers									
$\delta^{11}\text{B}$ (‰) *	2RSE $\delta^{11}\text{B}$ (‰) *	RSE $^{11/10}\text{B}$ (‰)*	$\delta^{11}\text{B}$ (‰) **	2RSE $\delta^{11}\text{B}$ (‰) **	RSE $^{11/10}\text{B}$ (‰)**	B ($\mu\text{g/g}$)	RSD B (%)	B/Ca (mmol/mol)	pH reconstructed
19.33	1.01	0.28	19.26	0.26	0.28	32	4.52	0.37	8.14
17.11	1.41	0.53	16.98	0.31	0.53	52	3.39	0.59	7.93
18.83	1.51	0.59	18.91	0.33	0.59	59	2.09	0.67	8.10
19.46	1.41	0.52	19.55	0.31	0.52	60	3.06	0.68	8.15
18.47	1.36	0.46	18.45	0.30	0.47	48	3.43	0.55	8.07
17.79	1.49	0.52	17.88	0.33	0.52	61	2.14	0.69	8.00
17.07	1.36	0.46	17.02	0.30	0.47	53	3.21	0.60	7.93
16.98	1.47	0.56	17.08	0.32	0.56	55	3.03	0.62	7.92
18.56	1.55	0.58	18.65	0.34	0.58	62	2.21	0.71	8.08
17.36	1.70	0.64	17.48	0.37	0.64	54	3.31	0.61	7.96
18.10	1.60	0.55	18.21	0.35	0.55	54	3.68	0.65	8.03
17.28	1.21	0.31	17.80	0.22	0.31	51	3.35	0.47	7.95
17.67	1.25	0.41	17.41	0.25	0.41	49	3.15	0.44	7.99
mean values									
$\delta^{11}\text{B}$ (‰)*	SD° $\delta^{11}\text{B}$ (‰)*	$\delta^{11}\text{B}$ (‰)**	SD° $\delta^{11}\text{B}$ (‰)**	B ($\mu\text{g/g}$)	SD° B ($\mu\text{g/g}$)	B/Ca (mmol/mol)	pH reconstructed	SD° pH reconstructed	pH seawater measured
18.00	0.83	18.05	0.04	53	7	0.588	8.02	0.08	8.08 ± 0.05

Table 7: Boron analysis of the coral. °SD calculated using single values. Details on errors see section 2.7.

single measurements of the coral					
$\delta^{11}\text{B}$ (‰)	2RSE $\delta^{11}\text{B}$ (‰)	RSE $^{11/10}\text{B}$ (‰)	B ($\mu\text{g/g}$)	RSD B (%)	B/Ca (mmol/mol)
21.32	0.51	0.32	60	2.73	0.55
21.64	0.45	0.33	61	2.62	0.56
21.29	0.48	0.23	62	2.35	0.57
21.67	0.45	0.27	65	1.89	0.60
21.83	0.49	0.33	65	2.94	0.60
20.81	0.5	0.31	60	2.22	0.56
20.74	0.48	0.27	57	2.93	0.53
20.36	0.48	0.36	55	3.12	0.51
21.72	0.46	0.24	62	1.63	0.58
21.92	0.50	0.29	65	2.04	0.60
20.19	0.46	0.35	62	3.11	0.57
20.23	0.44	0.28	60	2.01	0.55
20.13	0.47	0.28	59	2.85	0.55
mean values					
$\delta^{11}\text{B}$ (‰)	SD° $\delta^{11}\text{B}$ (‰)	B ($\mu\text{g/g}$)	SD° B ($\mu\text{g/g}$)	B/Ca (mmol/mol)	
21.07	0.65	61	3	0.564	

to the RSE of NISTSRM 610 (0.33‰ and 0.24‰) this result represents a worse B isotope homogeneity but lies still within the range of the required precision needed for paleo reconstructions. The relative counting statistic error of the highest amount of detected isotopes (^{10}B :6.4 million, ^{11}B 30 million cps during a detection time of 74 seconds) is 0.44‰, the relative counting statistic error of the smallest amount of detected isotopes is 0.45‰ (^{10}B :6 million, ^{11}B : 28 million cps during a detection time of 104 seconds).The RSE agrees with the counting statistical evolution. The mean external 2RSE is 1.44‰. However, this result represents the natural B isotope variability rather than the analytical uncertainty. The analytical uncertainty is assessed more adequately by the 2RSE of the reference material which is on average 0.9‰. A crucial point during B analysis were the thin chamber walls of the foraminifers which did not contain enough B for a gentle laser ablation. Since a sufficiently high intensity of B is important for reliable B isotope analysis foraminifers were ablated at a laser repetition rate which guaranteed an acceptable B signal. As a result holes in the tests of several foraminifers were observed when the laser ablated through the wall affecting the counting statistics negatively. Ablating through the test can

theoretically be avoided by setting the raster over a larger area. However, this is limited by the size of the area in the plane of focus. Since foraminifers do not have a flat surface, their round shape limits the focus area and therefore the ablation area. Figure 7a+b shows a comparison between a “rather” homogenous $^{11/10}\text{B}$ spectrum and a $^{11/10}\text{B}$ spectrum showing holes in the test where the laser ablated through. The simultaneous detection of B and Ca allows to reject parts in the spectra which represent holes typically visible as negative spikes. However, the counting statistic suffers from this correction. The test diameter of the foraminifers varied between 380 and 520 μm (Table 8) and the thickness of chamber walls was on average 10 μm . About 80% of the individuals from this size fraction show holes associated with laser ablation.

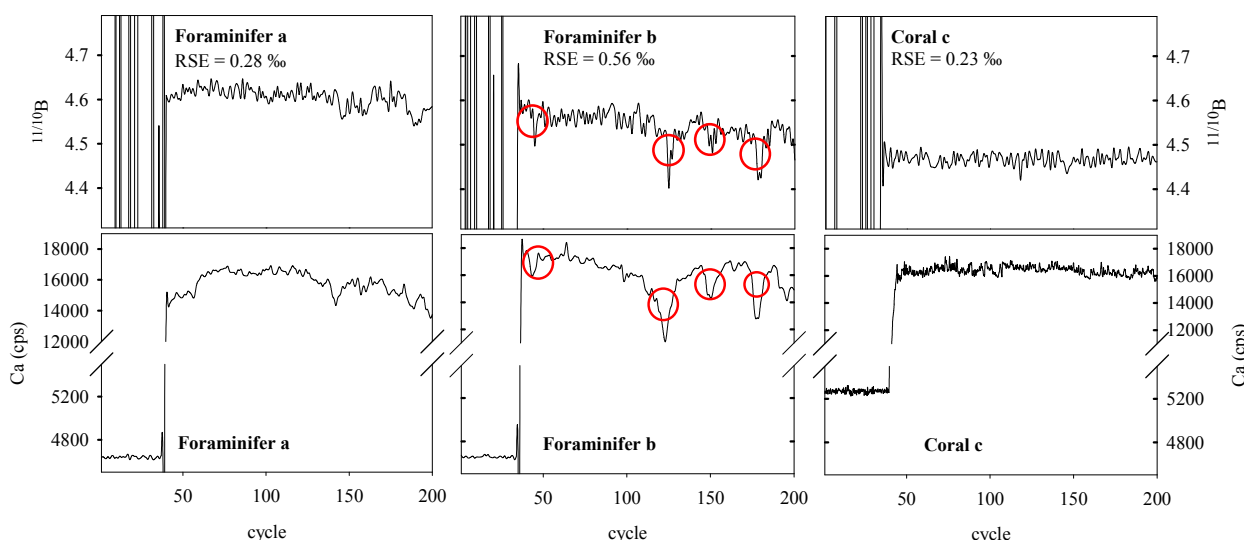


Figure 7: Graphs showing the ratio $^{11/10}\text{B}$ (above) and Ca cps (below) of two foraminifers (a+b) and one coral (c). The graph of the foraminifer b shows four holes (marked by circles) in the test as the laser penetrated the chamber wall. Additionally, a zoning in $^{11/10}\text{B}$ during the measurement can be seen. Both conditions lead to a worse RSE than for foraminifer a.

Foraminifers whose spectra show an internal RSE worse than 0.6‰ have been rejected. These observations do not necessarily mean that single tests of foraminifers are unsuitable for laser ablation. It is important to realize that the specimens investigated in this study grew from their juvenile stage for two months not reaching their final size. Natural growing *A. lessonii* reaches a test diameter of at least 1 mm (Walker et al., 2011) within a life span of at least one year. We chose to work with cultured specimens because this allows to control all important parameters of the culture media necessary for pH

Table 8: Size, estimated ablated calcite mass, and total B mass of ablated material.

foraminifer #	size (μm)	calcite mass ablated (ng)	total B corresponding to ablated mass (ng)
1	490	734	0.0235
2	460	1296	0.0674
3	450	1058	0.0624
4	430	1026	0.0616
5	400	1539	0.0739
6	400	1193	0.0728
7	450	1296	0.0687
8	380	1134	0.0624
9	380	1037	0.0643
10	470	1285	0.0694
11	460	1210	0.0653
12	510	1377	0.0702
13	520	1555	0.0762

reconstruction e.g. salinity, temperature and the B isotopic composition of the seawater. These remained constant over the course of the experiment and now allow us to reconstruct pH of seawater in which the specimens grew.

3.3.2 Coral Sample

In contrast to the foraminifers a better homogeneity of the $^{11/10}\text{B}$ was detected in the coral sample. On average, the internal RSE of $^{11/10}\text{B}$ is 0.29‰. The relative counting statistic error at the highest B intensity (^{10}B :18 million, ^{11}B 77 million cps during a detection time of 108 seconds) is 0.26‰, the relative counting statistic error at the lowest B intensity is 0.28‰ (^{10}B :16 million, ^{11}B : 69 million cps during a detection time of 140 seconds). The mean external 2RSE is 0.5‰. In contrast to the foraminifers the coral provides enough material for laser ablation resulting in a much better counting statistics. Furthermore, we did not observe any holes caused by laser ablation although the surface was ablated up to four times. The homogenous distribution of the B isotopes in the coral is occasionally as good as for SRM NIST 610 (Fig. 7c).

3.3.3. Sample Consumption

The amount of ablated material was calculated for both samples. For the coral the length, width and depth of the ablation craters was determined and the ablated volume calculated using a digital microscope (VHX 5000, Keyence). Figure 8 (a+b) shows an ablation crater of the coral sample corresponding to four ablation events. The volume of one ablation event is $\sim 680000 \mu\text{m}^3$ and the depth is $\sim 15 \mu\text{m}$. The ablation craters of foraminifers were measured using a laser microscope (VK-X200, Keyence) (Fig. 8c+d). The depth is defined as the distance between the surface of the test (orange to yellow area) and the so called “knob” a massive calcium carbonate part of the test with less pores (yellow to green area). Blue areas represent cavities between the chamber walls which are labelled in green.

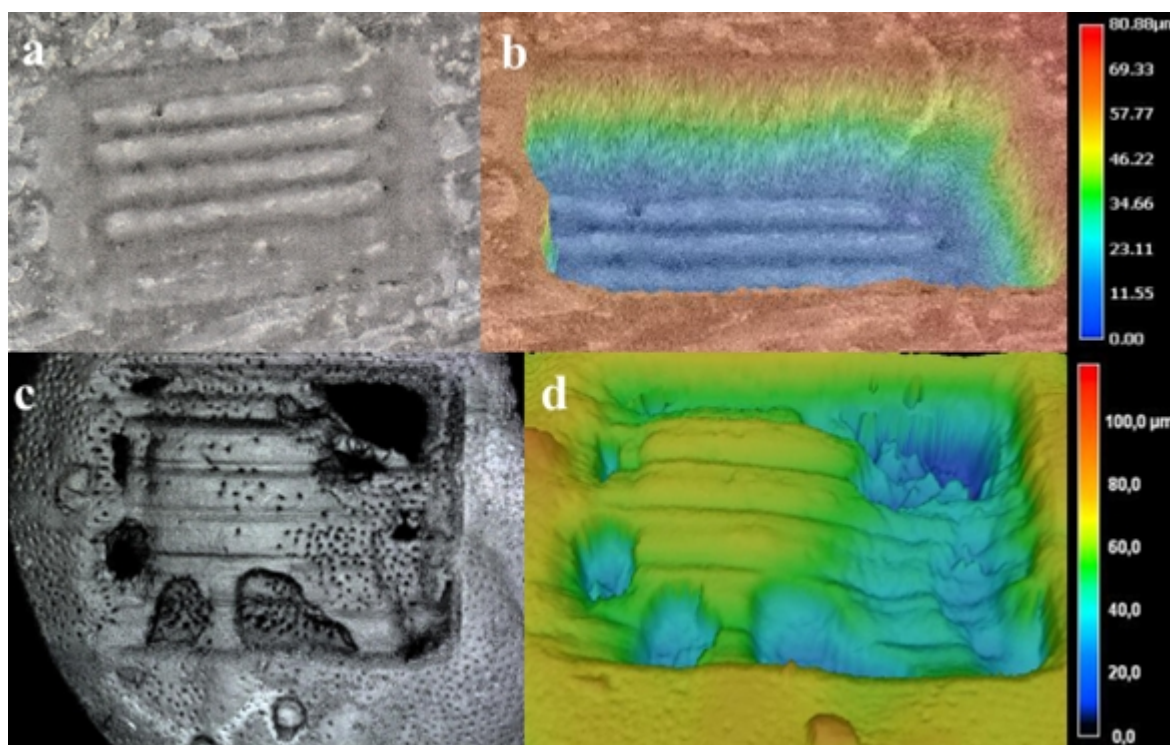


Figure 8: Pictures showing the depth profiles of both samples taken by a digital microscope (coral: a+b) and a laser microscope (foraminifer: c+d). The coral ablation crater corresponds to four ablation events yielding an ablated volume of $\sim 680000 \mu\text{m}^3$ ($250 \times 190 \times 15 \mu\text{m}$) per event. The foraminiferal crater corresponds to one ablation event. For the calculation of the volume ($\sim 450000 \mu\text{m}^3$; $160 \times 140 \times 20 \mu\text{m}$) pores and holes were not taken into account.

Giving a mean ablated depth of $20 \mu\text{m}$ the amount of ablated material per foraminifer would be on average 1200 ng containing a B concentration of 0.06 ng . For the calculation of the ablated mass pores

and holes in the tests were not taken into account. Therefore, our calculations represent a low overestimation. An overview of ablated material for each specimen is given in table 8. To date, (Fietzke et al., 2010) presented to our knowledge the only published study about *in situ* B isotope analysis of natural biogenic carbonates (corals) using LA MC-ICP-MS. The major difference between our studies is the use of faraday cups versus ion counters. The precision using faraday cups on small samples like foraminifers is limited by the noise level of these detectors. Ion counting detectors (as used in this study) show much lower noise levels, thereby increasing the signal to noise ratio significantly making these detectors more suitable for analysis of single foraminifers. Due to the high number of B cps required when using faraday cups, Fietzke et al. (2010) were forced to use a larger diameter of the laser beam (150µm). They ablated a sample containing 35 µg/g B at 30Hz for 30 s and to a depth of 100 µm, corresponding to 5 µg of sample, equivalent to 0.2 ng B. For a better comparison we chose a specimen containing a similar B concentration (32 µg/g, table 6). The material ablated is 0.73 µg calcite equivalent to 0.024 ng B. Hence, we use seven times less material.

In comparison to bulk analytical techniques the new method represented in this study consumes much less material. However, whereas bulk techniques provide a reliable mean value (mostly based on triplicate analysis of many dissolved tests) one $\delta^{11}\text{B}$ value from laser ablation is not necessarily representative due to inter- and intra- test variability, in addition to other factors as e.g. seasonality. Therefore, a representative number of samples has to be analyzed.

3.4. Implications for paleo applications

Unfortunately, we do not know the $\delta^{11}\text{B}_{\text{seawater}}$, in which the coral grew. Hence, a pH reconstruction can only be performed for the foraminifers. We reconstructed the pH of the seawater in which the foraminifers grew using (Zeebe and Wolf-Gladrow, 2001):

$$pH = pK_B - \log\left(-\frac{\delta^{11}\text{B}_{\text{seawater}} - \delta^{11}\text{B}_{\text{sample}}}{\delta^{11}\text{B}_{\text{seawater}} - \alpha \times \delta^{11}\text{B}_{\text{sample}} - \epsilon}\right) \quad (2.10)$$

Where pK_B is the dissociation constant of boric acid which is dependent on temperature (T) and salinity (S). pK_B was corrected for T and S after (Dickson, 1990). The corrected value is 8.59. The B isotopic

composition of seawater in which the foraminifers grew was measured using MC-ICP-MS at the university of Cambridge and is $39.77 \pm 0.44\%$ (SD). The B isotopic fractionation factor (α) between boric acid and borate is 1.0272 (Klochko et al., 2006), and $\epsilon = (\alpha - 1) \times 1000$. Reconstructed pH values are presented in table 4. On average, the reconstructed pH (8.02 ± 0.08) matches within errors the measured pH (8.08 ± 0.05) of the culture seawater. Previous studies on B isotopes in foraminiferal tests show that due to the so called “vital effects” foraminifers do not exactly record the pH of the seawater in which they grow (Sanyal et al., 1996; Hönisch and Hemming, 2004; Henehan et al., 2013). For example, symbiont activity strongly influences the pH near the surface of the foraminifers (Köhler-Rink and Kühl, 2000; Zeebe et al., 2003) shifting the B equilibria and consequently, impacts the $\delta^{11}\text{B}$ signature of the tests (Hönisch et al., 2003). Observations made by Foster (2008) and Rae et al. (2011) suggest that vital effects are more pronounced in planktonic than in benthic species, explaining why reconstructed pH values based on benthic species are in closer agreement with measured pH values. This notion is supported by this study. The good agreement between the measured and reconstructed pH values might be 1) exact knowledge of the parameters necessary for pH reconstruction 2) constant conditions (T, S, $\delta^{11}\text{B}_{\text{seawater}}$) during growth. We conclude that a change in the B isotopic composition by $\pm 0.5\%$ (which equals the mean internal precision) affects the reconstructed pH by ± 0.05 units. For paleo applications this resolution is acceptable. Changes during glacial to interglacial transitions are on the order of 0.3 pH units (Sanyal et al., 1995). However, the variability of $\delta^{11}\text{B}$ of 13 single measurements is 2.35‰ which is equivalent to a reconstructed pH change of 0.22 units.

Another application of the B proxy is based on its concentration itself. Unfortunately, the reported relationships between the B concentration and its controlling factor (CO_3^{2-} , HCO_3^-) are species specific e.g. (Yu & Elderfield, 2007; Brown et al., 2011; Rae et al., 2011). Since no calibration for *A. lessonii* exists yet we cannot verify the accuracy and precision of our target variable.

4. CONCLUSION

In this study we successfully applied a new in situ technique allowing the simultaneous determination of $\delta^{11}\text{B}$ and B/Ca ratios at the nanogram level (i.e. on single tests of foraminifers) providing two independent proxies for the reconstruction of the full carbonate system. Using the dual detection of B and Ca it is now possible to evaluate the data sets correctly by integrating signals intervals only where Ca was detected. The new technique considerably minimizes the sample size required for the simultaneous determination of B concentration and $\delta^{11}\text{B}$ as well as the time needed for sample preparation. It was tested on cultured benthic foraminifers and on a piece of coral. Our results show that a sufficient confidence in B analysis can only be achieved if a sufficient amount of material per one analysis is ablated (giving confidence in the precision) and enough individual tests are measured covering the range of the B variability. In the case of the foraminifers small test diameter and thin chamber walls limit the precision and application of laser ablation on single tests of foraminifers. Within a size range of 380 to 520 μm and a mean B concentration of 53 $\mu\text{g/g}$ the mean internal precision is 0.52‰. For future applications we recommend a careful selection of samples having at least the same size as investigated in this study. For the coral sample an internal precision of 0.29‰ was achieved which is mostly due to the fact that more material of higher homogeneity was ablated. This result is very promising for paleo pH reconstructions as well as investigations on seasonal variability in corals. Giving a homogenous $^{11/10}\text{B}$ distribution this new technique is able to provide a sufficient internal precision of the B isotopic composition for paleo pH reconstructions. From the pH reconstruction based on the cultured foraminifers we conclude that the mean reconstructed pH value calculated from 13 single measurements is in good agreement with the measured one.

ACKNOWLEDGEMENTS

We are grateful to Marlene Wall, Jan Fietzke, and Max Janse for providing the coral sample and the foraminifers. We thank Sambuddha Misra for the B analysis of the culture media and Keyence for the provision of the microscopic instruments. This project was financially supported by the DFG BI 432/7-1.

REFERENCES

- Aggarwal, J.K., Mezger, K., Pernicka, E., Meixner, A., 2004. The effect of instrumental mass bias on $\delta^{11}\text{B}$ measurements: a comparison between thermal ionisation mass spectrometry and multiple-collector ICP-MS. *International Journal of Mass Spectrometry*, 232(3): 259-263.
- Allison, N., Finch, A.A., 2010. $\delta^{11}\text{B}$, Sr, Mg and B in a modern Porites coral: the relationship between calcification site pH and skeletal chemistry. *Geochimica et Cosmochimica Acta*, 74(6): 1790-1800.
- Brown, R.E., Anderson, L.D., Thomas, E., Zachos, J.C., 2011. A core-top calibration of B/Ca in the benthic foraminifers *Nuttallides umbonifera* and *Oridorsalis umbonatus*: A proxy for Cenozoic bottom water carbonate saturation. *Earth and Planetary Science Letters*, 310(3-4): 360-368.
- Deschamps, F., Guillot, S., Godard, M., Chauvel, C., Andreani, M., Hattori, K., 2010. In situ characterization of serpentinites from forearc wedges: Timing of serpentinization and behavior of fluid-mobile elements in subduction zones. *Chemical Geology*, 269(3-4): 262-277.
- Dickson, A.G., 1990. Thermodynamics of the dissociation of boric acid in synthetic seawater from 273.15 to 318.15 K. *Deep Sea Research Part A. Oceanographic Research Papers*, 37(5): 755-766.
- Duchateau, N.L., de Bièvre, P., 1983. Boron isotopic measurements by thermal ionization mass spectrometry using the negative BO_2^- ion. *International Journal of Mass Spectrometry and Ion Processes*, 54(3): 289-297.
- Ernst, S. et al., 2011. BENTHIC FORAMINIFERA IN A LARGE INDO-PACIFIC CORAL REEF AQUARIUM. *The Journal of Foraminiferal Research*, 41(2): 101-113.
- Fietzke, J. et al., 2010. Boron isotope ratio determination in carbonates via LA-MC-ICP-MS using soda-lime glass standards as reference material. *Journal of Analytical Atomic Spectrometry*, 25(12): 1953-1957.
- Foster, G.L., 2008. Seawater pH, pCO_2 and $[\text{CO}_2-3]$ variations in the Caribbean Sea over the last 130 kyr: A boron isotope and B/Ca study of planktic foraminifera. *Earth and Planetary Science Letters*, 271(1-4): 254-266.
- Foster, G.L., Ni, Y., Haley, B., Elliott, T., 2006. Accurate and precise isotopic measurement of sub-nanogram sized samples of foraminiferal hosted boron by total evaporation NTIMS. *Chemical Geology*, 230(1-2): 161-174.
- Gaillardet, J.m., Allègre, C.J., 1995. Boron isotopic compositions of corals: Seawater or diagenesis record? *Earth and Planetary Science Letters*, 136(3-4): 665-676.
- Hemming, N.G., Guilderson, T.P., Fairbanks, R.G., 1998. Seasonal variations in the boron isotopic composition of coral: A productivity signal? *Global Biogeochemical Cycles*, 12(4): 581-586.
- Hemming, N.G., Hanson, G.N., 1992. Boron isotopic composition and concentration in modern marine carbonates. *Geochimica et Cosmochimica Acta*, 56(1): 537-543.
- Hemming, N.G., Hanson, G.N., 1994. A procedure for the isotopic analysis of boron by negative thermal ionization mass spectrometry. *Chemical Geology*, 114(1-2): 147-156.
- Henehan, M.J. et al., 2013. Calibration of the boron isotope proxy in the planktonic foraminifera *Globigerinoides ruber* for use in palaeo- CO_2 reconstruction. *Earth and Planetary Science Letters*, 364(0): 111-122.
- Heumann, K.G., Zeininger, H., 1985. Boron trace determination in metals and alloys by isotope dilution mass spectrometry with negative thermal ionization. *International Journal of Mass Spectrometry and Ion Processes*, 67(2): 237-252.
- Hönisch, B. et al., 2003. The influence of symbiont photosynthesis on the boron isotopic composition of foraminifera shells. *Marine Micropaleontology*, 49(1-2): 87-96.
- Hönisch, B., Hemming, N.G., 2004. Ground-truthing the boron isotope-paleo-pH proxy in planktonic foraminifera shells: Partial dissolution and shell size effects. *Paleoceanography*, 19(4): PA4010.
- Hou, K., Li, Y., Xiao, Y., Liu, F., Tian, Y., 2010. In situ boron isotope measurements of natural geological materials by LA-MC-ICP-MS. *Chinese Science Bulletin*, 55(29): 3305-3311.
- Hu, Z., Liu, Y., Li, M., Gao, S., Zhao, L., 2009. Results for rarely determined elements in MPI-DING, USGS and NIST SRM glasses using laser ablation ICP-MS. *Geostandards and Geoanalytical Research*, 33(3): 319-335.

- Jacob, D.E., 2006. High sensitivity analysis of trace element poor geological reference glasses by laser ablation-inductively coupled plasma-mass spectrometry. *Geostandards and Geoanalytical Research*, 30(3):221-235.
- Kasemann, S.A., Schmidt, D.N., Bijma J., Foster, G.L., 2009. In situ analysis in marine carbonates and its application for foraminifera and paleo-pH. *Chemical Geology*, 260(1-2): 138-147.
- Klochko, K., Kaufman, A.J., Yao, W., Byrne, R.H., Tossell, J.A., 2006. Experimental measurement of boron isotope fractionation in seawater. *Earth and Planetary Science Letters*, 248(1-2): 276-285.
- Köhler-Rink, S., Kühl, M., 2000. Microsensor studies of photosynthesis and respiration in larger symbiotic foraminifera. I The physico-chemical microenvironment of *Marginopora vertebralis*, *Amphistegina lobifera* and *Amphisorus hemprichii*. *Marine Biology*, 137(3): 473-486.
- Lazarov, M., Brey, G.P., Weyer, S., 2012. Evolution of the South African mantle- A case study of garnet peridotites from the Finsch diamond mine (Kaapvaal craton); part1: Inter-mineral trace element and isotopic equilibrium. *Lithos*, 154: 193-209.
- le Roux, P.J., Shirey, S.B., Benton, L., Hauri, E.H., Mock, T.D., 2004. In situ, multiple-multiplier, laser ablation ICP-MS measurement of boron isotopic composition ($\delta^{11}\text{B}$) at the nanogram level. *Chemical Geology*, 203(1-2): 123-138.
- Lécuyer, C., Grandjean, P., Reynard, B., Albarède, F., Telouk, P., 2002. $^{11}\text{B}/^{10}\text{B}$ analysis of geological materials by ICP-MS Plasma 54: Application to the boron fractionation between brachiopod calcite and seawater. *Chemical Geology*, 186(1-2): 45-55.
- Longerich, H.P., Jackson, S.E., Günther, D., 1996. Inter-laboratory note. Laser ablation inductively coupled plasma mass spectrometric transient signal data acquisition and analyte concentration calculation. *Journal of Analytical Atomic Spectrometry*, 11(9): 899-904.
- Liu, Y., Hu, Z., Gao, S., Günther, D., Gao, C., Chen, H., 2008. *In situ* analysis of major and trace elements of anhydrous minerals by LA-ICP-MS without applying an internal standard. *Chemical Geology*, 257(1-2): 34-43.
- Louvat, P., Bouchez, J., Paris, G., 2010. MC-ICP-MS Isotope Measurements with Direct Injection Nebulisation (d-DIHEN): Optimisation and Application to Boron in Seawater and Carbonate Samples. *Geostandards and Geoanalytical Research*, 35(1): 75-88.
- Ni, Y. et al., 2007. A core top assessment of proxies for the ocean carbonate system in surface-dwelling foraminifers. *Paleoceanography*, 22(3): PA3212.
- Rae, J.W.B., Foster, G.L., Schmidt, D.N., Elliott, T., 2011. Boron isotopes and B/Ca in benthic foraminifera: Proxies for the deep ocean carbonate system. *Earth and Planetary Science Letters*, 302(3-4): 403-413.
- Reynaud, S., Hemming, N.G., Juillet-Leclerc, A., Gattuso, J.-P., 2004. Effect of $p\text{CO}_2$ and temperature on the boron isotopic composition of the zooxanthellate coral *Acropora* sp. *Coral Reefs*, 23: 539-546.
- Rollion-Bard, C., Erez, J., 2010. Intra-shell boron isotope ratios in the symbiont-bearing benthic foraminiferan *Amphistegina lobifera*: Implications for $\delta^{11}\text{B}$ vital effects and paleo-pH reconstructions. *Geochimica et Cosmochimica Acta*, 74(5): 1530-1536.
- Rosner, M., Wiedenbeck, M., Ludwig, T., 2008. Composition-Induced Variations in SIMS Instrumental Mass Fractionation during Boron Isotope Ratio Measurements of Silicate Glasses. *Geostandards and Geoanalytical Research*, 32(1): 27-38.
- Sanyal, A., Hemming, N.G., Hanson, G.N., Broecker, W.S., 1995. Evidence for a higher pH in the glacial ocean from boron isotopes in foraminifera. *Nature*, 373: 234-236.
- Sanyal, A. et al., 1996. Oceanic pH control on the boron isotopic composition of foraminifera: Evidence from culture experiments. *Paleoceanography*, 11(5): 513-517.
- Tiepolo, M., Zannetti, A., Vannucci, R., 2005. Determination of lithium, beryllium, and boron at trace levels by laser ablation-inductively coupled plasma-sector field mass spectrometry. *Geostandards and Geoanalytical Research*, 29(2): 211-224.
- Tiepolo, M., Bouman, C., Vannucci, R., Schwieters, J., 2006. Laser ablation multicollector ICPMS determination of $\delta^{11}\text{B}$ in geological samples. *Applied Geochemistry*, 21(5): 788-801.
- Trotter, J. et al., 2011. Quantifying the pH "vital effect" in the temperate zooxanthellate coral *Cladocora caespitosa*: Validation of the boron seawater pH proxy. *Earth and Planetary Science Letters* 303: 163-173.

- Vengosh, A., Kolodny, Y., Starinsky, A., Chivas, A.R., McCulloch, M.T., 1991. Coprecipitation and isotopic fractionation of boron in modern biogenic carbonates. *Geochimica et Cosmochimica Acta*, 55(10): 2901-2910.
- Walker, R.A., Hallock, P., Torres, J.J., Vargo, G.A., 2011. PHOTOSYNTHESIS AND RESPIRATION IN FIVE SPECIES OF BENTHIC FORAMINIFERA THAT HOST ALGAL ENDOSYMBIONTS. *The Journal of Foraminiferal Research*, 41(4): 314-325.
- Wara, M.W., Delaney, M.L., Bullen, T.D., Ravelo, A.C., 2003. Possible roles of pH, temperature, and partial dissolution in determining boron concentration and isotopic composition in planktonic foraminifera. *Paleoceanography*, 18(4): 1100.
- Wunder, B., Meixner, A., Romer, R.L., Wirth, R., Heinrich, W., 2005. The geochemical cycle of boron: Constraints from boron isotope partitioning experiments between mica and fluid. *Lithos*, 84(3-4): 206-216.
- Yu, J., Elderfield, H., 2007. Benthic foraminiferal B/Ca ratios reflect deep water carbonate saturation state. *Earth and Planetary Science Letters*, 258(1-2): 73-86.
- Yu, J., Foster, G.L., Elderfield, H., Broecker, W.S., Clark, E., 2010. An evaluation of benthic foraminiferal B/Ca and $\delta^{11}\text{B}$ for deep ocean carbonate ion and pH reconstructions. *Earth and Planetary Science Letters*, 293(1-2): 114-120.
- Zeebe, R.E., Wolf-Gladrow, D.A., 2001. *CO₂ in seawater: equilibrium, kinetics, isotopes*. Elsevier Science B.V., Amsterdam.
- Zeebe, R.E., Wolf-Gladrow, D.A., Bijma, J., Hönisch, B., 2003. Vital effects in foraminifera do not compromise the use of $\delta^{11}\text{B}$ as a paleo-pH indicator: Evidence from modeling. *Paleoceanography*, 18(2): 1043.

APPENDIX

Table 1A

Boron isotopic signature of several *A. lessonii* specimens corrected using the conventional BG subtraction (*) and the time-resolved BG subtraction (**) (columns 1+2). The difference is up to 2.7‰. The reason is the highly decreasing BG signal (columns 3+4) and the low B intensity (columns 5+6). It should be noted that the foraminifers used here only served the purpose of initial test measurements. The B isotopic signature of the water in which they grew was not measured and probably variable. The water of the aquarium from which these foraminifers were picked was replaced once a month. Meanwhile algal growth and evaporation might have altered the B isotopic composition of the water. Therefore these samples are not included in further discussions in this study.

$\delta^{11}\text{B}$ (‰)*	$\delta^{11}\text{B}$ (‰)**	BG ^{10}B (cps)	BG ^{11}B (cps)	BG + sample ^{10}B (cps)	BG + sample ^{11}B (cps)	time (m)
10.47	11.09	25081	70251	46634	207938	0
8.64	10.04	23703	65380	71443	318209	14
9.63	8.55	22435	61013	50664	225091	26
11.22	10.29	21598	57691	42430	188737	40
13.26	10.51	21068	55894	78991	351429	53
12.18	10.02	20369	53484	75841	336276	67

Topic 3

Boron incorporation in the foraminifer *Amphistegina lessonii* under a decoupled carbonate chemistry

Karina Kaczmarek^{a*}

* corresponding author: karina.kaczmarek@awi.de

Gerald Langer^b

Gernot Nehrke^a

Ingo Horn^c

Sambuddha Misra^b

Max Janse^d

Jelle Bijma^a

^aAlfred-Wegener-Institut Helmholtz-Zentrum für Polar- und Meeresforschung, am Handelshafen 12, 27570 Bremerhaven, Germany

^bDepartment of Earth Science, University of Cambridge, Dowing Site, CB2 3EQ Cambridge, UK

^cInstitute of Mineralogy, Leibniz University, Callin street 3, 30167 Hannover, Germany

^dBurgers Zoo, Antoon van Hooffplein 1, 6816 SH Arnhem, The Netherlands

ABSTRACT

A number of studies have shown that the boron isotopic composition ($\delta^{11}\text{B}$) and the B/Ca ratio of biogenic carbonates (mostly foraminifers) can serve as proxies for two parameters of the ocean's carbonate chemistry, rendering it possible to calculate the entire carbonate system. However, identifying the carbonate system parameter influencing boron incorporation is difficult due to the co-variation of pH, CO_3^{2-} , and $\text{B}(\text{OH})_4^-$. To shed light on the question which parameter of the carbonate system is related to the boron incorporation, we performed culture experiments with the benthic symbiont-bearing foraminifer *Amphistegina lessonii* using a decoupled pH – CO_3^{2-} chemistry. The determination of the boron isotopic composition and B/Ca ratios was performed simultaneously by means of a new *in situ* technique combining optical emission spectroscopy and laser ablation MC-ICP-MS. The boron isotopic composition in the tests gets heavier with increasing pH and B/Ca increases with increasing $\text{BOH}_4^-/\text{HCO}_3^-$ of the culture media. The latter indicates that boron uptake of *A. lessonii*

features a competition between B(OH)_4^- and HCO_3^- . Furthermore, the simultaneous determination of B/Ca and $\delta^{11}\text{B}$ on single specimens allows for assessing the relative variability of these parameters. Among different treatments the B/Ca shows an increasing variability with increasing boron concentration in the test whereas the variability in the isotope distribution is constant. The $\delta^{11}\text{B}$ signature of *A. lessonii* tests is lighter than the boron isotopic composition of borate (the boron species thought to be incorporated into marine carbonates). The latter indicates that for this species the impact of respiration and calcification on the $\delta^{11}\text{B}$ signature might dominate over the one related to photosynthesis of symbionts.

1. INTRODUCTION

The oceans carbonate system comprises six co-varying parameters ($[\text{CO}_2]$, $[\text{HCO}_3^-]$, $[\text{CO}_3^{2-}]$, pH, total alkalinity (TA), and dissolved inorganic carbon (DIC)). Changes of the carbonate system caused by past changes in the atmospheric $p\text{CO}_2$ can be reconstructed if at least two of these parameters are known. A number of studies have shown that the boron isotopic composition ($\delta^{11}\text{B}$) and the B/Ca ratio of biogenic carbonates (mostly foraminifers) may serve as proxies that can provide these two parameters.

In seawater boron (B) mainly exists as boric acid (B(OH)_3) and borate (B(OH)_4^-). The isotopic composition and concentration of both species are pH dependent. Since the B isotopic composition of biogenic carbonates precipitated at a certain pH value is similar to that of B(OH)_4^- , Hemming & Hanson (1992) concluded that only B(OH)_4^- is incorporated into biogenic carbonates. Therewith, the B isotopic composition can be used as a proxy to infer the pH that prevailed during the formation of the biogenic carbonate. However, several studies show a deviation between the B isotopic composition of the biogenic carbonates and B(OH)_4^- of the sea water (Sanyal et al., 1996; Sanyal et al., 2001; Foster, 2008; Rae et al., 2011). This deviation is often explained by physiological processes like photosynthesis and respiration of symbionts (e.g. dinoflagellates) which modify the pH in the micro-environment around the foraminifera (Zeebe et al., 2003) leading to shifts in the B equilibria. Yet

another explanation for the observed deviation is that not only B(OH)_4^- is incorporated during the formation of calcium carbonate but to some extent also the isotopically heavier B(OH)_3 (Klochko et al., 2009). To account for physiological effects, species specific calibration experiments have been carried out to be able to apply this proxy and reliably reconstruct seawater pH (Sanyal et al., 2001; Hönisch et al., 2003; Henehan et al., 2013).

While the B isotope composition of biogenic carbonates is used to reconstruct past seawater pH, the B/Ca of foraminiferal calcite is often used to infer past seawater CO_3^{2-} concentrations e.g. (Yu et al., 2007; Brown et al., 2011). Inherent to all field studies and most experimental studies is that pH and CO_3^{2-} concentration of natural seawater are correlated. It is therefore impossible to determine which parameter of the carbonate system is in control of B/Ca. Not surprisingly, correlations between B/Ca and pH were described in addition to B/Ca and CO_3^{2-} concentration (Yu et al., 2007; Tripathi et al., 2011). The latter studies are based on field samples, but experimental studies suffer from the same ambiguity if the experimental setup uses a classical carbonate system manipulation, i.e. either DIC or TA manipulation. To identify the parameter of the carbonate system responsible for foraminiferal B/Ca, it is necessary to decouple pH and CO_3^{2-} concentration. Such an experimental setup will allow for excluding up to five out of the six parameters of the carbonate system. In an experimental study on the relationship between B/Ca and the seawater carbonate system Allen et al. (2012) showed “a competition between aqueous boron and carbonate species for inclusion into the calcite lattice” for *Orbulina universa*, *Globiberinoides ruber*, and *Globigerinoides sacculifer*. In this study we cultured *A. lessonii* under conditions in which pH and CO_3^{2-} concentration were decoupled in order to assess the controlling carbonate system parameter for B incorporation. The simultaneous determination of $\delta^{11}\text{B}$ and B/Ca on single specimens by means of a newly developed technique (based on a femto second laser ablation MC-ICP-MS connected to a fiber optic spectrometer) allows for the first time the determination of the elemental and isotope B variability among single specimens.

2. MATERIAL AND METHODS

2.1 Culturing and experimental setup

Live specimens of the benthic symbiont-bearing foraminifer *A. lessonii* were obtained from a coral reef aquarium at the Burgers Zoo (Arnhem, The Netherlands). SCUBA divers collected approximately 1 kg of sediment containing different species of foraminifers (Ernst et al., 2011). The sediment was transported to the Alfred Wegener Institute (Bremerhaven, Germany) immediately and transferred into a small aquarium (5L) filled with filtered (0.2 μm pore-size) North Sea seawater (NSW). The aquarium was equipped with a circulation pump to supply air and a time switched light source providing a light/dark cycle (12 h/12 h). About 100 specimens of *A. lessonii* were transferred to well plates containing NSW and placed in a temperature controlled room at 25°C (again exposed to a 12 h/12 h light/dark cycle). After two weeks ~20% of the specimens had asexually reproduced, yielding 10-30 juveniles per specimen. Subsequently, juvenile foraminifers were transferred into petri dishes containing NSW with a dedicated carbonate system (see 2.2. Preparation of culture media). Each petri dish was placed into one of six boxes each receiving a concentration of $p\text{CO}_2$ that was in equilibrium with the corresponding carbonate chemistry of the prepared NSW media. The supply of $p\text{CO}_2$ was realized by a gas-mixing system producing a constant gas flow of 40 L per hour for each box. Concentration of CO_2 was logged using CO_2 sensors (type FY0D00CO2B10 Ahlborn) and did not deviate by more than 25 μatm from the target-value. In order to avoid evaporation of culture media in the petri dishes, the gas was saturated with water by bubbling it through a fritted wash bottle filled with de-ionized water. The complete experimental setup was placed in a temperature-controlled (25°C) room. Because of heat produced by the lamps the temperature within the boxes containing the petri dishes increased by up to 2°C during the light cycle. Since this holds for all treatments, it did not impair the interpretation of results. Light intensity was 100-150 $\mu\text{mol photons m}^{-2}\text{s}^{-1}$. Every third day the culture media was replaced by a freshly opened aliquot from the corresponding batch of culture media, which was stored without headspace at ~3°C. Approximately 24 hours before the culture media was replaced it was filled in a petri dish and placed in the corresponding gas box to equilibrate. Each time when the culture media was replaced, foraminifers were fed with concentrated and sterilized

algae *Dunaliella salina* (20000 cells/ml). Before feeding algae were centrifuged to minimize dilution of the culture media, and exposed to 90°C for 20 minutes after centrifugation in order to reduce bacterial activity in the culture media. Foraminifers grew for three months. Afterwards specimens were harvested, bleached in NaOCl (active chlorine: 4.6%) for six hours, rinsed four times using de-ionized water, and dried for 12 hours at 50°C. For laser ablation analysis specimens were mounted on a glass slide using double sided adhesive tape.

The mortality of *A. lessonii* was 25% throughout all culture experiments. Mortality affected the entire clone rather than single specimens within a clone and dominantly juveniles in an early state (having ~3 chambers). The size of all foraminifers ranged between 400 and 900 µm. The morphology of the tests was indistinguishable from the one of specimens grown in the natural habitat.

2.2 Preparation of culture media

Six treatments of manipulated NSW were prepared: treatments 1 to 4 had a constant pH but different $[\text{CO}_3^{2-}]$. The labels are: pH_8.1¹⁶⁰, pH_8.1²⁶⁰, pH_8.1⁵⁴⁰, and pH_8.1⁶⁴⁰. The exponent represents the concentration of CO_3^{2-} in µmol/kg respectively. We will refer to the sum of treatments 1 to 4 as pH_8.1*. Treatment 5 yields a pH of 8.56 and a CO_3^{2-} concentration of 638 µmol/kg. It is labelled as pH_8.6⁶⁴⁰. Treatment 6 has a pH of 7.86 and a $[\text{CO}_3^{2-}]$ of 268 µmol/kg. It is labelled as pH_7.9²⁶⁰. Since our treatments are not in equilibrium with a $p\text{CO}_2$ of 380 µatm (except pH_8.1²⁶⁰), we used a CO_2 gas-mixing system providing each treatment with the associated equilibrium $p\text{CO}_2$. The required manipulation of the culture media was calculated by means of the computer program octave and the file csys.m (created by Richard E. Zeebe and Dieter Wolf-Gladrow, downloadable at http://www.soest.hawaii.edu/oceanography/faculty/zeebe_files/CO2_System_in_Seawater/csys.html). The csys.m file was modified to allow calculations of borate concentrations different from the natural concentration of seawater. The equilibrium constants of Mehrbach (for K1 and K2) and the total scale for pH were chosen. Temperature was set to 27°C, salinity to 32. Calculating the whole carbonate system chemistry requires at least two of its parameters. The input parameters for the pH constant treatments (pH_8.1*) were pH and $p\text{CO}_2$, for the $[\text{CO}_3^{2-}]$ constant treatments (pH_8.6⁶⁴⁰ + pH_8.1⁶⁴⁰ and pH_7.9²⁶⁰ + pH_8.1²⁶⁰) $[\text{CO}_3^{2-}]$ and $p\text{CO}_2$. The

basis for the different culture media was sterile filtered (0.2 μm pore size) NSW enriched in B (using $\text{B}(\text{OH})_3$, chemical purity: > 99.5%) to a final concentration of ~ 4 mmol/kg, which is ~ 10 times the B concentration of natural seawater. The enrichment with B was done to obtain a higher concentration within the test for better B analysis. For each treatment two litres of culture media were prepared and filled without headspace into 50 ml (for the replacement of culture media) and 200 ml (for chemical analysis) gastight, boron free, silicate flasks and stored at $\sim 3^\circ\text{C}$.

2.3 Analysis of the culture media

Since the amount of culture media in the petri dishes containing the foraminifers (which was replaced all three days) was not sufficient for all chemical analysis, approximately 200 ml of each batch of culture media were filled in polypropylene beakers and placed into the corresponding CO_2 box to equilibrate. Even though determining the chemical parameters once would have been sufficient, we performed this procedure bi-weekly to verify that all conditions stayed constant during the experimental period. After ~ 24 hours salinity and pH of these solutions were measured at *in situ* conditions and samples were taken for Ca, B, DIC, and TA analysis. Salinity measurements were performed using a conductivity meter (WTW Multi 340i) interfaced with a TetraCon 325 sensor. Measurements of pH were carried out by means of a combined pH glass electrode (Ectrode Plus, Metrohm) interfaced to a Radiometer pH-Meter (PHM240). Repeated measurements of buffers show a reproducibility of 0.05 pH units. After calibration (NBS buffer) the conversion to total scale was performed by measuring a Tris/Tris-HCl seawater buffer prepared in accordance with the recipe described in (Dickson et al., 2007). Calcium and B concentrations were determined by a Thermo Elemental (TJA) IRIS Intrepid ICP-OES Spectrometer using Merck 4 (multi element standard) as reference material. The average external error as estimated by multiple measurements of the reference material was $\pm 3.5\%$. Total alkalinity was calculated from linear Gran plots (Gran, 1952) after triplicate potentiometric titration (Bradshaw et al., 1981) using a TitroLine alpha plus auto sampler (Schott Instruments). Culture media samples were calibrated against an in-house standard (NSW) which is calibrated regularly against certified reference material batch No. 54 of Dickson (Scripps Institution of Oceanography). The average reproducibility is ± 10 $\mu\text{mol/kg}$. Determination of DIC was

performed photometrically in triplicates with a TRAACS CS800 QuaAAtro autoanalyzer with an average reproducibility of $\pm 10 \mu\text{mol/l}$ based on calibrations of an in-house standard (NSW) calibrated against Certified Reference Material Batch No. 54 of Dickson (Scripps Institution of Oceanography). Boron isotopic composition of the culture media were analyzed by means of a Thermo[®] Element XR, a single collector, sector field, high-resolution inductively coupled plasma mass spectrometer, fitted with a high sensitivity interface pump (Jet pump) as described in Misra et al. (2014). Boron isotopic composition is reported as per mil (‰) deviation from NIST SRM 951a ($^{11}\text{B}/^{10}\text{B} = 4.04362 \pm 0.00137$) (Catanzaro et al., 1970) where:

$$\delta^{11}\text{B}_{\text{sample}} (\text{‰}) = \left[\frac{(^{11/10}\text{B})_{\text{sample}}}{(^{11/10}\text{B})_{\text{NISTSRM 951a}}} - 1 \right] \times 1000 \quad (1)$$

Boron isotope analyses were made following a Sample – Standard Bracketing (SSB) technique. NIST 951a was used as the standard and samples were concentration matched, typically at $\pm 5\%$, with the standard and were analyzed in quintuplicate. The accuracy and precision of the analytical method was assessed by comparing $\delta^{11}\text{B}$ measurements of seawater and secondary boron standards (AE 120, 121, 122) with published (accepted) results. Our estimate of $\delta^{11}\text{B}_{\text{SW}}$ of $39.8 \pm 0.4\text{‰}$ (2σ , $n = 30$) are independent of sample size and are in agreement with published values of $39.6 \pm 0.4\text{‰}$ (Foster et al., 2010) and $39.7 \pm 0.6\text{‰}$ (Spivack & Edmond, 1987). Moreover, our $\delta^{11}\text{B}$ estimates of SRM AE-120 ($-20.2\text{‰} \pm 0.5\text{‰}$, $2s$, $n = 33$), SRM AE-121 ($19.8\text{‰} \pm 0.4\text{‰}$, $2s$, $n = 16$), SRM AE-122 ($39.6\text{‰} \pm 0.5\text{‰}$, $2s$, $n = 16$) are identical, within analytical uncertainty, to accepted values (Vogl & Rosner, 2012). Information about sample preparation for analysis can be found in the supplement.

2.4 Simultaneous determination of B isotopic composition and B concentration of single tests

The B analysis of the foraminifers was carried out as described in **topic 2** sections **2.1** till **2.6**.

3. RESULTS AND DISCUSSION

3.1 Carbonate system

The determination of pH, TA and DIC of the culture media yielded three parameters of the carbonate system. In theory, any two of these parameters can be used to calculate the entire carbonate system. However, it has been shown that the results can differ depending on the choice of input parameters (Hoppe, 2012). To evaluate in how far the choice of input parameters (pH/DIC, DIC/TA, and pH/TA) would affect the calculated carbonate system within the same treatment, calculations have been performed with all three combinations of input parameters. As can be seen from Table A1 (appendix) for this study the choice of input parameters does not result in significant differences. Therefore, further discussions and plots are based on the carbonate system calculated from the input parameters pH and DIC.

3.2 The B isotopic signature of *A. lessoniis*' tests

The measured boron isotopic composition of the foraminiferal tests is given in Table 1 (mean values calculated from single measurements of all foraminifers within one treatment) and Table A2 (single measurements of each foraminifer). For the treatments pH_8.1* the boron isotopic composition is identical (~ -32‰) while treatment pH_8.6⁶⁴⁰ shows an increase of the boron isotopic composition by 8.5‰. The boron isotopic composition determined for treatment pH_7.9²⁶⁰ shows a decrease of 3.4‰ compared to the values determined for the treatments pH_8.1*. The results show that the boron isotopic signature is clearly related to pH and independent of the CO₃²⁻ concentration (Fig.1).

3.2.1 The variation of the $\delta^{11}\text{B}$ data between treatments

The standard deviation of the measured $\delta^{11}\text{B}$ reflects the natural variation in the $\delta^{11}\text{B}$ for the different treatments. The standard deviations for the different treatments are nearly identical (~1.4‰) (see Table 1). Rollion-Bard & Erez (2010) used a different approach to evaluate the natural variation in $\delta^{11}\text{B}$ within the test of *Amphistegina lobifera*. Instead of the standard deviations they calculated the difference between the heaviest and lightest $\delta^{11}\text{B}$ value ($\Delta\delta^{11}\text{B}$), a method which overvalues data points outside the confidence interval. Using the latter approach Rollion-Bard & Erez (2010) described

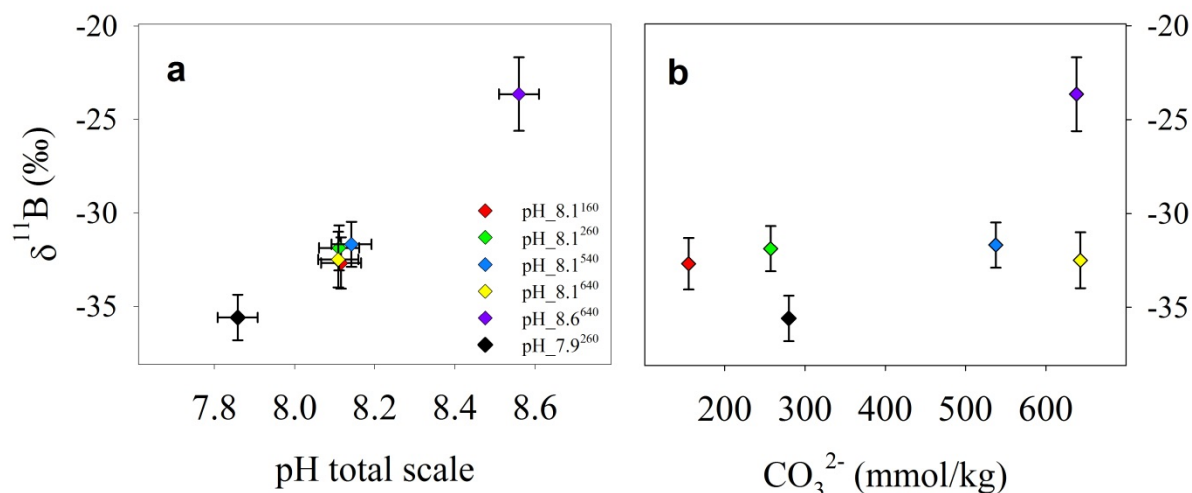


Figure 1: (a) Boron isotopic composition versus pH of the culture media for all treatments. The $\delta^{11}\text{B}$ data represent mean values obtained from single measurements within one treatment. Error bars for $\delta^{11}\text{B}$ represent SD. (b) Calculated carbonate ion concentration versus pH.

Table 1: Mean values of the B isotopic composition and B/Ca of *A. lessonii*. Errors are expressed as SD (calculated from single values within one treatment). Also listed is the isotopic composition of $\text{B}(\text{OH})_4^-$ (based on a calculated carbonate system using pH and DIC as input parameters) and the offset between the isotopic composition of foraminifers and $\text{B}(\text{OH})_4^-$ ($\Delta\delta^{11}\text{B}$).

Treatments	$\delta^{11}\text{B}$ (‰)	$\pm \delta^{11}\text{B}$ (‰)	$\delta^{11}\text{B}$ $\text{B}(\text{OH})_4^-$ cal (‰)	$\Delta\delta^{11}\text{B}$ (‰)	B/Ca (mmol/mol)	$\pm \text{B/Ca}$ (mmol/mol)
pH_8.1 ¹⁶⁰	-32.68	1.37	-28.65	4.04	5.12	1.14
pH_8.1 ²⁶⁰	-31.88	1.20	-28.81	3.07	2.95	0.53
pH_8.1 ⁵⁴⁰	-31.69	1.20	-28.37	3.32	1.75	0.11
pH_8.1 ⁶⁴⁰	-32.50	1.49	-28.59	3.90	1.58	0.13
pH_8.6 ⁶⁴⁰	-23.64	1.97	-22.75	0.90	6.36	1.30
pH_7.9 ²⁶⁰	-35.60	1.22	-31.30	4.29	1.20	0.08

$\Delta\delta^{11}\text{B}$ to be pH dependent in *A. lobifera*. In their study the $\Delta\delta^{11}\text{B}$ increased from 4.7‰ for foraminifers cultured at a pH of 8.45 to 12.2‰ for foraminifers cultured at a pH of 7.9. The authors explained the variability in terms of a calcification mechanism based on sea water vacuolization. It should be noted that the spot size of the analytical method they used to measure the $\delta^{11}\text{B}$ of the test (secondary ion mass spectrometry (SIMS)) was $\sim 30 \mu\text{m}$. This would require that areas, of at least this size, exist within the test, which are formed from vacuoles of the same pH. The latter is unlikely since the authors suggest themselves that the vacuoles cover a pH range starting at the bulk pH and ending with pH 9. Since in their study only a small portion of the test was grown under experimental conditions, the question arises whether the determined $\Delta\delta^{11}\text{B}$ would be the same if the whole test had been grown under experimental conditions. Furthermore, the hypothesis that seawater vacuolization is the only

source for calcification in foraminifers is controversially discussed (Nehrke et al., 2013). If we calculate $\Delta\delta^{11}\text{B}$ for our data as done in the study of Rollion-Bard & Erez (2010), the $\Delta\delta^{11}\text{B}$ for all treatments is $\sim 5\%$ being independent on the pH of the culture media (as already reflected in the standard deviation values).

It has been suggested that test size is an additional factor influencing the $\delta^{11}\text{B}$. Hönisch & Hemming (2004) report lighter $\delta^{11}\text{B}$ by 2.2‰ for individuals of *Globigerinoides sacculifer* in the sieve size class 250 -380 μm than for shells in the 515 – 865 μm size class. This observation is explained by a reduced photosynthetic activity in smaller specimens at greater depth. A study by Walker et al. (2011) showed a linear increase between size and symbionts in *A. lessonii*. If larger foraminifers accommodate more symbionts, smaller foraminifers experience less symbiotic activity, which might lead to lighter $\delta^{11}\text{B}$. However, in our study we do not observe either a correlation between the size of foraminifers and $\delta^{11}\text{B}$ or a correlation between growth rate and $\delta^{11}\text{B}$ (Fig. 2). In our experiment specimens grew for three months reaching a size between 400 and 900 μm . Although we observed different growth rates within each treatment, we do not see a correlation between the test size and the boron isotopic composition. If such an effect really exists in *A. lessonii*, it is very small and not reflected in the boron isotopic composition.

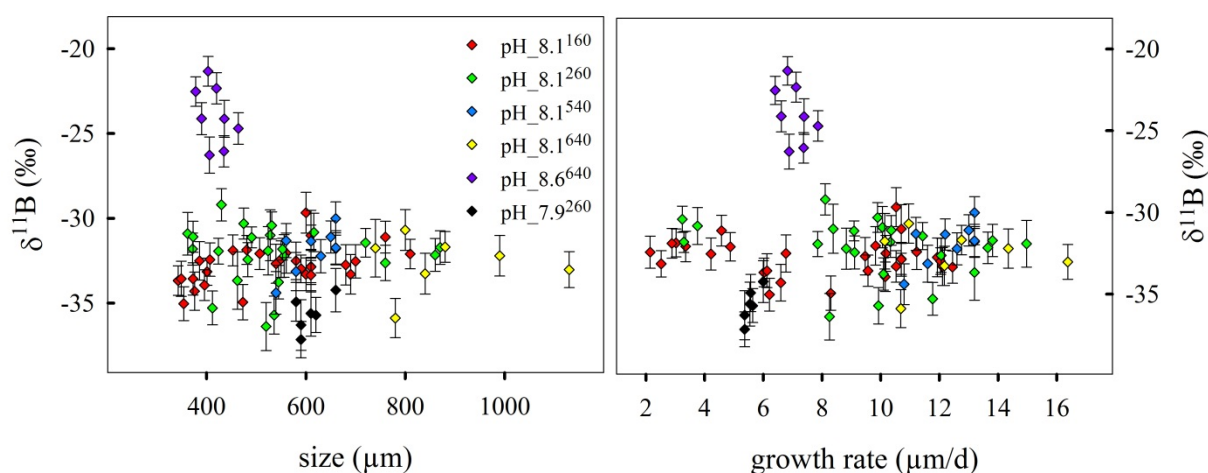


Figure 2: Size and growth rate (defined as size divided by the number of days in culture) versus B isotopic compositions of foraminifers.

3.2.2 $\delta^{11}\text{B}$ of the test versus $\delta^{11}\text{B}$ of $\text{B}(\text{OH})_4^-$

If the assumption that only $\text{B}(\text{OH})_4^-$ is incorporated into marine carbonates is correct, then the $\delta^{11}\text{B}$ of the foraminifers ($\delta^{11}\text{B}_{\text{foram}}$) should equal that of $\text{B}(\text{OH})_4^-$ of the culture media ($\delta^{11}\text{B}_{\text{B}(\text{OH})_4^-}$). The comparison between $\delta^{11}\text{B}_{\text{foram}}$ and $\delta^{11}\text{B}_{\text{B}(\text{OH})_4^-}$ is shown in Figure 3. One parameter needed to calculate $\delta^{11}\text{B}_{\text{B}(\text{OH})_4^-}$ is the boron fractionation factor α , which is defined as:

$$\alpha_{(\text{B}(\text{OH})_3)-\text{B}(\text{OH})_4^-} = \frac{{}^{11}\text{B}(\text{OH})_3/{}^{10}\text{B}(\text{OH})_3}{{}^{11}\text{B}(\text{OH})_4^-/{}^{10}\text{B}(\text{OH})_4^-} \quad (2)$$

Various values for α are reported in the literature. The first theoretical estimate of 1.01194 at 25°C was given by Kakihana et al. (1977) based on reduced partition function ratio calculations using data on molecular vibrations obtained from spectroscopic measurements. Zeebe (2005) showed that the calculation of α is sensitive to the choice of the theoretical methods used to calculate the forces in the molecule and to molecular vibration frequencies. Based on these observations α is suggested to vary between 1.02 and 1.05 (at 25°C). An experimental study was performed by Klochko et al. (2006) using spectrometric pH measurements in order to determine α from differences in the $\text{p}K_{\text{B}}$ of ${}^{11}\text{B}(\text{OH})_3$ and ${}^{10}\text{B}(\text{OH})_3$. The authors determined α to be 1.0272 at 25°C. Most recent studies on boron isotope fractionation (Rollion-Bard & Erez, 2010; Rae et al., 2011; Henehan et al., 2013) use the value 1.0272 for their calculations. According to Zeebe & Wolf-Gladrow (2001) $\delta^{11}\text{B}$ of $\text{B}(\text{OH})_4^-$ can be calculated if α is given by:

$$\delta^{11}\text{B}_{\text{B}(\text{OH})_4^-} = \frac{\delta^{11}\text{B}_{\text{sw}} \times [\text{B}_{\text{sw}}] - \epsilon_{\text{B}} \times [\text{B}(\text{OH})_3]}{[\text{B}(\text{OH})_4^-] + \alpha_{\text{B}} \times [\text{B}(\text{OH})_3]} \quad (3)$$

From Figure 3 it can be seen that $\delta^{11}\text{B}$ of the foraminifers is lighter than $\delta^{11}\text{B}$ of $\text{B}(\text{OH})_4^-$ except for treatment pH_8.6⁶⁴⁰. Since the boron isotopic composition of the culture medium ($\delta^{11}\text{B}_{\text{sw}}$) used in our experiments was measured regularly (every two weeks) and did not change significantly during the experiment, an offset in $\delta^{11}\text{B}$ caused by a changing isotopic composition of the culture media can be excluded. In the following we will discuss various reasons which may explain the offset assuming that α is 1.0272.

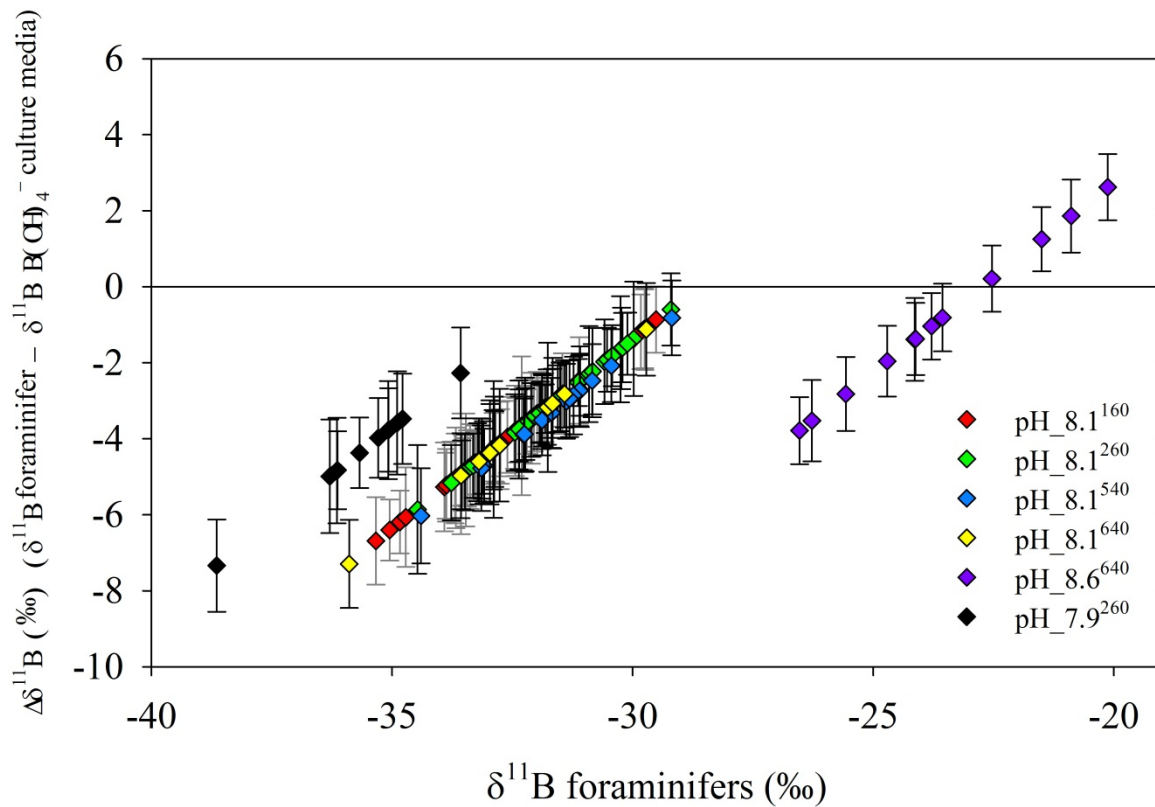


Figure 3: Difference between measured $\delta^{11}\text{B}$ of foraminifers and calculated $\delta^{11}\text{B}$ of $\text{B}(\text{OH})_4^-$ (y-axis) plotted against measured foraminiferal $\delta^{11}\text{B}$. The solid black line represents the B isotopic composition of $\text{B}(\text{OH})_4^-$.

The Boron standards

One factor that could explain the offset between $\delta^{11}\text{B}_{\text{foram}}$ and $\delta^{11}\text{B}_{\text{B}(\text{OH})_4^-}$ is the usage of two different standards. From equation 3 it can be seen that $\delta^{11}\text{B}$ of the culture media is needed to calculate $\delta^{11}\text{B}$ of $\text{B}(\text{OH})_4^-$. We used NIST 610 for the determination of $\delta^{11}\text{B}_{\text{foram}}$ and NIST 951 for the determination of $\delta^{11}\text{B}_{\text{culture media}}$. In order to compare $\delta^{11}\text{B}_{\text{foram}}$ and $\delta^{11}\text{B}_{\text{B}(\text{OH})_4^-}$, the boron isotopic difference in these standards have to be taken into account. NIST 610 and NIST 951 were compared by several studies (Kasemann et al., 2001; le Roux et al., 2004; Fietzke et al., 2010). The results of these studies show that both standards are on average within errors isotopically equal. Therefore, the usage of them cannot explain the deviation between $\delta^{11}\text{B}_{\text{foram}}$ and $\delta^{11}\text{B}_{\text{B}(\text{OH})_4^-}$ seen in the pH_8.1* treatments.

Vital effects

The most widely discussed reason for the $\delta^{11}\text{B}$ offset between foraminifers and $\text{B}(\text{OH})_4^-$ are the physiological processes involved in the calcification process, the so called vital effects. Symbiont activity strongly influences the pH near the surface of the foraminifers (Köhler-Rink & Kühl, 2000; Zeebe et al., 2003) and impacts the $\delta^{11}\text{B}$ signature of the test. The photosynthetic activity of symbionts consumes CO_2 leading to a pH increase while symbiont's respiration generates CO_2 leading to a pH decrease within the micro environment around the foraminifer. In theory, acidification of the microenvironment due to respiration and calcification would result in lighter $\delta^{11}\text{B}$ of the test whereas consumption of CO_2 by photosynthesis leads to heavier $\delta^{11}\text{B}$. The net impact of these different processes depends on their respective rates (Zeebe et al., 2003). The effect of photosynthesis on $\delta^{11}\text{B}$ was studied by Hönisch et al. (2003). From culture experiments with the planktonic symbiont bearing foraminifer *Orbulina universa* the authors report $\delta^{11}\text{B}$ values to be 1.5 ‰ higher under high light than under low light conditions. Furthermore, Lea et al. (1995) has shown that the calcification of the spherical shell in *O.universa* in culture experiments also takes place during night. If the timing of calcifications differs for single specimens of *A.lessonii*, the average of $\delta^{11}\text{B}$ of the tests would depend on which specimen calcifies when and how much. Using ^{14}C as a tracer Muller (1978) demonstrated that carbon fixation into the skeleton of *A. lessonii* is almost ten times higher in the light than in the dark suggesting that this species depend on symbiont photosynthesis for growth. The boron isotopic composition of *A.lessonii* obtained from our study is lower than for several planktonic species studied so far (Sanyal et al., 1996; Sanyal et al., 2001). This could indicate that photosynthetic activity in *A.lessonii* was lower than in planktonic species studied by Sanyal et al. (1996; 2001). A lower photosynthesis caused by low light levels in our experiments appears to be unlikely since Walker et al. (2011) show that in *A.lessonii* photosynthesis reaches its maximum at $170 \mu\text{mol photon m}^{-2}\text{s}^{-1}$. We used $120 \mu\text{mol photon m}^{-2}\text{s}^{-1}$ which is not suggestive of strong light limitation.

In benthic species without symbionts (*Neogloboquadrina dutertrei*, *Cibicidoides mundulus*, *Cibicidoides wuellerstorfi*) studied so far a lighter $\delta^{11}\text{B}$ is observed than for planktonic species (Foster, 2008; Rae et al., 2011). These findings support the notion that respiration and calcification of benthic

foraminifers are the dominant processes leading to an acidification in the micro environment. In support of this inference Glas et al. (2012) showed that the micro-environment pH of the symbiont-barren benthic species *Ammonia spec.* is, during chamber formation, by ca. 1.5 lower than bulk seawater.

The role of B(OH)₃

Another possible contribution of shifting foraminiferal $\delta^{11}\text{B}$ is the incorporation of B(OH)_3 (Klochko et al., 2009). This B species always has a heavier isotopic composition and therefore, additional incorporation of B(OH)_3 would result in heavier $\delta^{11}\text{B}$. In our study the $\delta^{11}\text{B}$ values of the benthic *A. lessonii* are lighter than the $\delta^{11}\text{B}$ values of B(OH)_4^- . Thus, an incorporation of B(OH)_3 at pH 8.1 cannot explain the measured values and seems unlikely. Even though, there is on average no offset at pH 8.6 incorporation of B(OH)_3 seems unlikely, too, as with increasing pH the concentration of B(OH)_3 decreases.

Boron enrichment of the culture media

We increased the boron concentration of all treatments ten times compared to the natural concentration of seawater. Borate has got a strong buffer capacity and its concentration is nearly doubled in the pH_{8.6}⁶⁴⁰ treatment (compared to pH_{8.1}*). This leads to a stronger compensation of the acidification in the microenvironment (Zeebe et al., 2008). This, in turn, could explain why foraminiferal samples from the pH_{8.6}⁶⁴⁰ treatment show a lower offset between $\delta^{11}\text{B}_{\text{foram}}$ and $\delta^{11}\text{B}_{\text{B(OH)}_4^-}$ compared to samples from the pH_{8.1}* and pH_{7.9}²⁶⁰ treatments.

3.3. The B/Ca of *A. lessonii*

The B/Ca data of single measurements is listed in table A2. Mean values of the foraminiferal tests plotted against pH and $[\text{CO}_3^{2-}]$ of the culture media are shown in Figure 4. No correlation between the plotted parameters is observed. In a culture study of Allen et al. (2011) it was shown that the pH of culture media and B/Ca of foraminiferal tests are positively correlated. An increase of pH is associated with changes in the carbonate system: The concentrations of CO_3^{2-} and B(OH)_4^- increase with increasing pH while the concentration of HCO_3^- decreases. Because of these

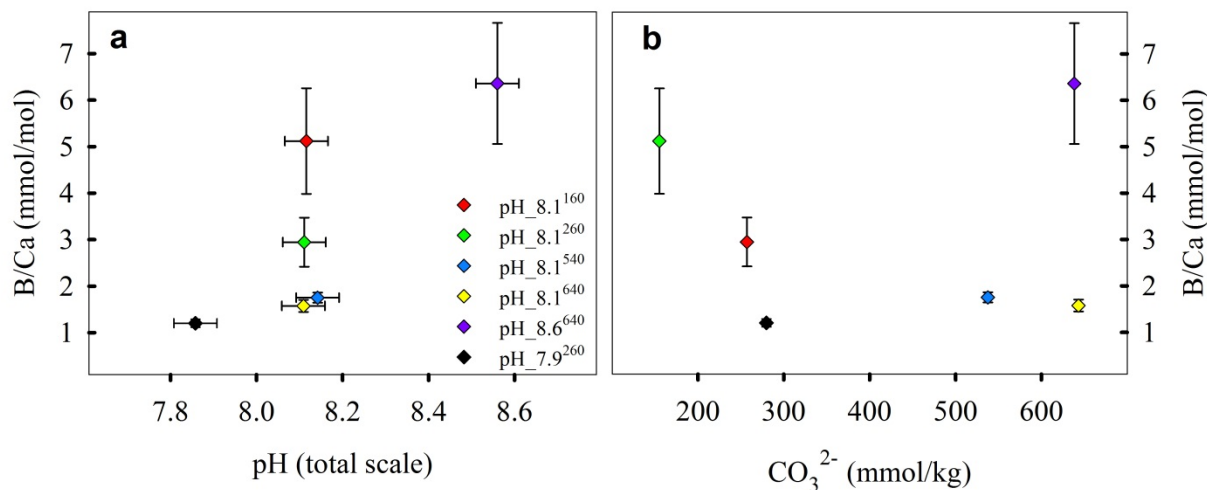


Figure 4: (a) B/Ca plotted against pH of culture media and (b) B/Ca plotted against $[\text{CO}_3^{2-}]$ of culture media. Both graphs show no correlation neither with pH nor with $[\text{CO}_3^{2-}]$. B/Ca data represents mean values of all measurements of foraminifers. Error bars are expressed as SD.

coupled processes it is, in the framework of a classical carbonate system perturbation study like the one of Allen and co-workers (2011), not possible to identify the causal agent. In a second study Allen and co-workers (2012) suggested based on data from a culture study on three different planktonic foraminiferal species using a decoupled carbonate chemistry a “competition between aqueous boron and carbon species for inclusion into the calcite lattice”. To further elaborate on this hypothesis we plot our B/Ca data against several possible candidates ($\text{B}(\text{OH})_4^-/\text{CO}_3^{2-}$, $\text{B}(\text{OH})_4^-/\text{HCO}_3^-$, and $\text{B}(\text{OH})_4^-/\text{DIC}$). The best correlation is given when B/Ca is plotted against $\text{B}(\text{OH})_4^-/\text{HCO}_3^-$ (Fig.5). This is in good agreement with the data shown in the publication of Allen and co-workers (2012) for cultured *G. sacculifer*, *G. ruber*, and *O. universa*. To summarise: if pH and subsequently $[\text{B}(\text{OH})_4^-]$ increase in the culture media, $[\text{HCO}_3^-]$ decreases resulting in less competition for $\text{B}(\text{OH})_4^-$ for uptake into the foraminifer’s test. In a natural system the competition between $\text{B}(\text{OH})_4^-$ and HCO_3^- support the underlying concept of the B/Ca proxy: the observed linearity of foraminiferal B/Ca and $[\text{CO}_3^{2-}]$ can be inferred from the inverse correlated relationship between $[\text{B}(\text{OH})_4^-]$ and $[\text{HCO}_3^-]$ with increasing pH.

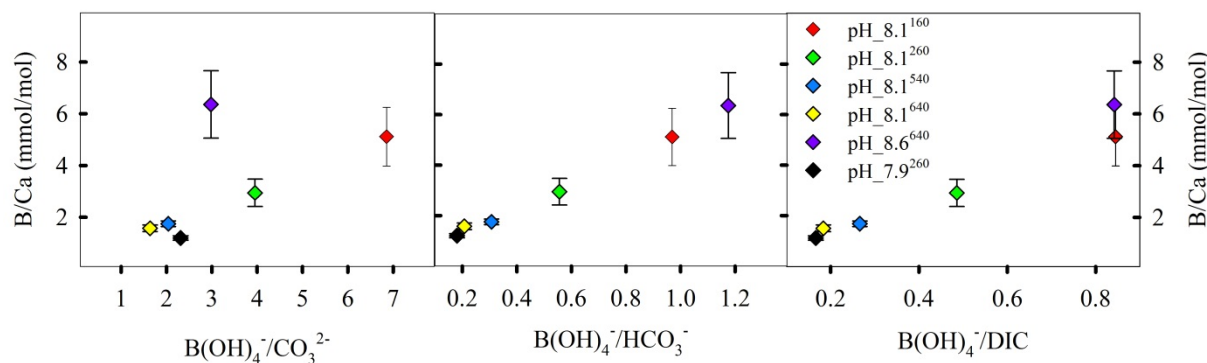


Figure 5: B/Ca plotted against $\text{B(OH)}_4^-/\text{CO}_3^{2-}$, $\text{B(OH)}_4^-/\text{HCO}_3^-$, and $\text{B(OH)}_4^-/\text{DIC}$. The best linear regression is given when B/Ca is plotted against $\text{B(OH)}_4^-/\text{HCO}_3^-$. B/Ca data represents mean values of all measurements. Error bars are expressed as SD.

Further observations

At this point we would like to draw the attention of the reader to two interesting observations within our data which cannot be elaborated further within the framework of this study, but that represent an interesting basis for further investigations. 1) Since both parameters ($\delta^{11}\text{B}$ and B/Ca) were determined simultaneously, the question arises whether a correlation between both parameters can be identified in the measurements. As can be seen from Figure 6 no preference for the incorporation of the lighter or heavier B isotope as a function of the B concentration in the test is observed. 2) It could be observed that the standard deviation for B/Ca does show a significant increase with increasing B incorporation (Fig. 5).

4. CONCLUSION

Culture experiments based on a decoupled pH and CO_3^{2-} chemistry indicate that the $\delta^{11}\text{B}$ of the test of *A. lessonii* is related to pH whereas the B/Ca of the foraminiferal shells show a positive correlation with $\text{B(OH)}_4^-/\text{HCO}_3^-$. The latter observation suggests a competition between B(OH)_4^- and HCO_3^- of the culture media for B uptake into the test. Furthermore, we observe a natural variability in $\delta^{11}\text{B}$ of $\sim 1.4\text{‰}$ (SD) or $\sim 5\text{‰}$ ($\Delta\delta^{11}\text{B}$) in the tests which seems to be independent of the carbonate chemistry. The B isotopic composition of the tests is lighter than the one of B(OH)_4^- at pH 8.1. We

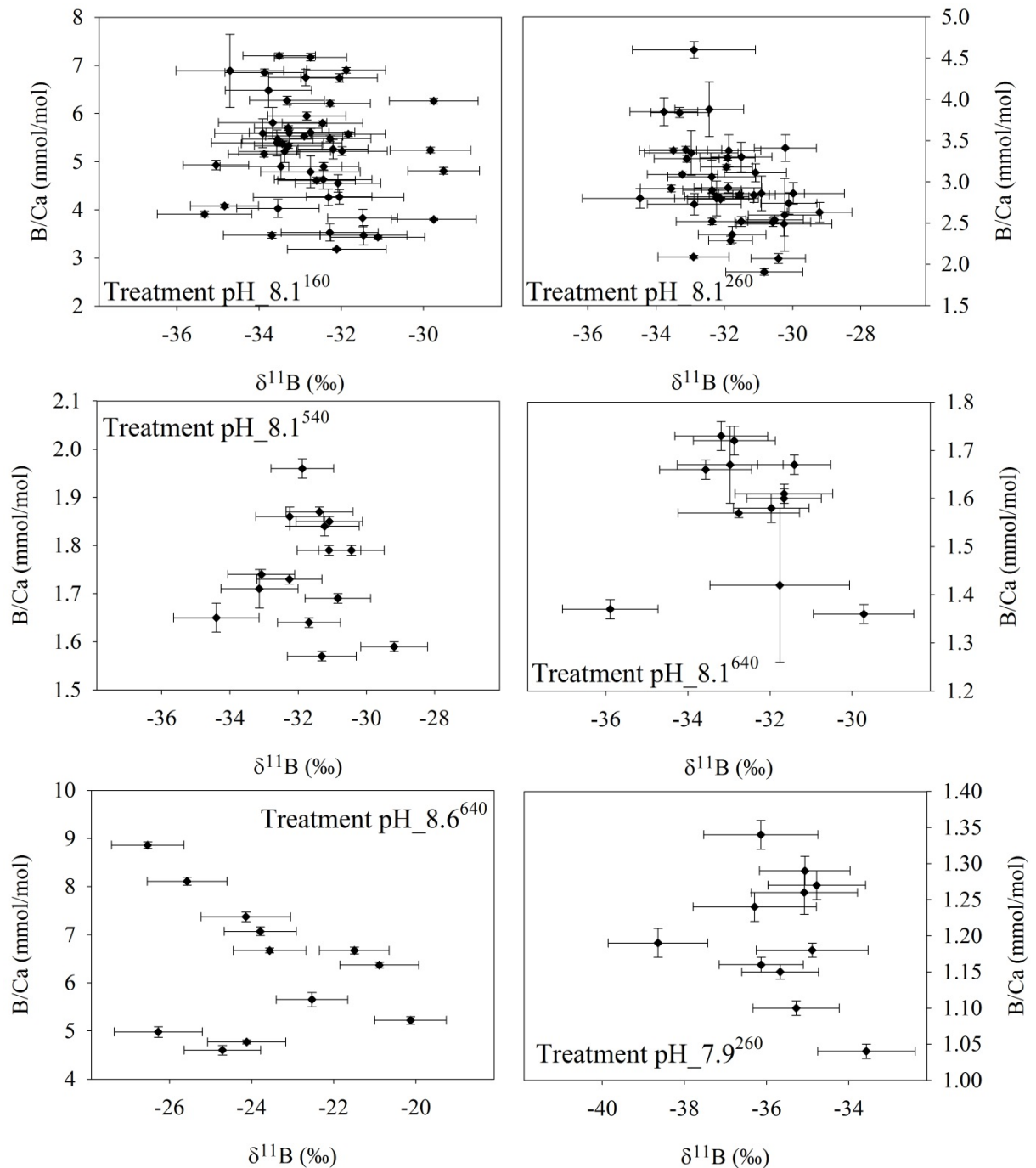


Figure 6: Single B/Ca values plotted against single $\delta^{11}\text{B}$ values. No correlation exists between the plotted parameters.

conclude that the effects of calcification and respiration on $\delta^{11}\text{B}$ dominating over the effects of photosynthesis are responsible for the offset between $\delta^{11}\text{B}_{\text{foram}}$ and $\delta^{11}\text{B}_{\text{B(OH)}_4}$. The distribution of B in

the tests is not homogenous: the variability in B/Ca increases with increasing B/Ca in the tests. Our data shows no correlation between B concentration and isotope fractionation.

ACKNOWLEDGMENTS

We thank Sarah Moser, Kerstin Oetjen, and Tina Brenneis for assistance during the culture experiments. For analysis of DIC and elemental measurements we thank Laura Wischnewski, Jana Hölscher, and Ilsetraut Stölting. We are grateful to Klaus-Uwe Richter for handling the CO₂ gas-mixing system. This project was financially supported by the DFG BI 432/7-1.

REFERENCES

- Allen, K.A., Hönisch, B., Eggins, S.M., Rosenthal, Y., 2012. Environmental controls on B/Ca in calcite tests of the tropical planktic foraminifer species *Globigerinoides ruber* and *Globigerinoides sacculifer*. *Earth and Planetary Science Letters* 351–352, 270-280.
- Allen, K.A., Hönisch, B., Eggins, S.M., Yu, J., Spero, H.J., Elderfield, H., 2011. Controls on boron incorporation in cultured tests of the planktic foraminifer *Orbulina universa*. *Earth and Planetary Science Letters* 309, 291-301.
- Bradshaw, A.L., Brewer, P.G., Shafer, D.K., Williams, R.T., 1981. Measurements of total carbon dioxide and alkalinity by potentiometric titration in the GEOSECS program. *Earth and Planetary Science Letters* 55, 99-115.
- Brown, R.E., Anderson, L.D., Thomas, E., Zachos, J.C., 2011. A core-top calibration of B/Ca in the benthic foraminifers *Nuttallides umbonifera* and *Oridorsalis umbonatus*: A proxy for Cenozoic bottom water carbonate saturation. *Earth and Planetary Science Letters* 310, 360-368.
- Catanzaro, E.J., Champion, C.E., Garner, E.L., Marinenko, G., Sappenfield, K.M., Shields, W.R., 1970. Boric Acid, Isotopic, and Assay Standard Reference Materials Nat. Bur. Stand. (U.S.) Spec. Publ. 260-17, 70.
- Dickson, A.G., Sabine, C.L., Christian, J.R., (Eds.), 2007. Guide to Best Practices for Ocean CO₂ Measurements. PICES Special Publication 3, 191.
- Ernst, S., Janse, M., Renema, W., Kouwenhoven, T., Goudeau, M.-L., Reichart, G.-J., 2011. BENTHIC FORAMINIFERA IN A LARGE INDO-PACIFIC CORAL REEF AQUARIUM. *The Journal of Foraminiferal Research* 41, 101-113.
- Fietzke, J., Heinemann, A., Taubner, I., Bohm, F., Erez, J., Eisenhauer, A., 2010. Boron isotope ratio determination in carbonates via LA-MC-ICP-MS using soda-lime glass standards as reference material. *Journal of Analytical Atomic Spectrometry* 25, 1953-1957.
- Foster, G.L., 2008. Seawater pH, pCO₂ and [CO₂-3] variations in the Caribbean Sea over the last 130 kyr: A boron isotope and B/Ca study of planktic foraminifera. *Earth and Planetary Science Letters* 271, 254-266.
- Foster, G.L., Pogge von Strandmann, P.A.E., Rae, J.W.B., 2010. Boron and magnesium isotopic composition of seawater. *Geochemistry, Geophysics, Geosystems* 11, Q08015.
- Glas, M.S., Langer, G., Keul, N., 2012. Calcification acidifies the microenvironment of a benthic foraminifer (*Ammonia sp.*). *Journal of Experimental Marine Biology and Ecology* 424-425, 53-58.
- Hemming, N.G., Hanson, G.N., 1992. Boron isotopic composition and concentration in modern marine carbonates. *Geochimica et Cosmochimica Acta* 56, 537-543.
- Hemming, N.G., Reeder, R.J., Hanson, G.N., 1995. Mineral-fluid partitioning and isotopic fractionation of boron in synthetic calcium carbonate. *Geochimica et Cosmochimica Acta* 59, 371-379.
- Henehan, M.J., Rae, J.W.B., Foster, G.L., Erez, J., Prentice, K.C., Kucera, M., Bostock, H.C., Martínez-Botí, M.A., Milton, J.A., Wilson, P.A., Marshall, B.J., Elliott, T., 2013. Calibration of the boron isotope proxy in the planktonic foraminifera *Globigerinoides ruber* for use in palaeo-CO₂ reconstruction. *Earth and Planetary Science Letters* 364, 111-122.

- Hönisch, B., Bijma, J., Russell, A.D., Spero, H.J., Palmer, M.R., Zeebe, R.E., Eisenhauer, A., 2003. The influence of symbiont photosynthesis on the boron isotopic composition of foraminifera shells. *Marine Micropaleontology* 49, 87-96.
- Hönisch, B., Hemming, N.G., 2004. Ground-truthing the boron isotope-paleo-pH proxy in planktonic foraminifera shells: Partial dissolution and shell size effects. *Paleoceanography* 19, PA4010.
- Hönisch, B., Hemming, N.G., 2005. Surface ocean pH response to variations in pCO₂ through two full glacial cycles. *Earth and Planetary Science Letters* 236, 305-314.
- Hoppe, C.J.M., Langer, G., Rokitta, S. D., Wolf-Gladrow, D. A., Rost, B, 2012. Implications of observed inconsistencies in carbonate chemistry measurements for ocean acidification studies. *Biogeosciences* 9, 2401-2405.
- Kaczmarek, K., Horn, I., Nehrke, G., Bijma, J. Simultaneous determination of $\delta^{11}\text{B}$ and B/Ca in marine biogenic carbonates at nano gram level. *Chemical Geology*, under review.
- Kakihana, H., Kotaka, M., Satoh, S., Nomura, M., Okamoto, M., 1977. Fundamental Studies on the Ion-Exchange Separation of Boron Isotopes. *Bulletin of the Chemical Society of Japan* 50, 158-163.
- Kasemann, S., Meixner, A., Rocholl, A., Vennemann, T., Rosner, M., Schmitt, A.K., Wiedenbeck, M., 2001. Boron and Oxygen Isotope Composition of Certified Reference Materials NIST SRM 610/612 and Reference Materials JB-2 and JR-2. *Geostandards Newsletter* 25, 405-416.
- Klochko, K., Cody, G.D., Tossell, J.A., Dera, P., Kaufman, A.J., 2009. Re-evaluating boron speciation in biogenic calcite and aragonite using ¹¹B MAS NMR. *Geochimica et Cosmochimica Acta* 73, 1890-1900.
- Klochko, K., Kaufman, A.J., Yao, W., Byrne, R.H., Tossell, J.A., 2006. Experimental measurement of boron isotope fractionation in seawater. *Earth and Planetary Science Letters* 248, 276-285.
- Köhler-Rink, S., Kühl, M., 2000. Microsensor studies of photosynthesis and respiration in larger symbiotic foraminifera. I The physico-chemical microenvironment of *Marginopora vertebralis*, *Amphistegina lobifera* and *Amphisorus hemprichii*. *Marine Biology* 137, 473-486.
- le Roux, P.J., Shirey, S.B., Benton, L., Hauri, E.H., Mock, T.D., 2004. In situ, multiple-multiplier, laser ablation ICP-MS measurement of boron isotopic composition ($\delta^{11}\text{B}$) at the nanogram level. *Chemical Geology* 203, 123-138.
- Lea, D.W., Martin, P.A., Chan, D.A., Spero, H.J., 1995. Calcium uptake and calcification rate in the planktonic foraminifer *Orbulina universa*. *The Journal of Foraminiferal Research* 25, 14-23.
- Longerich, H.P., Jackson, S.E., Gunther, D., 1996. Inter-laboratory note. Laser ablation inductively coupled plasma mass spectrometric transient signal data acquisition and analyte concentration calculation. *Journal of Analytical Atomic Spectrometry* 11, 899-904.
- Misra, S., Owen, R., Kerr, J., Greaves, M., Elderfield, H., 2014. Determination of $\delta^{11}\text{B}$ by HR-ICP-MS from Mass Limited Samples: Application to Natural Carbonates and Water Samples. *Geochimica et Cosmochimica Acta*, in review.
- Muller, P.H., 1978. 14 Carbon fixation and loss in a foraminiferal-algal symbiont system. *The Journal of Foraminiferal Research* 8, 35-41.
- Nehrke, G., Keul, N., Langer, G., de Nooijer, L.J., Bijma, J., Meibom, A., 2013. A new model for biomineralization and trace-element signatures of Foraminifera tests. *Biogeosciences* 10, 6759-6767.

- Ni, Y., Foster, G.L., Bailey, T., Elliott, T., Schmidt, D.N., Pearson, P., Haley, B., Coath, C., 2007. A core top assessment of proxies for the ocean carbonate system in surface-dwelling foraminifers. *Paleoceanography* 22, PA3212.
- Rae, J.W.B., Foster, G.L., Schmidt, D.N., Elliott, T., 2011. Boron isotopes and B/Ca in benthic foraminifera: Proxies for the deep ocean carbonate system. *Earth and Planetary Science Letters* 302, 403-413.
- Rollion-Bard, C., Erez, J., 2010. Intra-shell boron isotope ratios in the symbiont-bearing benthic foraminiferan *Amphistegina lobifera*: Implications for $\delta^{11}\text{B}$ vital effects and paleo-pH reconstructions. *Geochimica et Cosmochimica Acta* 74, 1530-1536.
- Sanyal, A., Hemming, N.G., Broecker, W.S., Lea, D.W., Spero, H.J., Hanson, G.N., 1996. Oceanic pH control on the boron isotopic composition of foraminifera: Evidence from culture experiments. *Paleoceanography* 11, 513-517.
- Sanyal, A., Bijma, J., Spero, H., Lea, D.W., 2001. Empirical relationship between pH and the boron isotopic composition of *Globigerinoides sacculifer*: Implications for the boron isotope paleo-pH proxy. *Paleoceanography* 16, 515-519.
- Sen, S., Stebbins, J.F., Hemming, N.G., Ghosh, B., 1994. Coordination environments of B impurities in calcite and aragonite polymorphs: A ^{11}B MAS NMR study. *American Mineralogist* 79, 819-825.
- Spero, H.J., Parker, S.L., 1985. Photosynthesis in the symbiotic planktonic foraminifer *Orbulina universa* and its potential contribution to oceanic primary productivity. *The Journal of Foraminiferal Research* 15, 273-281.
- Spivack, A.J., Edmond, J.M., 1987. Boron isotope exchange between seawater and the oceanic crust. *Geochimica et Cosmochimica Acta* 51, 1033-1043.
- Tripati, A.K., Roberts, C.D., Eagle, R.A., Li, G., 2011. A 20 million year record of planktic foraminiferal B/Ca ratios: Systematics and uncertainties in pCO₂ reconstructions. *Geochimica et Cosmochimica Acta* 75, 2582-2610.
- Vogl, J., Rosner, M., 2012. Production and Certification of a Unique Set of Isotope and Delta Reference Materials for Boron Isotope Determination in Geochemical, Environmental and Industrial Materials. *Geostandards and Geoanalytical Research* 36, 161-175.
- Walker, R.A., Hallock, P., Torres, J.J., Vargo, G.A., 2011. PHOTOSYNTHESIS AND RESPIRATION IN FIVE SPECIES OF BENTHIC FORAMINIFERA THAT HOST ALGAL ENDOSYMBIONTS. *The Journal of Foraminiferal Research* 41, 314-325.
- Yu, J., Elderfield, H., Hönisch, B., 2007. B/Ca in planktonic foraminifera as a proxy for surface seawater pH. *Paleoceanography* 22, PA2202.
- Zeebe, R.E., 2005. Stable boron isotope fractionation between dissolved $\text{B}(\text{OH})_3$ and $\text{B}(\text{OH})_4^-$. *Geochimica et Cosmochimica Acta* 69, 2753-2766.
- Zeebe, R.E., Wolf-Gladrow, D.A., 2001. CO₂ in seawater: equilibrium, kinetics, isotopes. Elsevier Science B.V., Amsterdam.
- Zeebe, R.E., Wolf-Gladrow, D.A., Bijma, J., Hönisch, B., 2003. Vital effects in foraminifera do not compromise the use of $\delta^{11}\text{B}$ as a paleo-pH indicator: Evidence from modeling. *Paleoceanography* 18, 1043.

Zeebe, R.E., Bijma, J., Hönisch, B., Sanyal, A., Spero, H.J., Wolf-Gladrow, D.A., 2008. Vital effects and beyond: a modelling perspective on developing paleoceanographical proxy relationships in foraminifera. Geological Society, London, Special Publications 303, 45-58.

APPENDIX

TABLES

Table A1: Chemical composition of the culture media. Calculated carbonate systems using different pairs of input parameters. m - measured, cal - calculated.* Calculation of $B(OH)_4^-$ was performed using a pK_B of 8.59 corrected for S and T according to Dickson 1990. For information about errors on measured parameters see paper text section 2.3.

Input pH and DIC	pH _m total	DIC _m μmol/kg	TA _m μmol/kg	TA _{cal} μmol/kg	CO ₃ ²⁻ _{cal} μmol/kg	HCO ₃ ⁻ _{cal} μmol/kg	B(OH) ₄ ⁻ _{cal} * μmol/kg	pCO ₂ _{cal} μatm	B _m μmol/kg	Ca _m μmol/kg	δ ¹¹ B _m ‰	δ ¹¹ B B(OH) ₄ ⁻ _{cal} ‰
pH_8.1 ¹⁶⁰	8.115	1257	2501	2456	155	1096	1062	213	4233	8503	-9.22	-28.65
pH_8.1 ²⁶⁰	8.111	2093	3232	3387	257	1826	1016	356	4063	9638	-9.00	-28.81
pH_8.1 ⁵⁴⁰	8.142	4128	5626	5748	538	3573	1098	652	4177	9692	-8.88	-28.37
pH_8.1 ⁶⁴⁰	8.109	5736	7392	7295	643	5064	1053	1006	4240	9360	-8.73	-28.59
pH_8.6 ⁶⁴⁰	8.560	2261	5387	4925	638	1620	1904	113	3944	9688	-9.00	-22.75
pH_7.9 ²⁶⁰	7.858	3890	4691	4789	280	3576	647	1254	4136	9580	-9.11	-31.30
Input pH and TA	pH _m total	TA _m μmol/kg	DIC _m μmol/kg	DIC _{cal} μmol/kg	CO ₃ ²⁻ _{cal} μmol/kg	HCO ₃ ⁻ _{cal} μmol/kg	B(OH) ₄ ⁻ _{cal} * μmol/kg	pCO ₂ _{cal} μatm	B _m μmol/kg	Ca _m μmol/kg	δ ¹¹ B _m ‰	δ ¹¹ B B(OH) ₄ ⁻ _{cal} ‰
pH_8.1 ¹⁶⁰	8.115	2501	1257	1297	160	1131	1062	220	4233	8503	-9.22	-28.65
pH_8.1 ²⁶⁰	8.111	3232	2093	1955	240	1706	1016	333	4063	9638	-9.00	-28.81
pH_8.1 ⁵⁴⁰	8.142	5626	4128	4020	524	3479	1098	635	4177	9692	-8.88	-28.37
pH_8.1 ⁶⁴⁰	8.109	7392	5736	5669	691	4952	1037	975	4240	9360	-8.73	-28.69
pH_8.6 ⁶⁴⁰	8.560	5387	2261	2348	663	1682	1904	117	3944	9688	-9.00	-22.75
pH_7.9 ²⁶⁰	7.858	4691	3890	3798	273	3491	647	1225	4136	9580	-9.11	-31.30
Input DIC and TA	pH _m total	pH _{cal} total	DIC _m μmol/kg	TA _m μmol/kg	CO ₃ ²⁻ _{cal} μmol/kg	HCO ₃ ⁻ _{cal} μmol/kg	B(OH) ₄ ⁻ _{cal} * μmol/kg	pCO ₂ _{cal} μatm	B _m μmol/kg	Ca _m μmol/kg	δ ¹¹ B _m ‰	δ ¹¹ B B(OH) ₄ ⁻ _{cal} ‰
pH_8.1 ¹⁶⁰	8.115	8.136	1257	2501	162	1090	1100	202	4233	8503	-9.22	-28.77
pH_8.1 ²⁶⁰	8.111	8.045	2093	3232	223	1858	901	424	4063	9638	-9.00	-29.42
pH_8.1 ⁵⁴⁰	8.142	8.100	4128	5626	494	3614	1022	725	4177	9692	-8.88	-28.81
pH_8.1 ⁶⁴⁰	8.109	8.086	5736	7392	667	5040	1012	1045	4240	9360	-8.73	-28.84
pH_8.6 ⁶⁴⁰	8.560	8.689	2261	5387	783	1476	2195	76	3944	9688	-9.00	-20.81
pH_7.9 ²⁶⁰	7.858	7.806	3890	4691	250	3601	714	1424	4136	9580	-9.11	-30.87

Table A2: Results from single B measurements of foraminifers. Errors are calculated according to formulas 2.8 (error of $\delta^{11}\text{B}$) and 2.9 (error of B/Ca) in topic 2.

Treatment pH 8.1 ¹⁶⁰				
Foram #	$\delta^{11}\text{B}$ (‰)	2RSE(‰)	B/Ca (mmol/l)	\pm (mmol/mol)
1	-33.88	0.87	5.16	0.06
1	-32.08	1.04	4.55	0.18
2	-33.43	1.00	5.37	0.05
2	-33.27	0.97	5.60	0.07
3	-31.98	1.10	5.22	0.09
3	-32.84	0.95	5.95	0.08
3	-33.69	1.18	3.47	0.06
4	-32.11	1.20	3.18	0.02
5	-35.33	1.15	3.91	0.06
5	-29.75	1.03	3.80	0.02
6	-31.11	1.14	3.43	0.03
7	-33.77	1.05	6.48	0.35
7	-33.38	1.12	5.21	0.23
8	-33.91	1.17	5.59	0.30
8	-33.47	1.48	4.90	0.26
9	-32.44	1.19	4.63	0.20
10	-32.20	0.85	5.26	0.20
11	-32.05	0.80	4.27	0.15
12	-33.32	0.91	6.27	0.09
12	-33.29	0.82	5.70	0.05
13	-32.27	0.99	5.48	0.06
13	-32.75	1.08	5.61	0.08
14	-31.83	0.90	5.57	0.05
14	-33.87	0.96	6.85	0.08
15	-32.05	0.93	6.74	0.09
16	-29.83	0.98	5.24	0.06
16	-29.51	0.87	4.81	0.07
17	-32.46	0.98	5.80	0.05
17	-32.90	0.94	5.53	0.06
18	-32.87	0.90	6.75	0.17
19	-31.88	0.96	6.90	0.06
19	-33.51	0.88	7.20	0.06
20	-32.27	0.98	6.21	0.06
20	-29.75	1.08	6.26	0.06
21	-32.75	0.88	7.17	0.08
22	-32.60	0.94	4.61	0.07
22	-32.43	0.85	4.90	0.08
23	-33.29	0.82	5.33	0.05
24	-33.55	0.86	5.47	0.06
24	-35.05	0.80	4.93	0.10
25	-34.84	0.83	4.08	0.04
26	-32.28	1.18	3.53	0.18
26	-31.46	1.06	3.47	0.20
27	-33.54	1.00	4.03	0.19
27	-32.75	1.21	4.79	0.33
28	-32.31	1.83	4.26	0.17
28	-31.48	0.85	3.83	0.18
29	-33.57	1.59	5.39	0.27
30	-34.71	1.31	6.89	0.76

31	-33.67	1.32	5.81	0.32
Treatment pH 8.1 ²⁶⁰				
Foram #	$\delta^{11}\text{B}$ (‰)	2RSE(‰)	B/Ca (mmol/l)	±(mmol/mol)
32	-33.13	1.05	3.39	0.04
32	-32.11	0.97	2.79	0.02
32	-32.22	0.94	2.82	0.03
32	-32.89	1.80	4.60	0.10
33	-33.23	1.03	3.09	0.03
33	-33.10	0.95	3.28	0.04
33	-33.49	1.00	3.38	0.03
34	-30.58	1.11	2.51	0.05
34	-32.90	1.04	2.09	0.02
34	-32.36	1.05	2.52	0.04
35	-29.98	1.50	2.86	0.13
35	-32.97	1.37	3.35	0.27
36	-32.23	1.23	2.80	0.21
36	-32.37	1.29	3.06	0.20
37	-30.25	1.40	2.49	0.15
37	-31.77	0.99	2.36	0.10
38	-34.47	1.69	2.80	0.12
38	-32.88	1.38	2.73	0.13
39	-30.91	1.26	2.86	0.21
40	-31.87	0.94	3.38	0.19
41	-31.50	0.90	3.30	0.18
41	-31.09	0.91	3.11	0.11
42	-29.21	0.95	2.63	0.12
43	-32.44	1.01	3.88	0.33
44	-30.23	1.07	2.60	0.44
44	-31.50	0.91	2.52	0.06
44	-33.56	0.90	2.92	0.04
45	-33.31	0.84	3.84	0.06
45	-31.89	0.99	2.93	0.06
45	-31.56	0.88	2.84	0.03
46	-31.91	0.81	3.29	0.03
46	-30.53	0.84	2.54	0.04
46	-32.36	0.86	2.90	0.03
47	-30.21	0.91	3.41	0.16
47	-30.11	0.82	2.74	0.13
48	-33.77	0.99	3.85	0.17
49	-31.94	0.76	3.18	0.03
50	-31.13	0.62	2.84	0.09
51	-30.42	0.80	2.07	0.06
52	-30.83	1.13	1.91	0.04
53	-31.82	0.64	2.29	0.05

Treatment pH 8.1 ⁵⁴⁰				
Foram #	$\delta^{11}\text{B}$ (‰)	2RSE(‰)	B/Ca (mmol/l)	\pm (mmol/mol)
54	-29.19	0.98	1.59	0.01
54	-30.84	0.96	1.69	0.01
55	-31.09	0.97	1.85	0.01
55	-31.10	0.93	1.79	0.01
56	-31.69	0.92	1.64	0.01
56	-31.88	0.92	1.96	0.02
57	-33.08	0.98	1.74	0.01
57	-31.38	0.98	1.87	0.01
58	-32.26	0.95	1.73	0.01
58	-30.44	0.96	1.79	0.01
59	-31.23	1.02	1.84	0.02
59	-32.25	0.99	1.86	0.02
60	-34.40	1.25	1.65	0.03
61	-31.31	1.01	1.57	0.01
62	-33.14	1.13	1.71	0.04

Treatment pH 8.1 ⁶⁴⁰				
Foram #	$\delta^{11}\text{B}$ (‰)	2RSE(‰)	B/Ca (mmol/l)	\pm (mmol/mol)
63	-31.66	1.19	1.61	0.02
63	-29.72	1.22	1.36	0.02
64	-35.89	1.16	1.37	0.02
65	-31.76	1.70	1.42	0.16
66	-33.19	1.13	1.73	0.03
66	-32.87	1.00	1.72	0.03
67	-32.76	1.48	1.57	0.01
67	-31.66	0.91	1.60	0.02
68	-33.57	1.12	1.66	0.02
68	-32.97	1.29	1.67	0.08
69	-31.41	0.89	1.67	0.02
69	-31.97	0.92	1.58	0.03

Treatment pH 8.6 ⁶⁴⁰				
Foram #	$\delta^{11}\text{B}$ (‰)	2RSE(‰)	B/Ca (mmol/l)	\pm (mmol/mol)
70	-26.53	0.88	8.86	0.07
70	-25.57	0.97	8.11	0.08
71	-26.27	1.07	4.98	0.11
72	-24.14	1.09	7.37	0.10
73	-24.71	0.93	4.60	0.10
74	-23.56	0.89	6.67	0.05
74	-21.50	0.85	6.67	0.07
75	-23.79	0.88	7.07	0.09
75	-20.89	0.96	6.37	0.06
76	-24.12	0.95	4.77	0.04
77	-22.53	0.87	5.65	0.15
77	-20.13	0.87	5.22	0.08

Treatment pH 7.9 ²⁶⁰				
Foram #	$\delta^{11}\text{B}$ (‰)	2RSE(‰)	B/Ca (mmol/l)	\pm (mmol/mol)
78	-33.57	1.19	1.04	0.01
78	-34.89	1.36	1.18	0.01
79	-36.14	1.39	1.34	0.02
79	-35.08	1.29	1.26	0.03
80	-36.29	1.50	1.24	0.02
81	-38.64	1.21	1.19	0.02
81	-35.67	0.93	1.15	0.01
82	-35.28	1.05	1.10	0.01
82	-36.13	1.02	1.16	0.01
83	-34.78	1.19	1.27	0.02
83	-35.07	1.10	1.29	0.02

Synthesis & Outlook

Topic 1

Effects of Temperature and Growth Rate on the B/Ca and $^{11}\text{B}/^{10}\text{B}$ Fractionation during Inorganic Calcite Formation

The major results of the inorganic precipitation experiments show that temperature and growth rate impact boron incorporation and isotope fractionation in calcite significantly. However, temperature and growth rate shift the incorporation and isotope fractionation of B in opposite directions, thereby masking their effects. Further major findings are:

1) At very low growth rate of calcite, representing almost thermodynamic **equilibrium conditions**, the B isotopic composition of calcite is equal to that of borate. This is an important finding because it implies that in an inorganic system at very slow calcite growth no fractionation of B isotopes between calcite and $\text{B}(\text{OH})_4^-$ occurs and confirms that the charged borate species is taken up. From studies dealing with biogenic calcium carbonates (corals, foraminifers) deviations between the B isotopic composition of carbonates and borate are often observed (Sanyal et al., 1996; Sanyal et al., 2001; Foster, 2008; Rae et al., 2011). These deviations are discussed in terms of vital effects but the incorporation of boric acid, which is isotopically heavier, has also been proposed (Klochko et al., 2009). My data demonstrate that boric acid is not incorporated. I conclude that the B isotopic signature in biogenic calcium carbonates is the result of a variety of different processes each influencing the B isotopic composition with different magnitudes and directions. As shown in this study the inorganic responses to changes in temperature and growth rate operate in opposing directions with nearly equal magnitudes: a change in temperature by 10 degrees shifts the B isotopic composition by $\sim 2\text{‰}$ to heavier values whereas doubling the growth rate results in lighter values by $\sim 2\text{‰}$. In a natural system (without decoupling) an increase in temperature will be probably accompanied by an increase in growth rate compensating the influence on the B isotopic composition. If

these two effects operate with the same magnitudes during calcification of foraminifers the B isotope composition represents a value influenced primary by calcification and respiration of the foraminifers and symbionts activity.

2) At higher growth rates of calcite, representing thermodynamic **disequilibrium conditions**, the B isotopic composition of calcite deviates from that of borate. Excluding the option of the incorporation of boric acid, this suggest that a fractionation between $^{10}\text{B}(\text{OH})_4^-$ and $^{11}\text{B}(\text{OH})_4^-$ occurs at the crystal surface. This fractionation can be explained with the surface entrapment model.

The results from the inorganic experiments suggest that temperature and growth rate might play an important role for calcium carbonates secreted by marine calcifiers. It has been observed that in the planktonic species *Globogerinoides sacculifer* $\delta^{11}\text{B}$ gets heavier with increasing shell mass, assuming higher growth rates with progressing ontogeny (Hönisch & Hemming, 2004; Wara et al., 2003). This observation is in disagreement with the inorganic trend. However, it is important to keep in mind that an increasing shell mass does not necessarily reflect increased growth rate, because chamber formation is not a continuous process and no data are available on the duration of chamber formation as a function of ontogeny. The problem for reconstructions based on sediment samples is that information about growth rate is not preserved (i.e. there are no proxies for growth rate). Determination of growth rate and its effect on foraminiferal $\delta^{11}\text{B}$ has not been investigated yet and can only be achieved by culture experiments growing foraminifers under one temperature and under constant chemical condition. The determination of growth rate requires strict protocols such as daily observations in order to determine the time span between consecutive chamber formation as well as the time required to calcify a chamber. The effect of temperature on foraminiferal $\delta^{11}\text{B}$ (which has not been investigated yet) should also be studied by culture experiments but it is very likely that a change in temperature will affect the growth rate, too. Therefore, it may turn out to be difficult to investigate the temperature effect on foraminiferal $\delta^{11}\text{B}$ in isolation in contrast to inorganic calcium carbonate.

The reported B/Ca ratios in foraminifers show two different patterns with respect to temperature: no impact (Allen et al., 2011) in the species *O. universa* or an increase with temperature (Wara et al., 2003;

Tripati et al., 2011) in the species *Globogerinoides sacculifer*, *Globorotalia inflata*, and *Globigerina bulloides*. The inorganic trend investigated in this thesis shows that an increase in temperature leads to lower B/Ca if growth rate is kept constant. In a natural system it is likely that an increase in temperature will lead to an increase in growth rate complicating the assessment of the exclusive effect of temperature in foraminifers. As suggested by the results from the inorganic calcite (investigated in this thesis) a simultaneous increase in temperature and growth rate will compensate the effects on B/Ca. Applying this principle to the observations on foraminifers discussed above give rise to the following scenarios: 1) An increase in temperature will lead to an increase in growth rate and the net effect on B/Ca with increasing temperature is compensated, explaining the absence of a temperature trend in *O.universa* 2) An increase in temperature is accompanied by an increase in growth rate but the magnitudes of the compensating effects are not equal resulting in a net change of B/Ca, explaining the observed correlation between temperature and B/Ca in some foraminifers (*Globigerinoides sacculifer*, *Globorotalia inflata*, *Globigerinoides bulloides*). Bijma et al. (1990) investigated temperature and salinity limits of some tropical spinose foraminifers and found that chamber formation and other vital processes such as feeding and rate of gametogenesis show a Gaussian or "bell curve" shape that falls off towards upper and lower temperature limits. Unfortunately, Bijma and co-workers (1990) did not measure the impact of temperature on calcification (rate). It can further be assumed that abiotic and vital effects interact in concert changing the chemistry at the site of calcification. From different responses of B/Ca to temperature observed for different foraminiferal species it is evident that these effects are species specific highlighting the need for species specific calibrations. However, calibration studies on B/Ca with respect to temperature and growth rate will face the same problems as calibration work on $\delta^{11}\text{B}$ mentioned above. The overall conclusion is that incorporation of B in inorganic calcite can be used as a baseline study for biogenic calcite but that biology may operate very differently. Nonetheless, the complex nature of minor/trace element incorporation during the biomineralisation process is often linked to inorganic calcite formation. For example, it is reported that the foraminiferal $\delta^{11}\text{B}$ deviates from the $\delta^{11}\text{B}$ of borate which is often explained by vital effects (Sanyal et al., 1996; Sanyal et al., 2001; Foster, 2008; Rae et al., 2011). The inorganic data obtained in this study shows an excellent agreement between the measured $\delta^{11}\text{B}$ of calcite and calculated $\delta^{11}\text{B}$ of borate if calcite grew close to thermodynamic equilibrium conditions.

However, if the offset between $\delta^{11}\text{B}$ of foraminiferal calcite and of borate is determined and stays constant it can be used to correct the foraminiferal signal. This corroborates the notion that “*vital effects do not compromise the $\delta^{11}\text{B}$ proxy*” (Zeebe et al., 2003). Nonetheless, investigations of element incorporation during inorganic calcite formation remain a helpful and essential tool to assess the complexity of a biogenic system. It provides a baseline from which first steps can be taken.

Topic 2

Simultaneous determination of $\delta^{11}\text{B}$ and B/Ca in marine biogenic carbonates at nano gram level

A new method for the simultaneous determination of $\delta^{11}\text{B}$ and B/Ca in single tests of foraminifers was developed by using a combination of optical emission spectroscopy and multiple ion counting MC-ICP-MS with laser ablation. The precision of the B isotope analysis is sufficient for paleo applications. In the coral sample an internal precision of 0.29‰ was achieved. Due to the higher inhomogeneity of the B isotope distribution in foraminifers, an internal precision of 0.5‰ was achieved. This precision translates to an uncertainty of 0.05 pH units. For glacial-interglacial transitions a pH change of 0.3 unit is predicted (Sanyal et al., 1995) therefore, analysis of B isotopes has to yield a precision better than 1‰ which, is provided by both samples.

The new technique offers several advantages towards conventional bulk analytical techniques:

- 1) The time for sample preparation and the amount of required samples is greatly reduced.
- 2) Two parameters of the carbonates systems can be determined simultaneously.
- 3) The B isotope signature and the corresponding B concentration signal in a single test can be determined. This opens the possibility to study the natural variability within one but also between different foraminiferal species. The latter might help to understand in how far B incorporation and isotope fractionation differs among specimens and whether any correlations between elemental and isotope incorporation exist.

Topic 3

Boron incorporation in the foraminifer *Amphistegina lessonii* under decoupled carbonate chemistry

By decoupling pH and the carbonate ion concentration it was demonstrated that the B isotopic composition in foraminifers is a function of pH and that B/Ca ratio is positively correlated with the $\text{B(OH)}_4^-/\text{HCO}_3^-$ ratio in seawater. The latter suggests a competition between B(OH)_4^- and HCO_3^- for the incorporation of boron in the calcite lattice and explains the positive correlation between foraminiferal B/Ca and $\text{pH}/\text{CO}_3^{2-}$ as already observed in foraminiferal studies. The observed B/Ca - $\text{pH}/\text{CO}_3^{2-}$ correlation stems from the fact that in a natural system an increase in pH is accompanied by an increase in $[\text{CO}_3^{2-}]$ and $[\text{B(OH)}_4^-]$ and a decrease in $[\text{HCO}_3^-]$. Without decoupling of pH and CO_3^{2-} one could conclude a close relationship between foraminiferal B/Ca and pH or B/Ca and $[\text{CO}_3^{2-}]$. By decoupling the carbonate chemistry, as done in this study, the parameters influencing foraminiferal B/Ca can be studied separately. The result of this study supports the underlying concept that HCO_3^- is substituted by borate during the absorption process on the calcite surface. Although the exact pathways of B in the calcite lattice are unknown, it is assumed that B substitutes in the carbonate site as HBO_3^{2-} (Hemming et al., 1995).

The B isotopic composition of the foraminifers is lighter than that of borate. The most widely discussed reasons for deviations from the B isotopic composition of borate are vital effects (Zeebe et al. 2003). Hönisch et al. (2003) grew *O. universa* at 10 times elevated B concentration as done in this study. Hönisch and co-workers (2003) found that symbionts activity raises $\delta^{11}\text{B}$ by 1.5‰. This translates to a pH shift of only 0.2 units whereas Rink et al. (1998) demonstrated that the pH difference in the ambient environment is ~ 0.8 pH units. This is due to the fact that at 10x natural boron concentration the buffering capacity of B(OH)_4^- in the ambient environment is much higher (Zeebe et al., 2003). A complicating factor for understanding the impact of vital effects (both photosynthesis and respiration) is the timing of chamber formation. On average 33% of the shell of *O. universa* is secreted during night (Lea et al., 1995). Furthermore, it has been shown that symbiont photosynthesis in *O. universa* has a daily periodicity (Spero & Parker, 1985). We conclude that the individual differences in respiration rate, number of symbionts,

rate of photosynthesis and calcification, as well as the timing of the latter contribute to the intra and inter test variability in B/Ca and $\delta^{11}\text{B}$ observed in this study. The pH in the proximity of a newly forming chamber in the benthic symbiont free species *Ammonia* sp was measured by Glas et al. (2012). This species shows a pH decrease by ca. 0.6 units during calcification which is expected to lead to a lighter $\delta^{11}\text{B}$ of the foraminiferal calcite than that of borate at bulk pH. In summary, vital effects have a strong impact on the B equilibrium and impacts of photosynthesis or respiration are different among different species. Applying the B proxies to paleo reconstructions requires species specific calibrations taking into account shifts in the chemistry in the microenvironment of the foraminifers. Although a lot of calibration studies have been performed on foraminifers in the last decades (Sanyal et al., 1996; Hönisch et al., 2003; Rae et al., 2011; Henehan et al., 2013) and the impact of temperature and salinity have been addressed (Allen et al., 2011; Allen et al., 2012) one parameter is still missing namely pressure. Paleo reconstructions are often based on benthic species such as *Cibicidoides wuellerstorfi*, *Cibicidoides mundulus* (Yu & Elderfield, 2007; Foster, 2008; Yu et al., 2010; Rae et al., 2011) whose growth habitat lies within a depth range of ~ 800 to 2500 m equivalent to a pressure range of 80 to 250 bars. Since dissociation constants are also pressure dependent, shifts in the species distribution of carbon and boron occur. For example, a change in pressure by 300 bars will shift pH by ~ 0.1 units (Zeebe & Wolf-Gladrow, 2001) and the borate concentration by 10%. So far, studies dealing with *C.wuellerstorfi* reveal only small deviations in $\delta^{11}\text{B}$ between foraminiferal calcite and borate. However, this good agreement might be misleading because changes in pressure affecting the carbon and boron speciation have not been considered. The reason why pressure based calibrations have not yet been performed is related to difficulties with *in situ* sample collection and culturing under *in situ* pressures. However, for correct data interpretation, pressure based calibrations are required for deep sea, barophilic, foraminifers.

Using the new *in situ* technique introduced in topic 2, it was possible to resolve the natural variability in *A. lessonii*: while the element distribution of B shows a higher variability with increasing B concentration in the test, the variability in the isotope distribution is ~1.4‰ (SD) or 5‰ ($\Delta\delta^{11}\text{B}$) being independent on the carbonate system chemistry. Natural variability of B/Ca and $\delta^{11}\text{B}$ in foraminifers has been poorly investigated yet. Most of the B data obtained from foraminifers is based on bulk analytical techniques

such as TIMS and MC-ICP-MS which do not allow analysis of single spots within one specimen. For boron based reconstructions bulk analytical techniques might represent a better approach since the results are generated from a large sample representing a reliable mean value. However, such techniques are not able to resolve B incorporation and B isotope fractionation patterns and thus do not help to gain more knowledge about B's behavior in single specimens. The latter is very important since it might help to obtain a better understanding of B incorporation.

REFERENCES

- Allen, K.A., Hönisch, B., Eggins, S.M., Rosenthal, Y., 2012. Environmental controls on B/Ca in calcite tests of the tropical planktic foraminifer species *Globigerinoides ruber* and *Globigerinoides sacculifer*. *Earth and Planetary Science Letters* 351–352, 270–280.
- Allen, K.A., Hönisch, B., Eggins, S.M., Yu, J., Spero, H.J., Elderfield, H., 2011. Controls on boron incorporation in cultured tests of the planktic foraminifer *Orbulina universa*. *Earth and Planetary Science Letters* 309, 291–301.
- Bijma, J., Faber, W.W., Hemleben, C., 1990. Temperature and salinity limits for growth and survival of some planktonic foraminifers in laboratory cultures. *The Journal of Foraminiferal Research* 20, 95–116.
- Foster, G.L., 2008. Seawater pH, pCO₂ and [CO₂–3] variations in the Caribbean Sea over the last 130 kyr: A boron isotope and B/Ca study of planktic foraminifera. *Earth and Planetary Science Letters* 271, 254–266.
- Glas, M.S., Langer, G., Keul, N., 2012. Calcification acidifies the microenvironment of a benthic foraminifer (*Ammonia* sp.). *Journal of Experimental Marine Biology and Ecology* 424–425, 53–58.
- Hemming, N.G., Reeder, R.J., Hanson, G.N., 1995. Mineral-fluid partitioning and isotopic fractionation of boron in synthetic calcium carbonate. *Geochimica et Cosmochimica Acta* 59, 371–379.
- Henehan, M.J., Rae, J.W.B., Foster, G.L., Erez, J., Prentice, K.C., Kucera, M., Bostock, H.C., Martínez-Botí, M.A., Milton, J.A., Wilson, P.A., Marshall, B.J., Elliott, T., 2013. Calibration of the boron isotope proxy in the planktonic foraminifera *Globigerinoides ruber* for use in palaeo-CO₂ reconstruction. *Earth and Planetary Science Letters* 364, 111–122.
- Hönisch, B., Bijma, J., Russell, A.D., Spero, H.J., Palmer, M.R., Zeebe, R.E., Eisenhauer, A., 2003. The influence of symbiont photosynthesis on the boron isotopic composition of foraminifera shells. *Marine Micropaleontology* 49, 87–96.
- Hönisch, B., Hemming, N.G., 2004. Ground-truthing the boron isotope-paleo-pH proxy in planktonic foraminifera shells: Partial dissolution and shell size effects. *Paleoceanography* 19, PA4010.
- Klochko, K., Cody, G.D., Tossell, J.A., Dera, P., Kaufman, A.J., 2009. Re-evaluating boron speciation in biogenic calcite and aragonite using ¹¹B MAS NMR. *Geochimica et Cosmochimica Acta* 73, 1890–1900.
- Lea, D.W., Martin, P.A., Chan, D.A., Spero, H.J., 1995. Calcium uptake and calcification rate in the planktonic foraminifer *Orbulina universa*. *The Journal of Foraminiferal Research* 25, 14–23.
- Rae, J.W.B., Foster, G.L., Schmidt, D.N., Elliott, T., 2011. Boron isotopes and B/Ca in benthic foraminifera: Proxies for the deep ocean carbonate system. *Earth and Planetary Science Letters* 302, 403–413.
- Rink, S., Köhl, M., Bijma, J., Spero, H.J., 1998. Microsensor studies of photosynthesis and respiration in the symbiotic foraminifer *Orbulina universa*. *Marine Biology* 131, 583–595.
- Sanyal, A., Bijma, J., Spero, H., Lea, D.W., 2001. Empirical relationship between pH and the boron isotopic composition of *Globigerinoides sacculifer*: Implications for the boron isotope paleo-pH proxy. *Paleoceanography* 16, 515–519.

- Sanyal, A., Hemming, N.G., Broecker, W.S., Lea, D.W., Spero, H.J., Hanson, G.N., 1996. Oceanic pH control on the boron isotopic composition of foraminifera: Evidence from culture experiments. *Paleoceanography* 11, 513-517.
- Sanyal, A., Hemming, N.G., Hanson, G.N., Broecker, W.S., 1995. Evidence for a higher pH in the glacial ocean from boron isotopes in foraminifera. *Nature* 373, 234-236.
- Spero, H.J., Parker, S.L., 1985. Photosynthesis in the symbiotic planktonic foraminifer *Orbulina universa*, and its potential contribution to oceanic primary productivity. *The Journal of Foraminiferal Research* 15, 273-281.
- Tripati, A.K., Roberts, C.D., Eagle, R.A., Li, G., 2011. A 20 million year record of planktic foraminiferal B/Ca ratios: Systematics and uncertainties in pCO₂ reconstructions. *Geochimica et Cosmochimica Acta* 75, 2582-2610.
- Wara, M.W., Delaney, M.L., Bullen, T.D., Ravelo, A.C., 2003. Possible roles of pH, temperature, and partial dissolution in determining boron concentration and isotopic composition in planktonic foraminifera. *Paleoceanography* 18, 1100.
- Yu, J., Elderfield, H., 2007. Benthic foraminiferal B/Ca ratios reflect deep water carbonate saturation state. *Earth and Planetary Science Letters* 258, 73-86.
- Yu, J., Foster, G.L., Elderfield, H., Broecker, W.S., Clark, E., 2010. An evaluation of benthic foraminiferal B/Ca and $\delta^{11}\text{B}$ for deep ocean carbonate ion and pH reconstructions. *Earth and Planetary Science Letters* 293, 114-120.
- Zeebe, R.E., Wolf-Gladrow, D.A., 2001. CO₂ in seawater: equilibrium, kinetics, isotopes. Elsevier Science B.V., Amsterdam.
- Zeebe, R.E., Wolf-Gladrow, D.A., Bijma, J., Hönisch, B., 2003. Vital effects in foraminifera do not compromise the use of $\delta^{11}\text{B}$ as a paleo-pH indicator: Evidence from modeling. *Paleoceanography* 18, 1043.